CZECH TECHNICAL UNIVERSITY IN PRAGUE

Faculty of Mechanical Engineering

Department of Fluid Mechanics and Thermodynamics

Analytical and Computational Methods for Transonic Flow Analysis and Design

Doctoral Thesis

Jiří Stodůlka

Field of Study: Thermomechanics and Fluid Mechanics

Supervisor: Pavel Šafařík

Supervisor Specialist: Helmut Sobieczky

Prague 2019

Abstract

The work deals with various solutions of the compressible transonic flows and their applications on academic and practical cases. The main motivation is to remind the classical methods, modify or modernize them with fast computational techniques and show their benefits even in todays modern era of commercial software tools. These may may be very powerful and useful, but sometimes lead to the lack of the basic understanding among the engineering community, mainly in such sensitive topic as transonic flow. The classical gas dynamics can describe, in simplified form, the process relations and individual regimes, but the nonlinear combined flow field behavior description requires deeper understanding and advanced approaches. In order to solve the combination of elliptic and hyperbolic equations describing the near sonic flow, the hodograph transformation based methods are introduced and rheograph solution to the near sonic flow is presented as well as the numerical methods which can solve directly Euler partial differential equations describing general compressible flow. All the approaches are compared and validated on the case of Guderley's cusp. For the benefit of the filed of study, classical methods are combined with modern computational abilities to create an academic case of supercritical nozzle, which prove the functionality for the internal aerodynamics and results with an interesting test example. The practical benefits of the analytical solution knowledge are presented on the ERCOFTAC case of transonic blade cascade SE 1050 with specific design and flow pattern with supersonic re-compression issue. The rheograph transformation is used for specific flow analysis and solutions to this problem are proposed.

Key words

compressible fluid flow, transonic flow, hodograph, rheograph transformation, method of characteristics, computational fluid dynamics, supercritical nozzle, blade cascade

Anotace

Práce se zabývá různými způsoby řešení transonického proudění stlačitelných tekutin a jejich aplikací na akademické i praktické úlohy. Hlavní motivací je připomenutí klasických metod, jejich modifikace využitím moderních výpočetních postupů a techniky a cílem je ukázat jejich benefity i v dnešní době rychlých numerických simulací. Tyto simulace jsou dnes velmi silným a efektivním nástrojem, avšak jejich schopnosti a robustnost mohou vést k ubývání potřebných základních znalostí mezi inženýry, zvláště pak v tak citlivé problematice jako je transonické proudění. Základní dynamika plynů dokáže popsat základní principy, vztahy a režimy, ale nelineární problematika chování smíšeného transonického proudění vyžaduje hlubší porozumnění a pokročilé postupy řešení. Pro potřebu řešení kombinace eliptických a hyperbolických rovnic popisujících proudění blízké rychlosti zvuku se využívají metody založené na hodografické transformaci. Je zde popsána rheografická metoda řešení a rovněž numerické metody řešící přimo Eulerovy rovnice proudění stlačitelné tekutiny. Všechny zmíněné metody jsou porovnány a validovány na úloze Guderleyho profilu. Pro přínos oboru je analytická rheografická metoda obohacena a rozšířena použitím moderních výpočetních metod a je tímto způsobem vytvořena akademická úloha superkritické trysky, která mimo jiné dokazuje možnost použití této metody i pro potřeby interní aerodynamiky a může dále sloužit jako zajímavá testovací úloha. Praktické výhody znalosti a využití analytických metod jsou prezentovány na úloze transonické lopatkové mříže SE 1050 z databáze ERCOFTAC. Tato mříž je známá svým specifickým charakterem a přítomností supersonické rekomprese. Rheografická transformace je použita na podrobnou analýzu specifického proudového pole a na jejím základu jsou navrženy opatření pro eliminaci tohoto nežádoucího chování.

Klíčová slova

proudění stlačitelné tekutiny, transonické proudění, hodograf, rheografická transformace, metoda charakteristik, CFD, superkritická tryska, lopatková mříž

Acknowledgement

At the first place I would like to thank to the supervisor of my thesis, prof. Pavel Šafařík, for his distinctive leadership and allround support during the study duties. The main acknowledgment belongs as well to the thesis supervisor specialist, prof. Helmut Sobieczky, who's academic work inspired me to choose the topic and who's helpful advices, ideas and effort led to interesting work. I also thank to the institutes of CTU in Prague in and TU Vienna.

Major thanks belongs also to my colleagues for various practical discussions and useful technical hints, likewise to my employers for understanding and all the material support as well as moral comprehension.

Last but not least, I would like to thank to my family, friends and the closest one.

The funding was supported by the Grant Agency of Czech Technical University in Prague, grant number SGS13/180/OHK2/3T/12.

Declaration

I declare I composed this thesis individually and using the references quoted at the end of the thesis.

.....

Some major portions of the thesis chapters have been already published as follows:

Chapter 4:

Stodůlka, J.: *Numerical Solution of Oblique Shock with Wall Interaction Using Finite Difference Method,* SKMTaT 2013, Žilina, pp. 275-278, 2013

Chapter 5:

Stodůlka J., Sobieczky, H.: *On Transonic Flow Models for Optimized Design and Experiment,* EPJ Web of Conferences 67, 02111, 2014

Stodůlka, J., Sobieczky, H.: *Theoretical and Numerical Solution of a Near Sonic Flow Considering the Off-Design Conditions,* Engineering Mechanics 2014, Svratka, pp. 588-591, 2014

Stodůlka, J., Šafařík, P.: *Analysis of Transonic Flow Past Cusped Airfoil Trailing Edge,* Acta Polytechnica, Prague, pp. 193-198, 2015

Chapter 6:

Stodůlka, J., Sobieczky, H., Šafařík, P.: *Analytical and Numerical Modifications of Transonic Nozzle Flows,* Journal of Thermal Science, Vol 27, Issue 4, pp. 382-388, 2018

Contents

Nomenclature

Symbols

a	speed of sound	m/s
A	area	m^2
A	scaling parameter	$-$
B	scaling parameter	$-$
c	velocity	m/s
c	specific heat capacity	$J/(kgK)$
c_p	pressure coefficient	$-$
C	chord length	m
d	wave distance	m
D	domain dimension	$-$
e	specific energy	J/kg
e	Euler number	$-$
E	mapping function E	$-$
E	electric potential	J
f	f vector	$-$
g	g vector	$-$
h	specific enthalpy	J/kg
h	conductor thickness	m
H	mapping function H	$-$
i	complex variable	$-$
I	current intensity	A
k	artificial viscosity parameter	$-$
k	switch parameter	$-$
K	coefficient K	$-$
l	switch parameter	$-$
L	convective flux	$-$
m	switch parameter	$-$
M	Mach number	$-$

n	normal direction	$-$
p	pressure	Pa
P	chamber/thickness parameter	$-$
q	velocity magnitude	m/s
r	specific gas constant	$J/(kgK)$
r	gradient ratio	$-$
s	rheograph coordinate s	$-$
t	time	s
t	rheograph coordinate r	$-$
T	temperature	K
T	pitch	m
u	velocity in x direction	m/s
U	u velocity in rheograph plane	$-$
v	velocity in y direction	m/s
v	specific volume	m^3/kg
V	y velocity in rheograph plane	$-$
w	conservative variable vector	$-$
W	current function	$-$
x	x coordinate	m
X	x coordinate in rheograph plane	$-$
y	y coordinate	m
Y	y coordinate in rheograph plane	$-$
z	z coordinate	m
α	angle of attack	$^\circ$
β	wave angle	$^\circ$
γ	stagger angle	$^\circ$
δ	flow turning angle	$^\circ$
ϵ	viscosity parameter	$-$
ζ	working plane ζ	$-$
η	η characteristic	$-$

ϑ	flow angle	$^\circ$
κ	specific heat capacity ratio	$-$
λ	solution parameter	$-$
Λ	conductivity	S/m
ν	Prandtl-Meyer angle	$-$
ξ	ξ characteristic	$-$
π	Ludolph number	$-$
ρ	density	kg/m^3
σ	similarity parameter	$-$
ς	loss coefficient	$-$
τ	thickness to chord ratio	$-$
Υ	convective constant	$-$
ϕ	velocity potential	m^2/s
Φ	conservative variable	$-$
χ	similarity parameter	$-$
ψ	stream function	m^2/s
Ψ	limitter	$-$
ω	camber to chord ratio	$-$

Indexes

$'$	perturbation variable
$*$	critical state
0	stagnation state
1	state 1
2	state 2
3	state 3
4	state 4
∞	infinity

a	region a
b	region b
D	domain boundary
h	derivative in h direction
i	step i in spatial direction
j	step j in spatial direction
n	step n in time
p	constant pressure
P	camber/thickness parameter
s	derivative in s direction
s	constant entropy
ss	second derivative in s direction
t	time
t	derivative in time
t	derivative in t direction
tt	second derivative in t direction
v	constant volume
x	derivative in x direction
xx	second derivative in x direction
y	derivative in y direction
yy	second derivative in y direction

Dwn	down
Lft	left
max	maximum
min	minimum
red	reduced parameter
ref	reference value
$Rght$	right
TE	trailing edge
Up	up

η	first derivative in η direction
ϑ	first derivative in ϑ direction
ν	first derivative in ν direction
ξ	first derivative in ξ direction

1 Introduction

Among various aerospace vehicle speeds and machinery operating states, the transonic regime has always posed remarkably difficult challenges to systematic design and experimental techniques. The unknown physical limits and by this time unexpected behavior at reaching and exceeding sonic velocities were hard to understand and describe for the first observers. Until only theoretical methods to understand transonic flow phenomena developed in past time shed light into transonic testing techniques by solving the underlying physical relations in various stages of their simplifications. Such analytical models led to the geometrical description of basic aerodynamic shapes and subsequently to realistic wing sections including qualitative insight into the structure of surrounding transonic flow. At the same time, first numerical simulations of these physical relations were developed so that prior to experimental investigations a quantitative results were obtained. These, finally, allowed for a calibration of wind tunnels which are needed to aid the industry in their development of efficient flight vehicles and blades in rotating machinery. Accelerated computational technology and numerical codes development then enabled the expansion and introduced this field to the wider community of engineers. After that moment, the industry also started to be filled with fast tools for evaluation, design and optimization, but with no more need for understanding the underlying flow characteristics and theoretical analysis they originated from.

The work makes use of classical concepts for transonic and supersonic flows [1], [2] which have been used for developing design methods for aircraft wings and turbomachinery blades in the past century [3], [4]. These methods might be aging today, but can still be cheap and capable and compared to presently operational computational methods based on pure computational power, they offer valuable extra benefit of understanding the transonic flow phenomena and gas dynamic basic principles and behavior mostly unknown to current engineers. Various applications for different cases in aerospace field were developed mainly during the supersonic transport era, but the possible extensions of the classical methods can be applied as well on internal aerodynamics as a nozzle type flows [5]. To make these methods [6] still relevant, they can now arise and advance from modern computational and programing abilities, allowing fast numerical solution to different types of partial differential equations and characteristic methods and provide a new sights to the problematics. These still theoretically and mathematically valid concepts and cases may be perfectly suitable for validation and application of new approaches, however, the seek for direct practical usage example

of any method requires application on a industry relevant case. Besides the supersonic wing sections, shock-free airfoils and other aviation concepts solving mainly the external flow, the solution of transonic internal aerodynamics already implies the possible practical application for the turbomachinery blades and cascades [7]. Concerning this, the main idea is to show that all the classic theory, even though up to date renovated, widely used CFD solutions as well as experiments can be used in cooperation and occasionally provide new, more advanced view on flow field analysis and also potentially help with a clever shape design.

In general, elegant analytical solutions were developed using the hodograph formulations to linearize the gas dynamic equations and thanks to that, large number of solutions were presented in the past century. The skillful application and composition of these methods to create exact solutions to practical fluid dynamics in the transonic flow regime has led modern aerodynamics to become a mature science. While this is of course quite beneficial to the engineering community, one negative aspect seems to remain, A large portion of phenomena-based knowledge base is no more part of academic education, simply because it is seen as replaced by software to solve practical problems. Design concepts, however, rest on this knowledge of mathematical models and feed the creativity of engineers interested in innovative projects.

Specifically, still very suitable for today applications, the rheograph transformation method [4] was repeatedly proved to be very efficient for aerodynamic design in various forms. Validated and extended with new available tools, it could remind the justification of the classical knowledge and prove its relevancy among other, more common approaches.

1.1 Motivation

As the described problematics reaches the limits of simple mathematical methods and derived solutions are results of complicated and combined theories, the more attention should be paid to the level of knowledge amongst the researchers. There are many new possibilities which can improve the by decades verified, nowadays maybe old fashioned, but still effective approaches and make them more pleasant and available. However, the tools of the new engineering era sometimes tends to turn in different direction.

The new modern generation of engineers and even scientists may be skilled in use of modern computational software and hardware tools, but the complexity and abilities of nowadays technology requires less and less of user involvement. On one hand, there are the commercial CFD codes

which allow to simulate all imaginable problems no matter the complexity of geometry model or physics. They are getting more and more accurate, robust and user friendly. On the other hand, the IT technology marches forward resulting in hardware and computational power getting cheaper and accessible, what leads to popularity of methods like design of experiments and other hardware based optimization methods. No doubt that there are many benefits of such technological progress, but the side effect of the overall knowledge no more being necessary to be present among the research and development society is also apparent due to this evolution. Especially in such complicated and sensitive field of study as the transonic flow regime, where the understanding of general principles and characteristics is crucial for precise flow analysis or correct problem evaluation, optimization and design.

The main philosophical message of the thesis is to remind the basic principles of high speed compressible fluid flow analysis and techniques and show that it is still beneficial to have at least a basic theoretical knowledge among engineering community. To show that the modern numerical computational methods do not have to mean the old practice to be forgotten but may be used in cooperation with theoretical methods and lead to better understanding of the transonic flow basics and smarter, creative engineering.

1.2 Topics and Scheme

Previous thoughts already point out the main theme of the following chapters, however, for the informational impact, some applicable conclusions are important too. Besides the general reminder of those mostly forgotten methods, the methods that led to the current state of the art in the filed of compressible fluid flows and brought designs and machines the civilization today uses on daily basis, new solutions and applications can still be carried out. In order to satisfy the mentioned ideas and thoughts and give the work an academical, practical and educational purpose and meaning, the following tasks and topics in consecutive sections are solved in this thesis.

The first task is to briefly introduce the compressible gas dynamics problematics, its basics and general principles as well as possible solutions to subsonic, supersonic and transonic problems and flow fields. In more detail, to describe methods based on theoretical approaches like is the hodograph-based rheograph transformation and explain their benefits. And besides that, introduce direct numerical methods developed for solution of the full nonlinear partial differential equation systems.

Not only CFD simulations, but also other computational methods are today irreplaceable techniques for solution of various research and development challenges. The basics of modern numerical modeling methods are described with the aim of evaluation of the the most suitable schemes for high speed compressible fluid flow application. And although in comparison with this, the foundation of the theoretical analytical methods for high speed design methods may be aging, the known and well described Guderley's cusp and its lifting variations [3], [8] problem can serve as a perfect test case for comparison of the hodograph-based methods, classical gas dynamics principles and modern computational techniques. This mutual validation should show the relevance and accuracy of all those techniques for current challenges no matter the era of origin and on the top, provide new views on classical cases.

After understanding the principles and managing all the methods for transonic flow analysis and design, the next task is to preview the idea of combination of the flow field numerical computation and theoretical methods. In other words, to outline the revitalization of the rheograph transformation method [5] and elliptic continuation using modern computational tools. Specifically, solve simultaneously the elliptical equations described flow and hyperbolic equations based characteristics on mathematically valid theoretical example for internal supercritical nozzle throat flow. Usage of manual based analytical methods for solution of equations describing underlying flow required wide knowledge in advanced mathematics what may led to unpopularity of this design methods between some of the general community in the past. Numerical computational solution could lead, overall, to easier to use method and remove this drawback.

To demonstrate the ability, functionality and possible benefits of such method on a relevant practical case, it is applied on a real geometry and real flow field of the blade cascade SE 1050 [7]. This cascade is well know for it's specific flow pattern given by the specific shaping resulting in the formation of supersonic re-compression during the flow expansion. This case has been a subject to numerous experiments [9], numerical simulations [10] and analysis and some ideas for re-design were proposed [11], but their functionality was not validated. The goal here is to show how the results obtained from numerical simulations or experiments can be used the initial condition for the transonic flow behavior analysis with respect to previously discussed approaches and investigate if those methods can help be used to shape modification.

2 The Theory and Solutions of the Compressible Fluid Flows

The effect of compressibility brings the high speed aerodynamics to the new level of understanding due to reaching the natural physical limits. The barrier of sound distinguishes the flow in two differently behaving and differently described regimes, yielding from the combination of elliptic and hyperbolic equation systems for subsonic and supersonic flow. The only way of analytical solutions to the transonic flow fields leads to transformations into linearized nonphysical planes, which are not easy to understand nor use, but necessary to keep in mind. Modern computational era arrives then with new possibilities and numerical methods and computational fluid dynamics to solve directly the general equations.

Before solving the concrete applications, it is appropriate to introduce the known theory and describe general state of knowledge. Therefore, the overview of compressible flow basic principles and introduction to later used flow solutions is described in this chapter.

2.1 Compressible Fluid Flow Classification

Compressible fluid flow implies variation of density in the flow field resulted principally from pressure changes between two points in the flow. Compressibility can be easily defined on small element with volume v. If pressure from original value p is increased by infinitesimal amount dp, the volume of the element will be correspondingly compressed by the amount dv [12].

$$\upsilon = -\frac{1}{v}\frac{dv}{dp} \tag{2.1}$$

The rate of change in density with respect to pressure is then closely connected with the velocity propagation of small pressure disturbances, or in other words the speed of sound, defined by [12]

$$a = \sqrt{\left(\frac{dp}{d\rho}\right)_s} \tag{2.2}$$

If the flow reaches sonic conditions where the local velocity equals local speed of sound, such state is then called critical and local velocity is the critical velocity.

$$a^* = c^* \tag{2.3}$$

In the Figure 2.1, different regimes with respect to the disturbance propagation or the speed of sound are depicted. In the subsonic regime, nothing unexpected appears, but for higher velocities

closer to the speed of sound, the effect of compressibility, obviously, needs to be considered. The sonic regime, where the object velocity and a local speed of sound are equal, leads to formation of common normal wave. And finally, if the velocity exceeds the speed of sound, a conical wave is formed as a wrap of the individual sound waves. This phenomenon is also known as a Mach cone or a Mach wedge.

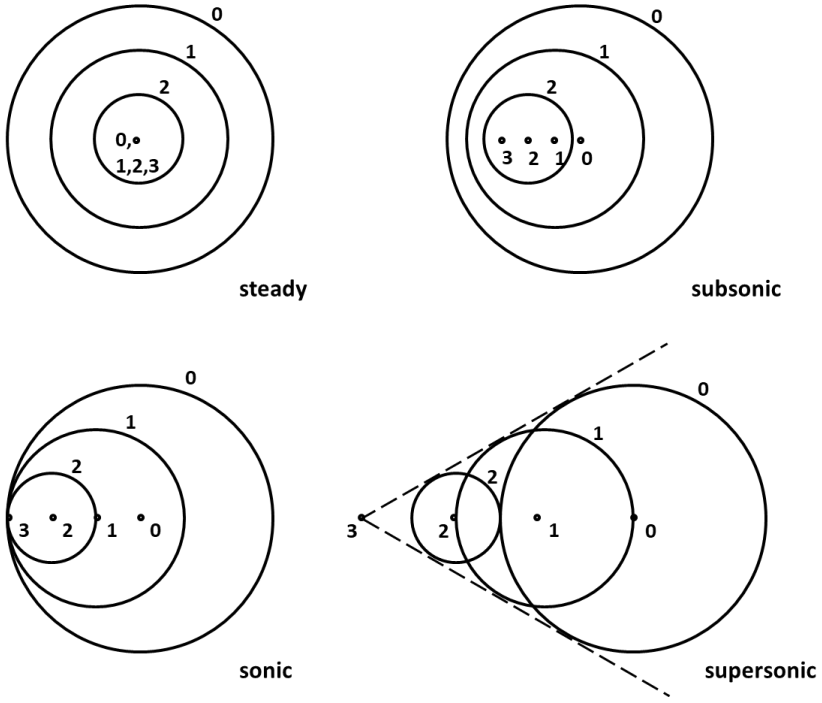

Figure 2.1: Speed regimes

For easy classification of the flow, a characteristic dimensionless number defined as a ratio of the flow velocity and the speed of sound called the Mach number is introduced.

$$M = \frac{c}{a} \tag{2.4}$$

The barrier of sound $M = 1$ distinguishes the flow regimes into subsonic regime for $M < 1$ and supersonic regime for $M > 1$. Subsonic flow is characterized by smooth streamlines and continuously varying properties and due to elliptic nature of the subsonic regime, free stream is already deflected far upstream the obstacles. Supersonic flow, with speeds exceeding the propagation of pressure disturbance, characterized by hyperbolic character behaves entirely different and usually forms waves and sudden discontinuities of parameters, or shocks, in the flow field already apparent form the Figure 2.1. Upstream flow is independent of obstacles as they affect the flow only downstream the perturbation. Flows reaching very high Mach numbers, generally $M > 5$, where temperatures

become the main role in flow parameters are called hypersonic. The graphical expression of the regime distribution is depicted in the Figure 2.2.

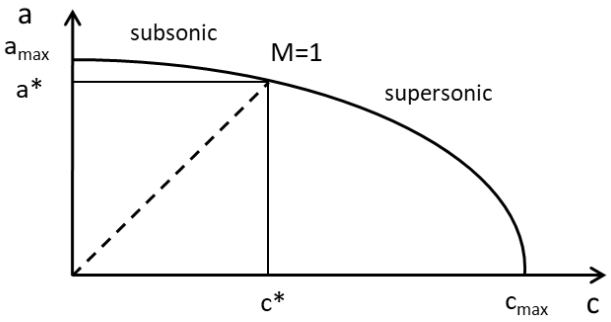

Figure 2.2: Flow regimes

For velocities close to the speed of sound, both types of fluid can occur together and form a transonic flow field. If subsonic flow is accelerated enough, it can reach sonic speed and continue supersonic to form expansion or shock waves. Transonic regime is extremely sensitive to any changes mainly in areas closest to the sonic conditions, where only minor changes in geometry mean dramatic changes in the flow field. And while the basics of subsonic and supersonic theory can be described by linear theory, much more difficult situation as a transonic regime always leads to nonlinear description with various theoretical difficulties.

2.2 Governing Equations and General Principles

High-speed compressible fluid flow, in general, is described by partial differential equation system of the Euler equations. These describe the law of conservation of mass, momentum and energy in the upcoming form.

Continuity equation:

$$\frac{\partial \rho}{\partial t} + \nabla \cdot (\rho \vec{c}\,) = 0 \tag{2.5}$$

Momentum equation:

$$\frac{\partial (\rho \vec{c}\,)}{\partial t} + \nabla \cdot (\rho \vec{c}\,\vec{c}\,) + \nabla p = 0 \tag{2.6}$$

Energy equation:

$$\frac{\partial (\rho e)}{\partial t} + \nabla \cdot [\vec{c}\ (\rho e + p)] = 0 \tag{2.7}$$

Unlike the low Reynolds number Navier-Stokes equations, viscosity plays minor role to the compressible flow phenomena and for better understanding of the general principles, the flow can be considered as inviscid.

At the velocities, temperatures and pressure characteristics of the compressible flow, the flowing medium can be considered as a perfect or ideal gas, represented by the state equation

$$\frac{p}{\rho} = rT \tag{2.8}$$

with r being the specific gas constant. Another important constant for ideal gas widely used throughout the whole compressible flow regime is the ratio of specific heat capacities.

$$\kappa = \frac{c_p}{c_v} \tag{2.9}$$

As mentioned for Euler equations, neglecting dissipation effects like boundary layers or heat conduction in high velocity flows over airfoils or in nozzles allow them to be considered as isoentropic. This assumption allows easier derivation of relations directly applicable to many types of practical flow problems. Basic equation that relate pressure, density and temperature for an isoentropic process can be derived [13].

$$\frac{p_2}{p_1} = \left(\frac{\rho_2}{\rho_1}\right)^{\kappa} = \left(\frac{T_2}{T_1}\right)^{\frac{\kappa}{\kappa-1}} \tag{2.10}$$

Similarly, mainly for the one-dimensional internal aerodynamics cases, other flow properties and aerodynamic functions can be easily derived using general equations and properties between two states [13].

The geometrical or shape effects are important for understanding the differences in the transonic flow and flow transitions. In terms of accelerated and decelerated flow, substituting relation for speed of sound into continuity equation leads to Hugoniot equation which expresses the relationship between change in cross-section area and change in velocity [13].

$$\frac{dA}{A} = \frac{dc}{c}\left(M^2 - 1\right) \tag{2.11}$$

From this simple equation is obvious that the flow accelerated in convergent nozzle shape geometry in subsonic regime is decelerated in the same geometry in supersonic regime and thus, the same geometry acts like a diffuser in speeds exceeding sonic velocities. On the other hand, decelerated flow in subsonic divergent diffuser is accelerated in the same geometry in supersonic regime acting like a supersonic nozzle. Graphical explanation is depicted in the Figure 2.3.

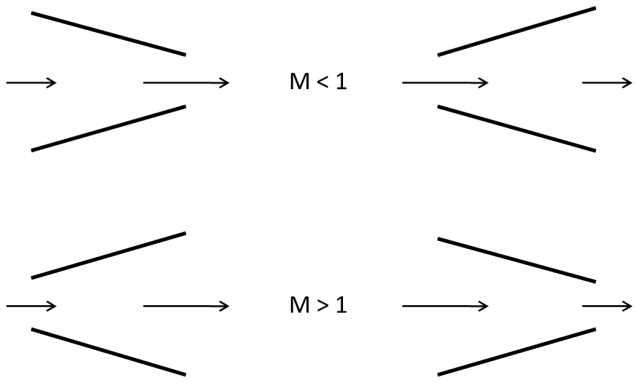

Figure 2.3: Nozzle and diffuser for different flow regimes

Previous relations already imply that in order to accelerate the flow from slow subsonic regime all the way to supersonic speeds, the nozzle needs to have a convergent-divergent shape (Eq. (2.12)) with sonic point in the smallest cross-section area, or the nozzle throat, where $dA/A = 0$. This also means that the mass flow is limited to the sonic conditions in the nozzle throat. This phenomenon is called aerodynamic choke.

$$\frac{dA}{A} > 0 \quad for \quad M < 0, \quad \frac{dA}{A} < 0 \quad for \quad M > 0 \tag{2.12}$$

For certain combinations of initial and final pressures the, basic isoentropic theory of compressible flow provide no solution to some of the flow problems. If the flow is rapidly forced to slow down from supersonic speeds, instead of gradual and continuous decrease of velocity and increase of pressure, very rapid changes and discontinuities may occur. The velocity in such situations drops instantly from supersonic values to subsonic and a normal shock wave is formed. Because shock waves work only one way, always from supersonic to subsonic and never vice versa, the process cannot be considered as reversible and thus isoentropic. Adiabatic relations have to be used instead. The main relation of normal shock determines that the product of velocity in front of and behind the wave equals to the critical velocity squared.

In planar case where two dimensional effects like turning of the flow form, compression oblique shock waves are often formed in slowed supersonic flow field (Fig. 2.4). Oblique shocks appear at convex boundary shape change, on real geometries typically at the leading and trailing edges of the airfoil or blade. They represent the same abrupt parameter change, but unlike the normal shocks, due to geometrical aspects of normal and tangential direction, oblique shocks usually act as weak waves and velocity behind the wave remains supersonic.

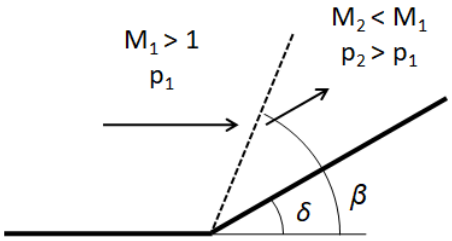

Figure 2.4: Oblique shock

Although naturally inclining to weak solution, if forced, strong oblique shocks can appear as well, one for subsonic outlet Mach number and one for supersonic. Resulting from adiabatic equations, both solutions are valid. The normal shock wave is here just a special extreme variant of the oblique shock. This ambiguity is one of the very typical properties of compressible flow reaching supersonic speeds.

Acceleration of the supersonic flow occur on concave boundary shape change in form of Prandtl-Meyer expansion (Fig. 2.5). Despite still having the wavy character, expansion accelerates the flow in smooth continuous rate.

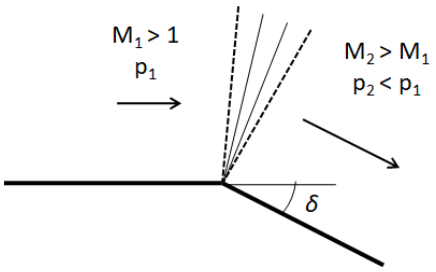

Figure 2.5: Prandt-Meyer expaansion

Parameters of above phenomena are all obtained using relatively simple gas dynamics equations and relations and thus are easy to solve or calculate. To describe and find a solution of the whole, multidimensional flow filed, more advanced approaches have to be used and many theories stand on the basics of the potential flow. The potential flow theory allows separation of continuity, momentum and energy equation into one equation solving a new variable called velocity potential for special case of irrotational flow. So the steady state two-dimensional potential flow is defined by the continuity equation and irrotationality.

$$div\,(\rho\vec{c}\,) = 0 \tag{2.13}$$

$$rot\,(\vec{c}\,) = 0 \tag{2.14}$$

The application for compressible flows resulting from combining continuity and momentum equation with relation of speed of sound into a potential equation [13] (here for two dimensional flow) with $a = a(\phi_x, \phi_y)$

$$\left(1 - \frac{\phi_x^2}{a^2}\right)\phi_{xx} + \left(1 - \frac{\phi_y^2}{a^2}\right)\phi_{yy} - \frac{2\phi_x\phi_y}{a^2}\phi_{xy} = 0 \tag{2.15}$$

However, the nonlinear character disallows direct simple solution of the potential equation and thus, a special case of potential flow theory for slender profiles with small velocity change and flow angle deviation can be used to linearize the equation. Defining perturbation velocity and perturbation potential solving a perturbations from the uniform flow yelding the approximate equation [13]

$$\left(1 - M^2\right)\phi'_{xx} + \phi'_{yy} = 0 \tag{2.16}$$

For subsonic regime, this equation becomes elliptical and can be solved using Prandtl transformation similarly to conformal mapping method. Hyperbolic wavy character in supersonic regime leads to the method of characteristics, which is based on principle of characteristic lines with constant invariants along them.

$$\frac{dy}{dx} = \pm\frac{1}{\sqrt{M^2 - 1}} \tag{2.17}$$

Positive sign for left running characteristics and negative sign for right running characteristics.

2.3 Near Sonic Flow and Hodograph Based Methods

The proper full mathematical solution of transonic flow phenomena resulting in the co-existence of elliptic and hyperbolic basic differential equations have to bring together classical hydraulic methods with the wave propagation solutions. To understand the basics of such theory, the flow can be restricted, so that the velocity magnitude is close to speed of sound. These restrictions allow the simplifications of the basic potential equations resulting in the analytically exact solution of a flow past slender airfoil in this sonic free stream. The upcoming theory and resulting relations were written using [4].

Velocity potential ϕ and stream function ψ are defined with $q = |\vec{c}\,|$ and ϑ the flow angle.

$$\phi_x = \frac{\rho_0}{\rho}\psi_y = u = qcos\vartheta \tag{2.18}$$

$$\phi_y = \frac{\rho_0}{\rho}\psi_x = u = qsin\vartheta \tag{2.19}$$

where density as function of Mach number is

$$\frac{\rho}{\rho_0} = \left(1 + \frac{\kappa - 1}{2} M^2\right)^{-\frac{1}{\kappa - 1}} \tag{2.20}$$

This system, Eq. (2.18) and Eq. (2.19), of nonlinear equations after elimination of ϕ and ψ yields

$$\phi_{xx} + \phi_{yy} = -\frac{\rho_x}{\rho}\phi_x - \frac{\rho_y}{\rho}\phi_y \tag{2.21}$$

$$\psi_{xx} + \psi_{yy} = \frac{\rho_x}{\rho}\psi_x + \frac{\rho_y}{\rho}\psi_y \tag{2.22}$$

To avoid the nonlinearity of this basic system, the transformation of the solution to the hodograph plane can be applied replacing the physical coordinates x, y with new ones, the flow angle ϑ and Prandtl-Meyer turning angle ν with a^* being the critical velocity.

$$\nu = \int_{a^*}^{q} \sqrt{|M^2 - 1|}\frac{dq}{q} \tag{2.23}$$

These new variables lead to define a hodograph plane wherein the basic system becomes linear Beltrami system:

$$\phi_\nu = K(\nu)\,\psi_\vartheta \,(\nu \geq 0, M \geq 1) \tag{2.24}$$

$$\phi_\nu = -K(\nu)\,\psi_\vartheta \,(\nu \leq 0, M \leq 1) \tag{2.25}$$

with

$$K = K(M(\nu)) = \frac{\rho_0}{\rho}\sqrt{|M^2 - 1|} \tag{2.26}$$

ϑ and ν are also functions of a computational working plane obtained from the basic ν, ϑ hodograph by conformal (subsonic) or characteristic (supersonic) mapping. For subsonic including sonic conditions conformal mapping defines working plane ζ. E is the mapping function.

$$\zeta_0 = \nu + i\vartheta \tag{2.27}$$

$$\zeta = s + it = E(\zeta_0) \tag{2.28}$$

The basic system in ζ becomes

$$\phi_s = -K(\nu(s,t))\,\psi_t \tag{2.29}$$

$$\phi_t = K(\nu(s,t))\,\psi_s \tag{2.30}$$

$\nu(s,t)$ is then the real and $\vartheta(s,t)$ imaginary part of $E^{-1}(\zeta)$. These equations, Eq. (2.29) and Eq. (2.30) form the linear Beltrami system and elimination of ψ and ϕ leads to linear Poisson equations:

$$\phi_{ss} + \phi_{tt} = \frac{K_s}{K}\phi_s + \frac{K_t}{K}\phi_t \tag{2.31}$$

$$\psi_{tt} + \psi_{tt} = \frac{K_s}{K}\psi_s + \frac{K_t}{K}\psi_t \tag{2.32}$$

New characteristic variables occur for supersonic region with a suitable mapping function H.

$$\xi = H\left(\vartheta + \nu\right) \tag{2.33}$$

$$\mu = H\left(\vartheta - \nu\right) \tag{2.34}$$

The system is then valid in ξ, μ plane

$$\phi_\xi = K\left(\nu\left(\xi, \mu\right)\right)\psi_\xi \tag{2.35}$$

$$\phi_\mu = -K\left(\nu\left(\xi, \mu\right)\right)\psi_\mu \tag{2.36}$$

or

$$\left(\frac{d\psi}{d\phi}\right)_{\xi,\mu=const.} = \pm K^{-1}. \tag{2.37}$$

That is the basic relation to integrate the flow equations for method of characteristics for supersonic flow.

This solution allows the integration of physical coordinates x, y by

$$dz = dx + idy = e^{i\vartheta}\left(d\phi + i\frac{\rho_0}{\rho}d\psi\right)q^{-1} \tag{2.38}$$

for flows with small perturbations to a sonic parallel flow so that

$$(M - 1) \ll 1 \tag{2.39}$$

$$\vartheta \ll \pi/2 \tag{2.40}$$

and by eliminating ϕ and ψ a system for physical plane coordinates can be obtained. The transonic similarity laws containing a similarity parameter σ for reduction of variables for place and state x, y, q, ϑ are:

$$s = \pm 2 \cdot 3^{-1} \cdot \sigma^{-1}\left(\kappa - 1\right)^{1/2} a|1 - \frac{q}{a^*}|^{3/2} \tag{2.41}$$

$$t = \sigma^{-1}\vartheta \tag{2.42}$$

$$x = \phi/a^* \tag{2.43}$$

$$y = \sigma^{-1/3} \cdot 3^{1/3}\left[2^{-1}\left(\kappa - 1\right)\right]^{\frac{1}{\kappa-1}+\frac{1}{3}} \cdot \psi/a^* \tag{2.44}$$

s is positive for supersonic, negative for subsonic and equal to zero for sonic conditions. The basic system (2.24) and (2.25) then yields to corresponding Beltrami system for reduced physical plane parameters s and t.

$$X_s = \pm|s^{1/3}|Y_t \tag{2.45}$$

$$X_t = \pm|s^{1/3}|Y_s \tag{2.46}$$

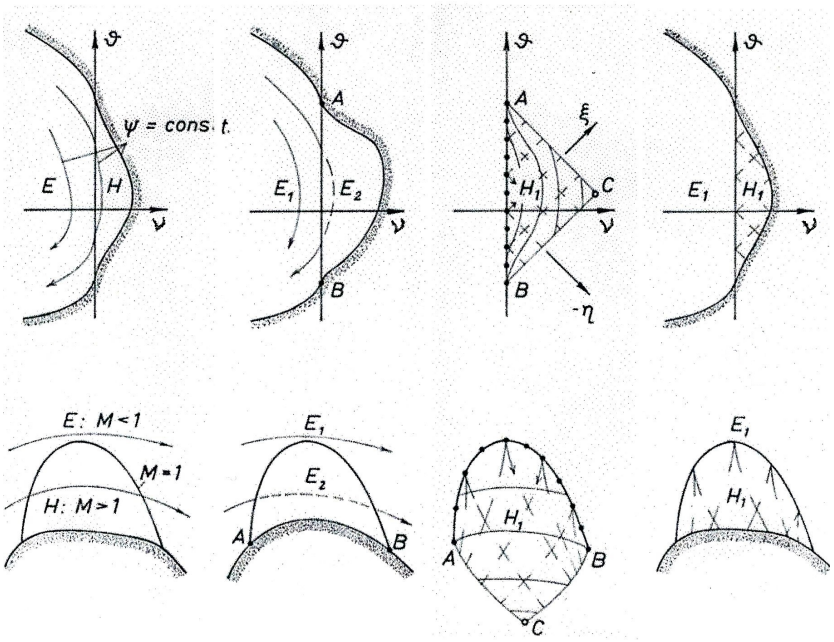

Figure 2.6: Conformal and characteristic mapping [4]

The idea of whole process is symbolized in the Figure 2.6. To describe the flow field correctly, the elliptical and hyperbolic description of the flow should be used all together (scheme on the left). As this is technically impossible, the described process can be used instead. The whole field can be solved as elliptical using techniques related to conformal mapping, so everything up to the sonic line is correct, but the supersonic region as well as surface shape is not (second scheme). Now, knowing that the sonic line can still be considered as correct, the data form it can be used to grow new supersonic region using characteristics (third scheme). Finally by integrating the characteristic field a new surface shape can be obtained and the whole flow field is correct. So practically, the shape is deformed to correspond with the pre-calculated flow.

2.4 Electric Rheograph Analogy

The specific structure of supercritical flow containing singularities and mathematically problematic patterns requires specific treatment. Sonic lines and isotachs saddle points regularly appearing in the transonic flow fields represent very weakly singular behavior and due to this, the flow surface may fold into multivalued hodograph. This effect is why the special rheograph plane needs to be used in order to obtain single-valued characteristics grid.

This can be described imagining an airfoil in transonic flow field and mapping using plane ζ_0. First, the stagnation point is logically mapped into infinity and second, the saddle point N folds the domain and forms a "second deck" of ζ_0 [4].

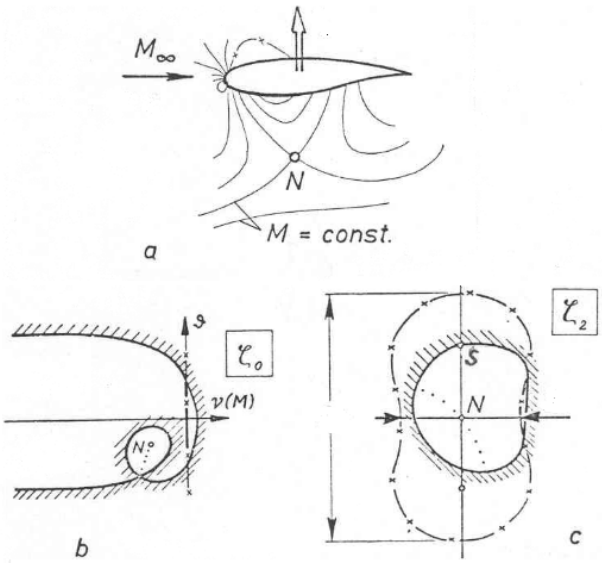

Figure 2.7: Hodograph and rheograph transformation [4]

To achieve a single sheeted problem of closed structure, the stagnation point is moved into finite domain with the mapping

$$\zeta_1 = e^{\zeta_0} \tag{2.47}$$

and then another mapping unwraps the loop and single sheeted plane is obtained

$$\zeta_2 = a\left(\zeta_1 - \zeta_{1N}\right)^{1/2} \tag{2.48}$$

with a being an arbitrary scaling factor and

$$\zeta_{1N} = e^{\nu(M_N)+i\vartheta_N} \tag{2.49}$$

The idea leads to the analogy between the plane electric conductor and the coefficient K [4]. Considering the electric potential E and conductivity Λ, the current intensity dI, which crosses a surface element dA is given by Ohm's law.

$$dI = -\Lambda \frac{dE}{dn} dE \tag{2.50}$$

For two dimensional case, the conductivity of material is constant but the overall conduction can be varied with variable thickness distribution.

$$dI = -\Lambda \cdot h\,(x, y)\, \frac{dE}{dn} dA \tag{2.51}$$

and a conservation within the conductor

$$div\,(h \cdot grad \cdot E) = 0 \tag{2.52}$$

a partial differential equation can be obtained for E

$$E_{xx} + E_{yy} = -\frac{h_x}{h} E_x - \frac{h_y}{h} E_y \tag{2.53}$$

There exists a current function W, which is associated to the electrical potential by Beltrami system

$$E_x = \frac{1}{\Lambda_h} W_y \tag{2.54}$$

$$E_y = -\frac{1}{\Lambda_h} W_x \tag{2.55}$$

The similarity between gas flow and electric current variable is obvious and is called a rheo-electric analogy

$$\begin{aligned} \phi &= E \\ \psi &= W \\ \Lambda h &= K^{-1} \end{aligned} \tag{2.56}$$

This revelation then also led to design of inclined electrolytic water tank, which allows the similar to electric continuation of the analog flow beyond the sonic line in rheograph plane [4].

2.5 Numerical Methods for Compressible Fluid Flows

From previous sections is apparent that complete solution of subsonic and supersonic flows is a challenging task for theoretical methods. Modern computational abilities on the other hand allow to solve

directly the partial differential equations numerically using computational fluid dynamics methods [14]. These methods in general transform differentials to differentiations using finite computational grids.

Simple partial differential equation for conservative variable Φ can be written as

$$\frac{\partial \Phi}{\partial t} = \frac{\partial^2 \Phi}{\partial x^2} \tag{2.57}$$

This equation can be directly rewritten for method of finite differences:

$$\frac{\Phi_i^{n+1} - \Phi_i^n}{\Delta t} = \frac{\Phi_{i-1}^n - 2\Phi_i^n + \Phi_{i+1}^n}{\Delta x^2} \tag{2.58}$$

Other and widely used approach is transformation into integral form using method of finite volumes:

$$\int_t \int_D \frac{\partial \Phi}{\partial t} dx dt = \int_t \int_D \frac{\partial^2 \Phi}{\partial x^2} dx dt \tag{2.59}$$

which applying mean value theorem and Green's theorem yields

$$\Phi_i^{n+1} = \Phi_i^n - \frac{\Delta t}{D} \oint_D \frac{\partial \Phi}{\partial x}|^n = \Phi_i^n + \frac{\Delta t}{D} \sum_{k=1}^{K} \frac{\partial \Phi}{\partial x}|_k^n \Delta x \tag{2.60}$$

There are more approaches for numerical flow solution like finite element method or Lattice-Boltzman method, but the previous two are the most common for compressible fluids problematics.

The process of discretization of partial differential equations is called the approximation. There are many approximation schemes used in CFD codes, but the most common for all relevant fluid problems is the central difference or upwind spatial discretization. Consider a differential term

$$\frac{\partial \Phi}{\partial t} + \Upsilon \frac{\partial \Phi}{\partial x} = 0 \tag{2.61}$$

central difference approximation of the term is then expressed by

$$\Upsilon \frac{\Phi_{i-1} - \Phi_{i+1}}{2\Delta x} = 0 \tag{2.62}$$

Second order upwind scheme is taking into account the direction of the flow and helps with the stability

$$\Upsilon \frac{3\Phi_i - 4\Phi_{i-1} + \Phi_{i-2}}{2\Delta x} = 0 \quad for \quad \Upsilon > 0 \tag{2.63}$$

$$\Upsilon \frac{-\Phi_{i+2} + 4\Phi_{i+1} - 3\Phi_i}{2\Delta x} = 0 \quad for \quad \Upsilon < 0 \tag{2.64}$$

The stability of approximation is given by Courant-Friedrichs-Lewy condition. The CFL number puts in relation time and spatial step.

$$CFL = \Upsilon \frac{\Delta t}{\Delta x} \leq 1 \tag{2.65}$$

Time marching methods are common even for steady state simulations, where time derivation term is added to stationary equations and solution is obtained after variables are settled in fictitious time. Other way are the iterative methods [15]. For e.g. the simple Jacobi iteration method for equation $\frac{\partial^2 \Phi}{\partial x^2} + \frac{\partial^2 \Phi}{\partial y^2} = 0$ is defined as:

$$\Phi_{i,j}^{n+1} = \frac{1}{4} \left(\Phi_{i-1,j}^{n} + \Phi_{i+1,j}^{n} + \Phi_{i,j-1}^{n} + \Phi_{i,j+1}^{n} \right) \tag{2.66}$$

or in matrix form

$$Ax = B \tag{2.67}$$

$$(D - E - F)\, x = B \tag{2.68}$$

$$Dx = (E + F)\, x + B \tag{2.69}$$

$$x^{n+1} = D^{-1} (E + F)\, x + D^{-1} B \tag{2.70}$$

where

$$A = \begin{bmatrix} D & -F \\ -E & D \end{bmatrix} \tag{2.71}$$

3 State of the Art Summary and New Objectives

The previous chapter summarize available techniques and already implies their benefits. Simplified exact relations of the basic gas dynamics provide direct possibilities for phenomena verification and direct analysis, but the range of usage is limited. Transformation techniques allow linearizion of flow describing equations enabling analytical solution of the complete flow fields, but the complexity of such approach requires deep understandings. CFD codes and numerical methods can solve and simulate almost any possible case or situation, however, such powerful tool still demands experienced user for case definition and results analysis in order to preform at maximum potential.

This work concentrates mainly on the the rheograph transformation method, which originated from the need for solution of the flow regimes reaching and exceeding the speed of sound long ago computational era, mainly for, at that time widely developed, aerospace applications. The classical gas dynamics and even the known hodograph method could not provide enough for the complex flow fields so far and the extra transformation into single valued plane was developed [1], [16]. The rheograph transformation method has been proven as an relevant and effective tool for design, mainly for the external aerodynamics and thus the aerospace field [3], [8]. Internal and other flows were not much a subject, but some variations for nozzle like [5] or multidimensional cases were suggested. As numerical methods started to rise, these analytical concepts were later also a subject to comparison with the CFD simulations [17] with already positive results. With new possibilities that arrived with computational technology, a new graphics could be added and modified models for other relevant cases were developed [6], but still suffered from the need for wide theoretical and mathematical background. With that said, an interesting question arises and that is, if this issue could be reduced with a help from the computational techniques and make the transformation applicable and usable tool for design and analysis.

The numerical methods are continually marching forward and are no longer a privilege for only a few. The commercial software [18] cover still more and more and provide high level of robustness. For special cases, the known methods and schemes [19], [15] allow the creation of specific purpose in house codes. Besides aeronautics, one of the fields that rose with the expansion of computational methods is turbomachinery with cascades and turbine or compressor blades [7]. Thus, the focus on the internal flows, never much studied by the hodograph based transformation methods, could be a relevant contribution.

One of the biggest advantages of the rheograph transformation is the ability of handling the singular points often present in transonic flow field. The knowledge of both, the rheograph transformation technique [5] and computational methods can lead to the effective combination of them in creation of an academic example of supercritical nozzle design with singular sonic throat point. One of the practical turbomachinery applications to work on is the SE 1050 blade cascade [7], which was already a subject of various experimental [9] and numerical [10] tests. They showed a very specific behavior of this cascade at transonic regime and creation of a re-compression region [11]. Although many times studied, could be good example that provides a space for new point of view.

3.1 Thesis Goals

In general, the main point to prove is that the hodograph based methods with a fresh touch of computational techniques can provide a working, powerful and even today relevant analysis and design tool for both academic and practical cases. The thesis goals to verify this hypothesis are therefore formulated as:

- To validate described solutions to the compressible and transonic flows and their functionality and accuracy on a case of sonic cusped airfoils.
- To reduce the need for manual analytical solution and complex mathematics and extend the rheograph transformation method using computational techniques for solution of linearized flow equations and method of characteristics.
- To describe the application for internal aerodynamics and apply the solution on a novel academic example of a supercritical nozzle.
- To test the abilities of such approach on a practical case of the blade cascade SE 1050. To analyze the specific flow field pattern using the rheograph transformation and propose possible design solutions.
- To discuss the functionality of developed method for wide usage in relevant academic and practical applications.

4 Numerical Schemes Verification

Besides the emphasis of analytical basis, the numerical computations and simulations play and will play the leading role of modern engineering tool, including this thesis. Therefore, this section is dedicated to the introduction of compressible fluid flow suitable schemes and verification of their functionality in CFD codes.

An example of oblique shock is used here to compare different schemes, from simple Lax-Friedrichs and MacCormac to advanced AUSM scheme [JS1]. This simple example can show how different schemes deal with one of the characteristics of the compressible flow, the shock waves and their interactions with solid boundaries. Due to an exact analytical solution, this example is perfect for testing the accuracy of the methods as well.

4.1 Oblique Shock Case and Numerical Schemes

Shock waves, representing an abrupt sudden change in the medium parameters, are great example of hyperbolic equation systems. Consider a supersonic flow of $M_1 = 3$ approaching oblique shock with the wave angle $\beta_1 = 33°$. This situation is schematically depicted in the Figure 4.1. Knowing these two numbers, there is no problem to exactly compute the properties of the generated flow field using e.g. The Compressible Aerodynamics Calculator [20]. The task here is to perform the numerical solution using different methods and schemes for compressible inviscid flow and compare obtained results with the analytical ones.

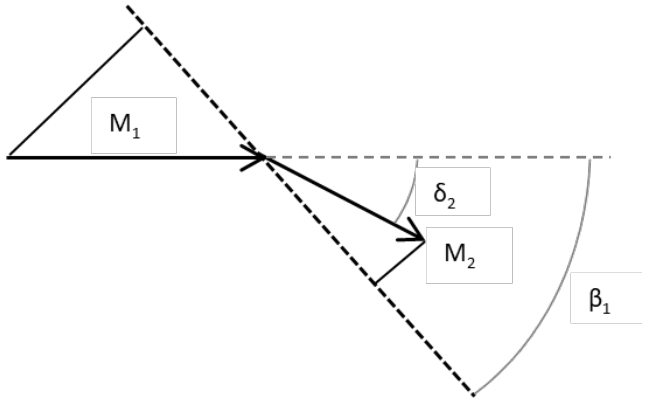

Figure 4.1: Oblique shock scheme

Mach numbers M_1 and M_2 represent Mach number in front of and behind the shock. Vectors in the Figure 4.1 already show that the velocity drops through the shock, pressure analogically rises.

Angle β is the angle of the oblique shock and angle δ is the change of flow direction, or the deflection angle.

Euler equations for two dimensional inviscid compressible flow can be written in basic vector form:

$$W_t + F(W)_x + G(W)_y = 0 \tag{4.1}$$

or in form with conservative variables

$$\begin{pmatrix} \rho \\ \rho u \\ \rho v \\ e \end{pmatrix}_t + \begin{pmatrix} \rho u \\ \rho u^2 + p \\ \rho uv \\ (e+p)\,u \end{pmatrix}_x + \begin{pmatrix} \rho u \\ \rho uv \\ \rho v^2 + p \\ (e+p)\,v \end{pmatrix}_y = 0 \tag{4.2}$$

where e is the ideal gas total energy

$$e = \rho \left[\frac{1}{2}\left(u^2 + v^2\right) + c_v T \right] \tag{4.3}$$

This system is then closed with equation of state in form

$$p = (\kappa - 1)\left[e - \frac{1}{2}\rho\left(u^2 + v^2\right) \right] \tag{4.4}$$

For this case, a rectangular domain was created with dimensions 1.5x1. While the left and top side of the rectangle form the inlet into the domain, right side is the outlet and the bottom side is the solid wall. Different boundary conditions setup is symbolized in the Figure 4.2. The domain was meshed with the cartesian grid with 80 nodes in both directions.

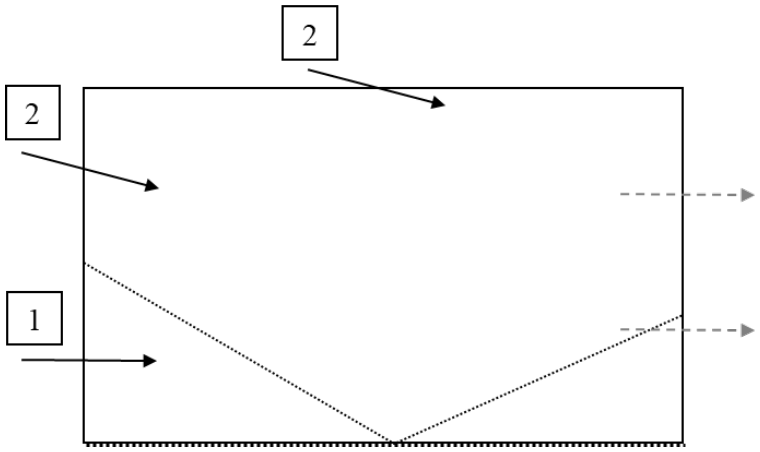

Figure 4.2: Computational domain

The idea is to arrive into the domain with already formed right running oblique shock and for this purpose, the inlet was separated in two parts and each of them corresponds to conservative variable values for appropriate region – in front of and behind the wave. The wave then reflects from the wall and exits the domain. Parameters on boundary conditions correspond with exact analytically calculated values. Considering both inlet and outlet being supersonic, values for individual boundaries are defined as:

Table 4.1: Boundary conditions for conservative variables

	p	**u**	**v**	**T**
inlet 1	100 000	1 040	0	300
inlet 2	294 000	880	-246	423
outlet	ext.	ext.	ext.	ext.
wall	$p_y = 0$	$u_y = 0$	0	$T_y = 0$

Extrapolation at the outlet boundary is solved by a scheme

$$\Phi_i = 2\Phi_{i-1} - \Phi_{i-2} \tag{4.5}$$

As a first type of scheme for this case, the first order Lax-Friedrichs scheme which can be written for two dimensional domain as [21] was used

$$\begin{aligned} w_{i,j}^{n+1} = w_{i,j}^n &- \frac{\Delta t}{2\Delta x}\left(f_{i+1,j}^n - f_{i-1,j}^n\right) - \frac{\Delta t}{2\Delta y}\left(g_{i,j+1}^n - g_{i,j-1}^n\right) \\ &+ \frac{\epsilon}{4}\left(w_{i+1,j}^n - 2w_{i,j}^n + w_{i-1,j}^n\right) + \frac{\epsilon}{4}\left(w_{i,j+1}^n - 2w_{i,j}^n + w_{i,j-1}^n\right) \end{aligned} \tag{4.6}$$

where the last two terms represent the artificial viscosity and parametr $\epsilon \in (0, 1)$.

Next scheme was the second order two step MacCormac Lax-Wendroff scheme with Jameson artificial viscosity [21][22]:

$$w_{i,j}^{n+\frac{1}{2}} = w_{i,j}^n - \frac{\Delta t}{2\Delta x}\left(f_{i+1,j}^n - f_{i-1,j}^n\right) - \frac{\Delta t}{2\Delta y}\left(g_{i,j+1}^n - g_{i,j-1}^n\right) \tag{4.7}$$

$$\widehat{w_{i,j}^{n+1}} = \frac{1}{2}\left(w_{i,j}^n - w_{i,j}^{n+\frac{1}{2}}\right) - \frac{\Delta t}{2\Delta x}\left(f_{i,j}^{n+\frac{1}{2}} - f_{i-1,j}^{n+\frac{1}{2}}\right) - \frac{\Delta t}{2\Delta y}\left(g_{i,j}^{n+\frac{1}{2}} - g_{i,j-1}^{n+\frac{1}{2}}\right) \tag{4.8}$$

and the Jameson artificial viscosity is given by:

$$\begin{aligned} w_{i,j}^{n+1} = \widehat{w_{i,j}^{n+1}} &+ k_1\left(w_{i+1,j}^n - 2w_{i,j}^n + w_{i-1,j}^n\right)\frac{|p_{i-1,j}^n - 2p_{i,j}^n + p_{i+1,j}^n|}{|p_{i-1,j}^n + 2p_{i,j}^n + p_{i+1,j}^n|} \\ &+ k_2\left(w_{i,j+1}^n - 2w_{i,j}^n + w_{i,j-1}^n\right)\frac{|p_{i,j-1}^n - 2p_{i,j}^n + p_{i,j+1}^n|}{|p_{i,j-1}^n + 2p_{i,j}^n + p_{i,j+1}^n|} \end{aligned} \tag{4.9}$$

From this term, it is obvious that the artificial viscosity plays role in locations where the pressure difference is high and on the other hand have no influence where the pressure distribution is continuous.

The two previous schemes are good for their simplicity and for demonstration of the basic functions of numerical codes. But for the practical cases of today, they do not provide enough accuracy and stability. That is why the widely practically used AUSM scheme was chosen as next. AUSM is advanced high order scheme used in ANSYS Fluent CFD code as well as many others suitable for compressible flows and will be used in the later flow simulation cases below. Advection Upstream Splitting Method belongs to the so called flux-splitting methods, or methods based on decomposition of the convective fluxes vector, specifically for AUSM, to the convective and pressure part. Such scheme is close to the upwind methods and approximates according to the flow direction.

All according to [19], convective fluxes for i and j directions are formed

$$f_{i+\frac{1}{2}} = Mu_{i+\frac{1}{2}} \begin{pmatrix} \rho a \\ \rho a u \\ \rho a v \\ (e+p)\, a \end{pmatrix}_{Lft/Rght} + \begin{pmatrix} 0 \\ p \\ 0 \\ 0 \end{pmatrix}_{i+\frac{1}{2}} \tag{4.10}$$

$$g_{j+\frac{1}{2}} = Mv_{j+\frac{1}{2}} \begin{pmatrix} \rho a \\ \rho a u \\ \rho a v \\ (e+p)\, a \end{pmatrix}_{Up/Dw} + \begin{pmatrix} 0 \\ 0 \\ p \\ 0 \end{pmatrix}_{j+\frac{1}{2}} \tag{4.11}$$

L is used for $Mu_{i+\frac{1}{2}} \geq 1$, R otherwise (U/D analogically).

Pressure is obtained from

$$p_{i+\frac{1}{2}} = p^{+}_{Lft} + p^{-}_{Rght} \tag{4.12}$$

with the split pressures given by

$$p^{+}_{Lft} = \begin{pmatrix} p_{Lft} & for & M_{Lft} \geq 1 \\ \frac{p_{Lft}}{4}\left(M_{Lft}+1\right)^2\left(2-M_{Lft}\right) & for & |M_{Lft}| < 1 \\ 0 & for & M_{Lft} \leq -1 \end{pmatrix} \tag{4.13}$$

$$p^{-}_{Rght} = \begin{pmatrix} p_{Rght} & for & M_{Rght} \geq 1 \\ \frac{p_{Rght}}{4}\left(M_{Rght}+1\right)^2\left(2-M_{Rght}\right) & for & |M_{Rght}| < 1 \\ 0 & for & M_{Rght} \leq -1 \end{pmatrix} \tag{4.14}$$

Similarly then for $i\,(j) - \frac{1}{2}$

Values in $i\,(j) \pm \frac{1}{2}$, L/R value can be interpolated using MUSCLE interpolation method [19]:

$$f_{i+\frac{1}{2}}^{Lft} = f_i + \frac{1}{2}\Psi\,(r_i)\,(f_{i+1} - f_i) \tag{4.15}$$

$$f_{i-\frac{1}{2}}^{Lft} = f_{i-1} + \frac{1}{2}\Psi\,(r_{i-1})\,(f_i - f_{i-1}) \tag{4.16}$$

$$f_{i+\frac{1}{2}}^{Rght} = f_{i+1} - \frac{1}{2}\Psi\,(r_{i+1})\,(f_{i+2} - f_{i+1}) \tag{4.17}$$

$$f_{i-\frac{1}{2}}^{Rght} = f_i - \frac{1}{2}\Psi\,(r_i)\,(f_{i+1} - f_i) \tag{4.18}$$

and for node value using central approximation:

$$f_{x_i} = \frac{1}{\Delta x_i}\left(f_{i+\frac{1}{2}}^n - f_{i-\frac{1}{2}}^n\right) \tag{4.19}$$

$\Psi\,(r)$ is a limiter necessary for problems with shock waves. For e.g. Minmod limiter [19] looks like

$$\Psi_{min}\,(r_i) = max\,[0, min\,(1, r)] \tag{4.20}$$

$$\lim_{r\to\infty} \Psi_{min}\,(r_i) = 1 \tag{4.21}$$

where r_i is the gradient ratio

$$r_i = \frac{f_i - f_{i-1}}{f_{i+1} - f_i} \tag{4.22}$$

Time discretization is solved using 2nd order Runge-Kutta TVD [23]. TVD or Total Variation Diminishing is based on total variation conservation and total minimum and maximum conservation. This should restrict solution oscillation on discontinuities.

$$w^{n+\frac{1}{2}} = w^n + \Delta t L\,(w^n) \tag{4.23}$$

$$w^{n+1} = \frac{1}{2}w^n + \frac{1}{2}w^{n+\frac{1}{2}} + \Delta t L\left(w^{n+\frac{1}{2}}\right) \tag{4.24}$$

where $L\,(w^n)$ is convective flux $f_x + g_y$

Final form of the AUSM scheme for usage in finite difference method can be written as:

$$w_{i,j}^{n+\frac{1}{2}} = w_{i,j}^n - \Delta t\left[\frac{1}{\Delta x}\left[\left(\frac{u}{a}\right)_{i+\frac{1}{2},j}^n f_{i+\frac{1}{2}}^n + px_{i+\frac{1}{2}}^n - \left[\left(\frac{u}{a}\right)_{i+\frac{1}{2},j}^n f_{i+\frac{1}{2}}^n + px_{i+\frac{1}{2}}^n\right]\right] + \frac{1}{\Delta y}...\right] \tag{4.25}$$

4.2 Results and Conclusion

All three simulations led successfully to a converged solution and the contours of pressure for all tested codes are shown in the Figures 4.3 - 4.5. The wave angles and pressure values in formed regions correspond to the analytically calculated values, as the angle of reflected wave should be close to $44°$ and the pressure behind the reflected wave close to 700 000 Pa for such setup. Main differences between used codes and schemes appear concentrating on the discontinuous drops along the waves.

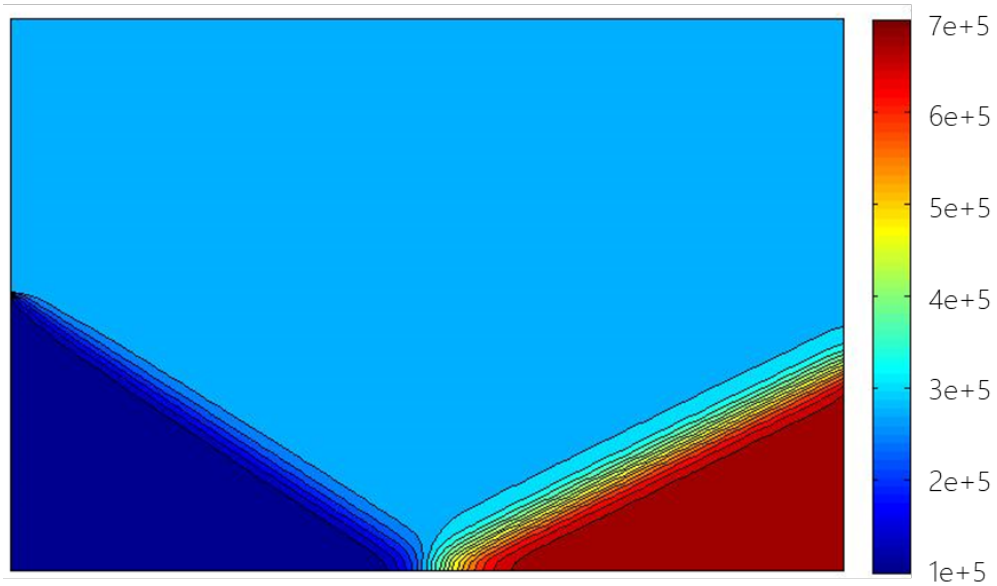

Figure 4.3: Contours of pressure [Pa] - LF

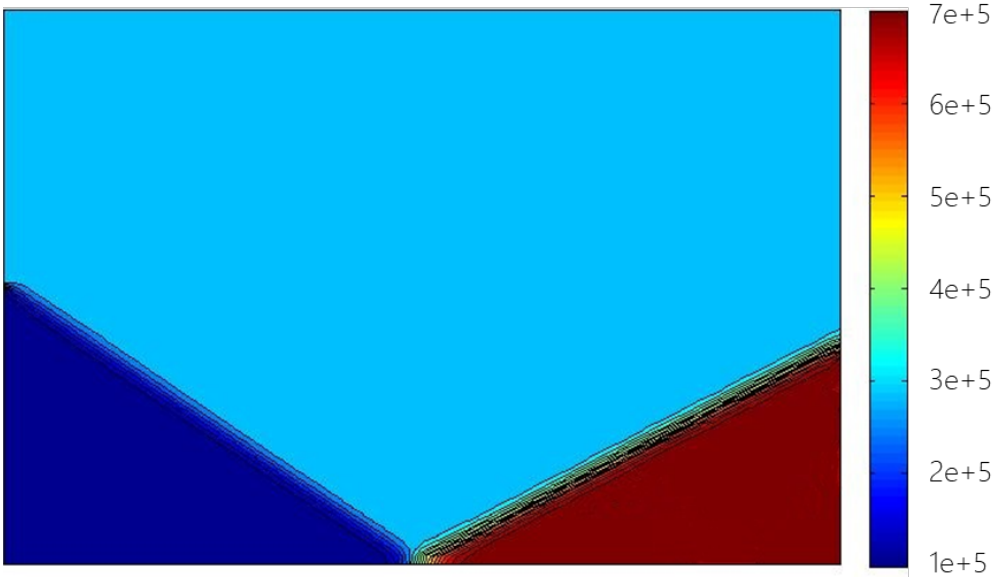

Figure 4.4: Contours of pressure [Pa] - MC

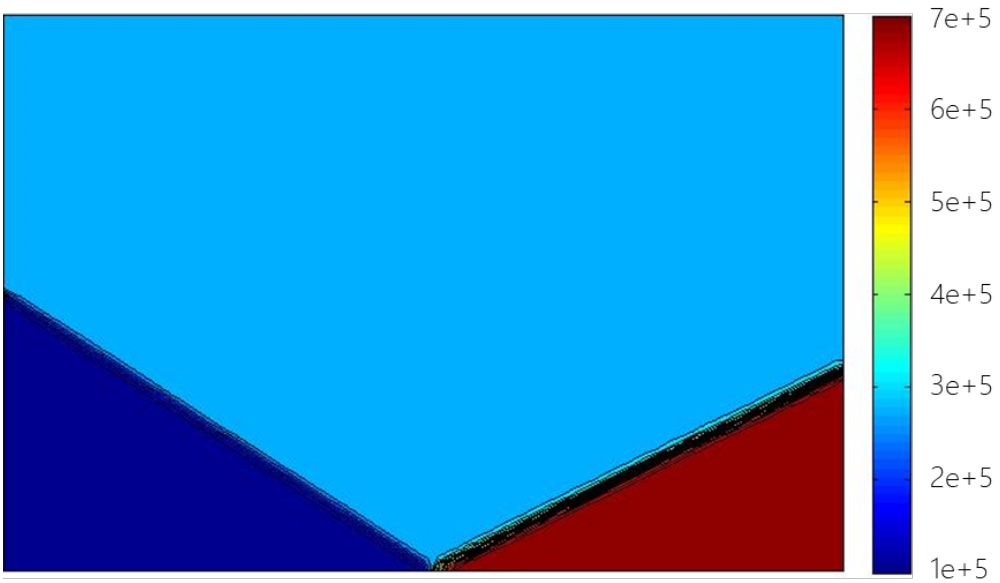

Figure 4.5: Contours of pressure [Pa] - AUSM

The pressure distribution on the wall for each code is shown in the Figure 4.6. The solid line represents the analytical solution.

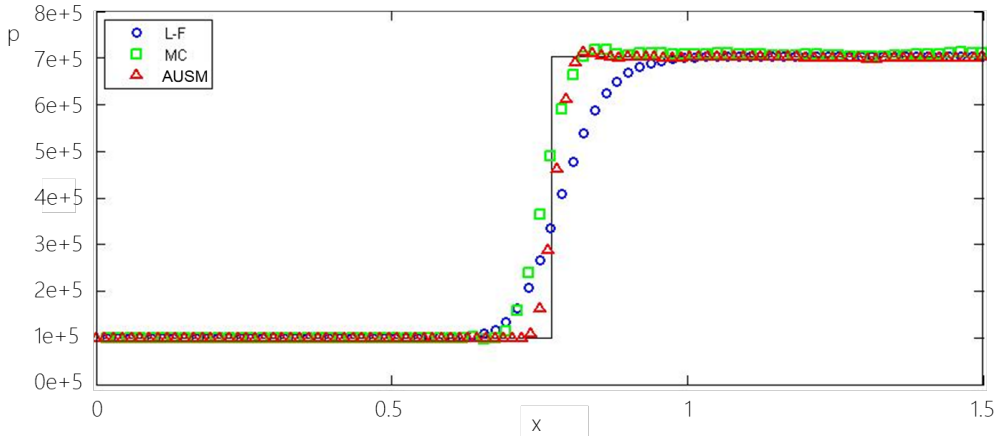

Figure 4.6: Wall pressure distribution [Pa]

The previous results lead to a conclusion that the Lax-Friedrich scheme shows its natural characteristic of a strong dissipation, even with very low artificial viscosity coefficients. On the other hand the MacCormac Lax-Wndroff scheme acts much more accurately in this way but thanks to strong oscillations near the shocks the influence of the artificial viscosity term had to be raised what causes that the pressure change along the wave is still not as steep as the AUSM scheme results show. That proves the AUSM as a reasonable choice for upcoming CFD simulations.

5 Guderley's Cusp as a Validation Case

This section is dedicated to remembering of some analytically defined methods and airfoil geometries as a test cases and to comparison of analytical flow description with numerical results [JS2], making use of a commercially available computational fluid dynamics code and with classical gas dynamics analysis.

The main point of the use of Guderley's case is to arrive at a high degree of understanding typical transonic challenges and remind on this example that accelerated optimization strategies may be carried out with a reduced set of input parameters, before costly experiments may focus directly on optimum design cases.

5.1 Exact Solution

Finding analytical solutions to above hodograph relations described in Chapter 2.4 allows to derive the formulae defining the shape, flow conditions and pressure coefficient for cusped airfoils in a uniform sonic flow $M_\infty = 1$ [3], [17]. The solution of such airfoil is described in the Figure 5.1 and the schematic view on a cusp with all defined parameters is in the Figure 5.2.

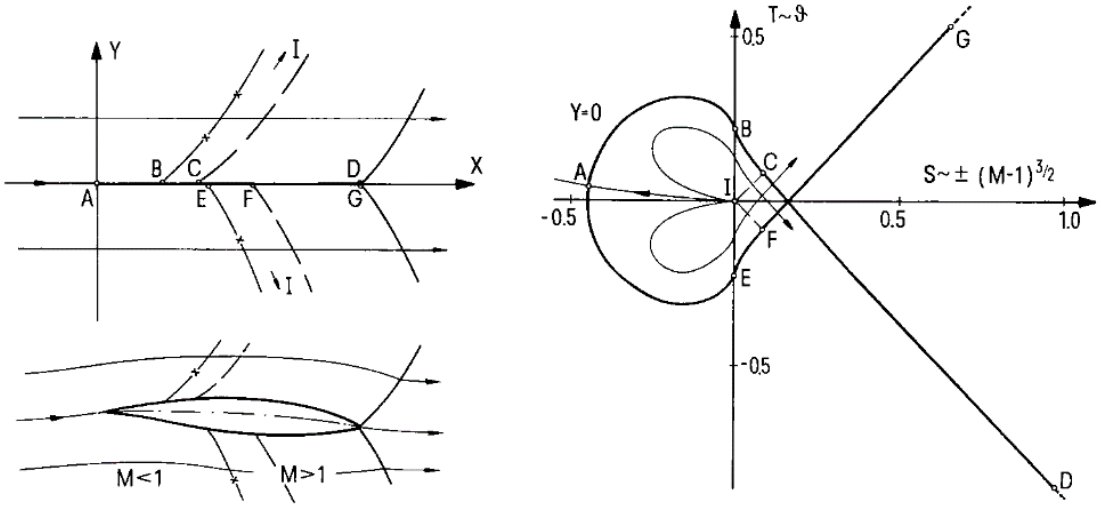

Figure 5.1: Cusp solution in the real and the rheograph plane [3]

The solution in real plane is on the left in the Figure 5.1, the modified hodograph plane on the right with axes t corresponding to flow angle and s being a function of the Mach number or eventually the Prandtl-Meyer angle. As can be seen, the sharp leading edge (point A) cuts through the sonic flow at a certain angle. Due to smooth acceleration of the transonic flow from subsonic to supersonic

past the airfoil, crossed sonic lines appear (B,E). Up to these points, the quasi-conformal mapping is used and from here, it is necessary to switch to the characteristic mapping. The characteristics (C,F) and the flow are still accelerating smoothly up to the trailing edge where the oblique shocks are formed (D,G).

Such solution results in the cusp shape described with two parameters - thickness and camber parameter. Thickness to chord ratio is τ and camber to chord ratio ω. The solution is exact for $\tau \to 0$ and practically valid for slender airfoils with $\tau \leq 0.5$. The case with camber to chord ratio $\omega = 0$ is the symmetrical one also known as "Guderley's cusp". Limit of validity for cambered airfoils is given by ratio $\omega/\tau \leq 0.5$.

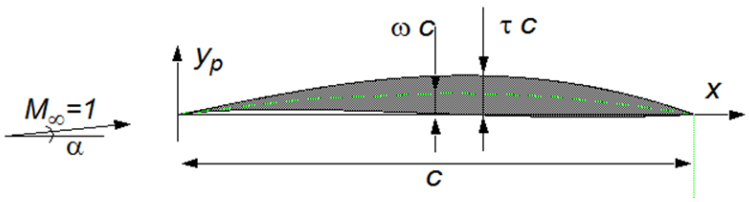

Figure 5.2: The cusp solution and parameters [17]

The camber/thickness parameter, which is afterwards used for generation of geometry and the flow description, is given by [3]:

$$P\left(\frac{\omega}{\tau}\right) = 2^{13/2} \cdot 3^{3/2} \cdot 5^{-7/2} \cdot \frac{\omega}{\tau}\left[1 + 2^{12} \cdot 3 \cdot 5^{-6}\left(\frac{\omega}{\tau}\right)^2\right]^{-1/2} \tag{5.1}$$

When the cusp is cambered, it is pointing into the flow and it is smoothly passed by the stream so the flow is not forced to change direction around sharp leading edge. The angle of attack is then:

$$\alpha = \tau \cdot 2^{-9/2} \cdot 3^{-1/2} \cdot 5^{5/2} \cdot P\frac{1 - 2^{-1} \cdot 3^{-4} \cdot 5 \cdot 13P^2}{\left(1 - 2^{-1} \cdot 3^{-2} \cdot 5P^2\right)^{3/2}} \tag{5.2}$$

The geometry vertex data for family of cambered airfoils is given by:

$$y_P(x) = \tau \cdot x(1-x)\left(2^2 \cdot \frac{\omega}{\tau} \pm 2^{-2} \cdot 3^{-3/2} \cdot 5^{5/2} \cdot x^{1/2}\right) \tag{5.3}$$

and finally the pressure coefficient:

$$c_p = \frac{\left(5^2 \cdot \tau\right)^{2/3}}{\left[2^2 \cdot 3 \cdot (\kappa + 1)\right]^{1/3}}\left[\frac{1 - 2^{-2} \cdot 3^{-2} \cdot 5P^2}{1 - 2^{-1} \cdot 3^{-2} \cdot 5P^2} - 2^1 \cdot 5x \mp \frac{2^{-1/2} \cdot 3^{-1} \cdot 5Px^{1/2}}{\left(1 - 2^{-1} \cdot 3^{-2} \cdot 5P^2\right)}\right] \tag{5.4}$$

Knowing these, a complete analytical solution of this problem of sharp cusped airfoil in a sonic free stream is known.

5.2 Numerical Solution

For the numerical simulations, the upcoming three variants of cusped airfoils were investigated. The symmetrical cusp, the limit variant with thickness to chord ratio $\tau = 0.1$ and parameter $\omega/\tau = 0.5$ together with the case with parameters somewhere in the middle of the exact solution bounds, $\tau = 0.05$ and $\omega/\tau = 0.02$. The computational domain is 20x as big as the chord length in all directions. The mesh for all cases was mapped with quad cells with total count of approximately 100000 cells, except for the symmetrical case, where only the half of the plane needed to be used. The detail of the mesh for one of the cases is shown in the Figure 5.3.

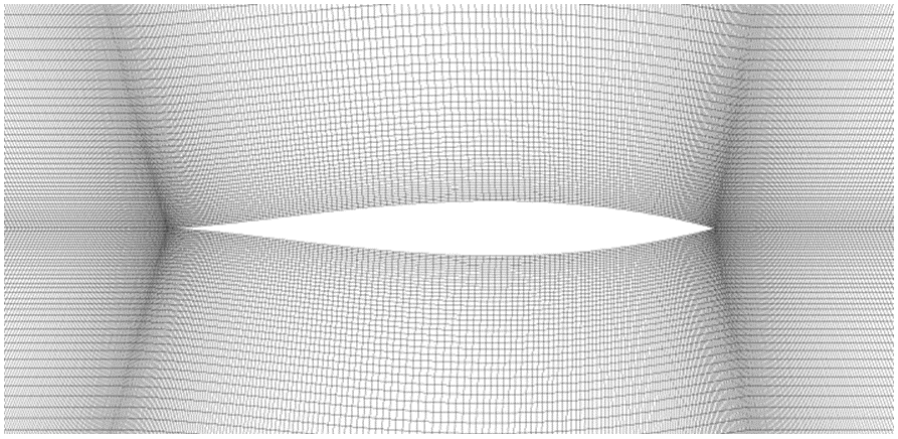

Figure 5.3: Symmetrical cusp computational mesh

For flow simulations, the inviscid – Euler model with ideal gas implemented in a commercial CFD software ANSYS Fluent [18] was used. The numerical flux scheme was the AUSM scheme with second order upwind. The only outer boundary condition was set as the non-reflective pressure far field boundary condition and its value is computed using the gas dynamics equation [18]:

$$\frac{p_0}{p} = \left(1 + \frac{\kappa - 1}{2} M^2\right)^{\frac{\kappa}{\kappa - 1}} \tag{5.5}$$

where p_0 is the total or atmospheric pressure and Mach number exactly one for this case. Pressure p then gives the boundary value for the far field.

All three tested cases successfully led to a converged solution using implicit solver after 10 - 15 thousand iterations. Contours of Mach number to visualize the simulated flow field are shown in Figures 5.4 - 5.6. The most important thing that can be noticed from these figures is the fact that no shock appears anywhere near the leading edge or along the airfoils. The velocities around the leading edge are subsonic and along the airfoil the velocity continually rise to supersonic values what forms

the oblique shocks propagating from the trailing edge. The flow is smooth for all cases along whole length as the theory suggests.

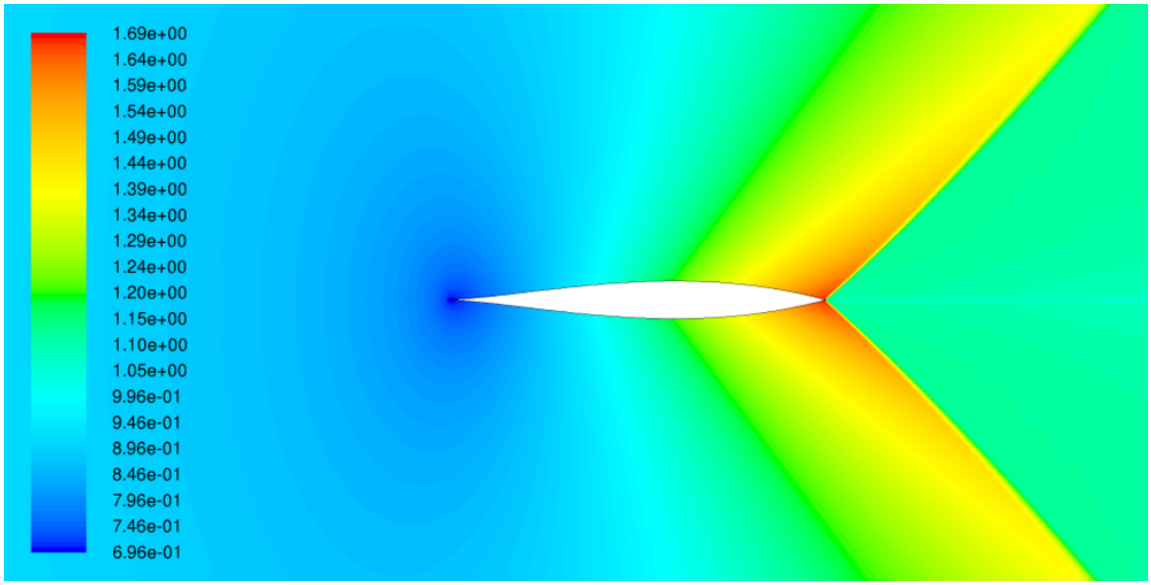

Figure 5.4: Contours of Mach number for symmetrical airfoil: $\tau = 0.1$ and parameter $\omega/\tau = 0$

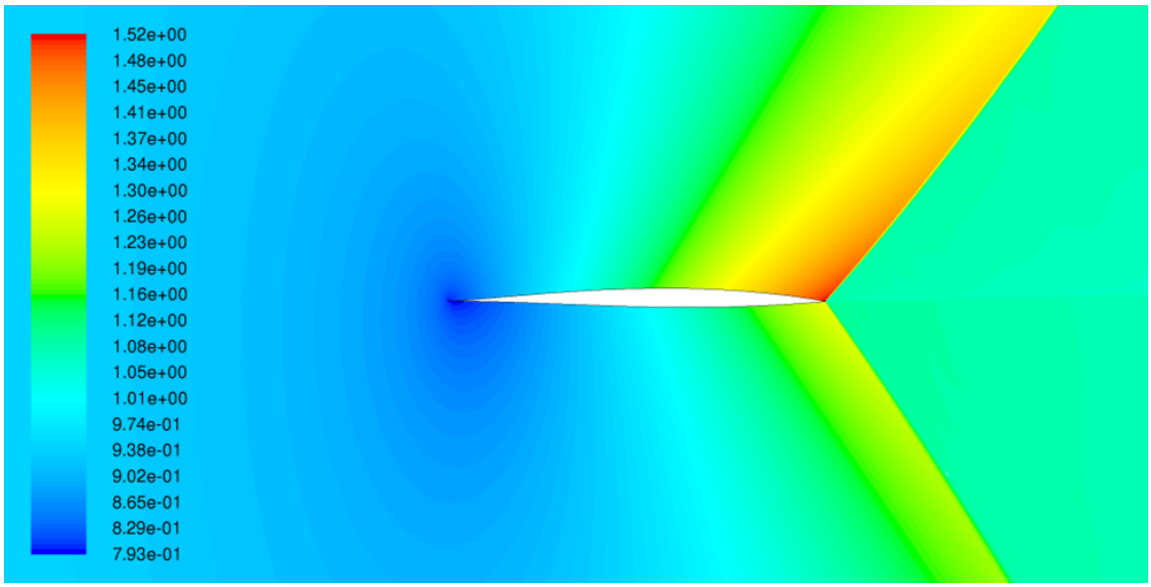

Figure 5.5: Contours of Mach number: $\tau = 0.05$ and parameter $\omega/\tau = 0.02$

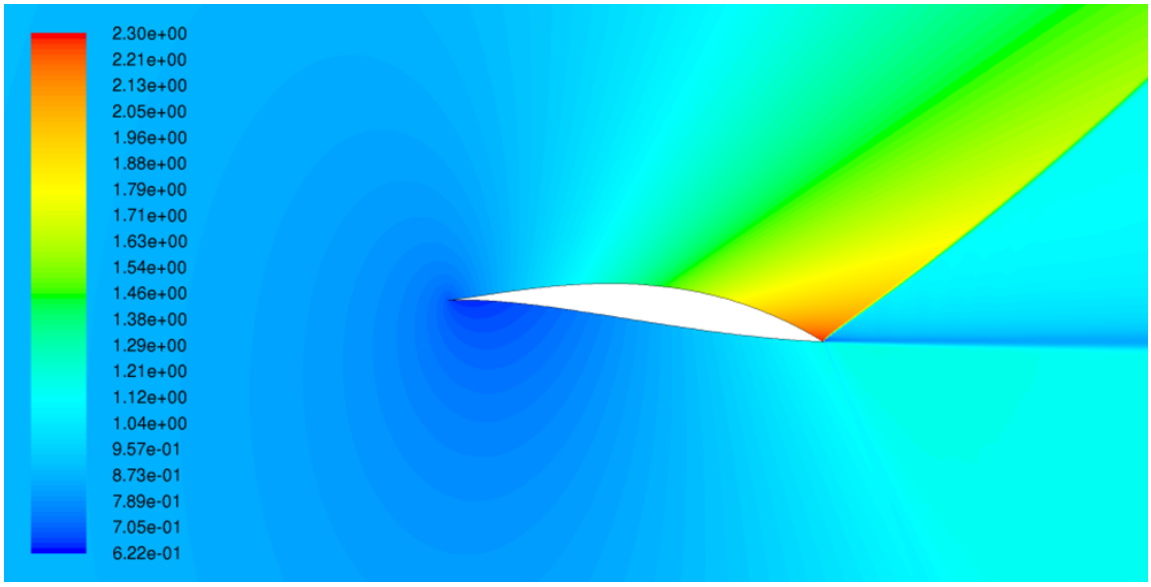

Figure 5.6: Contours of Mach number: $\tau = 0.1$ and parameter $\omega/\tau = 0.5$

The differences between the cases are obvious and depend on the input thickness and camber to chord ratio parameters. The flow for the symmetrical case is, as expected, symmetrical with two oblique shocks starting at the trailing edge, but for the thickest and most cambered limit airfoil the shock is formed only on the upper side of the airfoil while the flow is not accelerated enough along lower side and it remains shock free till the end as the velocity near the end of the airfoil is similar to the velocity behind. This critical setup leads to a so called slip line generation behind the profile. For different illustration, the contours of entropy produced by oblique shock and this tangential discontinuity which occurred in the limiting case are shown in the Figure 5.7. The thin and less cambered case is somewhere between two previous variants as it forms two shocks but with different strength. With the rising thickness and camber a higher Mach numbers are also reached.

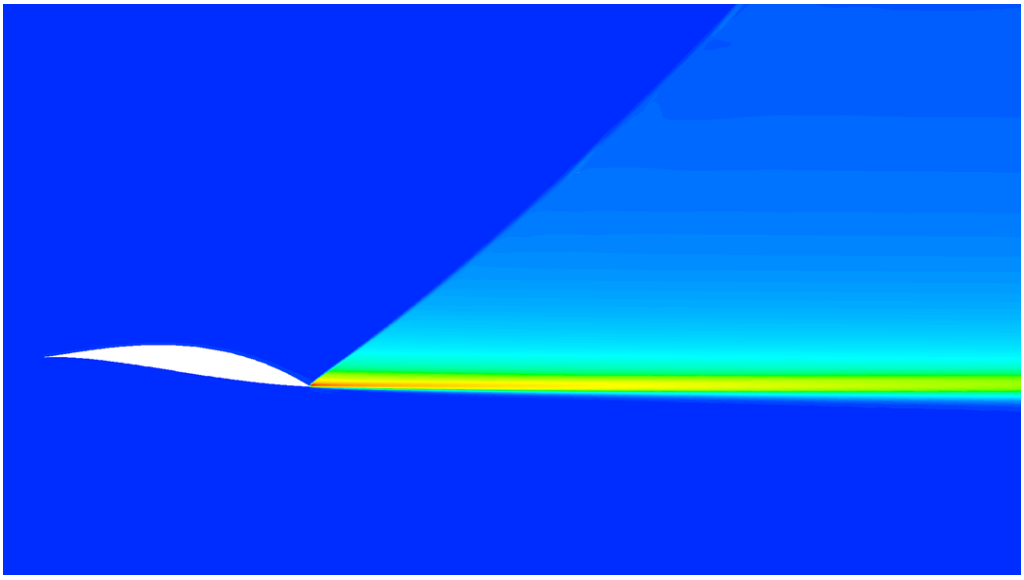

Figure 5.7: Contours of entropy $\tau = 0.1$ and parameter $\omega/\tau = 0.5$

The way how to compare the results with the theoretical ones is via the pressure coefficient c_p distribution along the cusp as described above. Theoretically correct pressure coefficient distribution on the airfoil surface is given by Eq. (5.4) and Figures 5.8 - 5.10 show the comparison with the numerical data. Dashed lines represent the theory and solid lines are results from the numerical simulation.

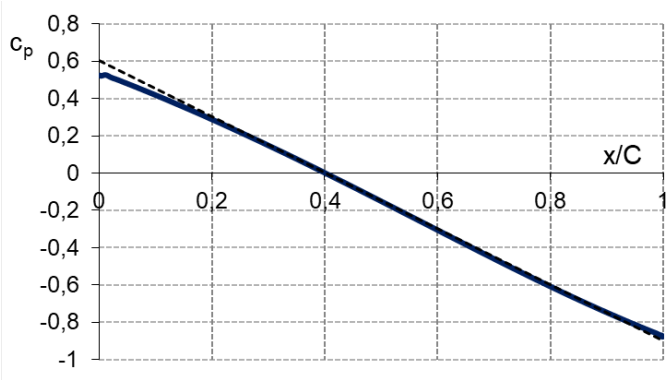

Figure 5.8: Pressure coefficient distribution for symmetrical airfoil: $\tau = 0.1$ and parameter $\omega/\tau = 0$

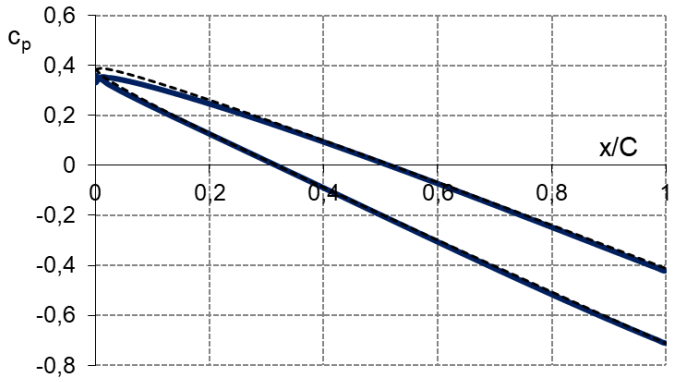

Figure 5.9: Pressure coefficient distribution: $\tau = 0.05$ and parameter $\omega/\tau = 0.02$

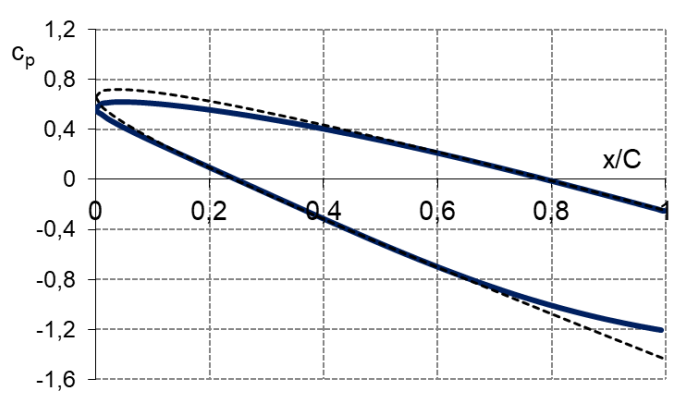

Figure 5.10: Pressure coefficient distribution: $\tau = 0.1$ and parameter $\omega/\tau = 0.5$

From correct flow behavior already obvious from contour figures, it is expectable that the pressure coefficient distribution along the airfoil surface will also correspond at least tendentiously with the theoretical lines and data in the Figures 5.8 - 5.10 confirm that. In areas where the pressure coefficient values lay between 0.3 and -0.8 are numerical results almost identical with dashed theoretical. As the values rise from these bounds, noticeable deviations appear. Even when there is no flow separation on the leading edge and shocks appear only at the trailing edges, so the character of the flow corresponds with the theoretical assumptions, some differences appear right in these areas. This may be given by the fact that the flow velocities start to differ from a near sonic flow here as Mach numbers reached in these areas vary from 0.6 to 2.3 depending on thickness and camber parameter. The Mach numbers where the results correspond are approximately from 0.8 to 1.6. So the highly supersonic or subsonic areas can cause some deviation, but rest of the flow field is described very well.

5.3 Clasical Gas Dynamics Analysis

The situation of the two nonsymmetrical cases in terms of shock waves formation will be now analyzed using classical gas dynamics relation. For the evaluation of oblique shock parameters, upcoming physical model [JS3] of supersonic flows interaction on a sharp trailing edge is formulated, as depicted in the Figure 5.11. The shock wave a is shock wave of the first family (left-running shock wave) and the shock wave b is shock wave of the second family (right running shock wave).

The total pressures are equal

$$p_{01} = p_{02} \tag{5.6}$$

The basic conditions on the discontinuity downstream of the sharp trailing edge hold equality of static pressures

$$p_3 = p_4 \tag{5.7}$$

and equality of azimuthal flow angles

$$\vartheta_3 = \vartheta_4 \tag{5.8}$$

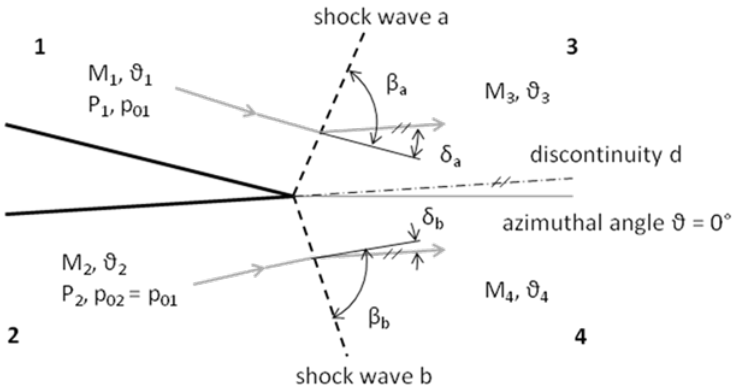

Figure 5.11: Trailing edge oblique shocks configuration

For solution of flow conditions, the shock polar diagrams are used. These diagrams give a family of possible solutions in terms of pressure ratio to turning angle dependencies for given values of Mach numbers M and angle of shock waves to incoming flow β as a parameter. The pressure ratio on the shock wave a is given by formula [12]

$$\frac{p_3}{p_1} = \frac{\kappa - 1}{\kappa + 1}\left(\frac{2\kappa}{\kappa - 1} M_1^2 sin^2\beta_a - 1\right) \tag{5.9}$$

where κ is ratio of specific heat capacities, M_1 is Mach number in the region 1 in the Figure 5.11, β_a is angle of shock wave a to incoming flow. Analogously, the pressure ratio on the shock wave b is

given by

$$\frac{p_4}{p_2} = \frac{\kappa - 1}{\kappa + 1}\left(\frac{2\kappa}{\kappa - 1}M_2^2 sin^2\beta_b - 1\right) \tag{5.10}$$

Ratios of total to static pressures in regions 1 and 2 are given by isentropic formula

$$\frac{p_{01}}{p_1} = \left(1 + \frac{\kappa - 1}{2}M_1^2\right)^{\frac{\kappa}{\kappa-1}} \tag{5.11}$$

and

$$\frac{p_{02}}{p_2} = \left(1 + \frac{\kappa - 1}{2}M_2^2\right)^{\frac{\kappa}{\kappa-1}} \tag{5.12}$$

Turning angles of flow on the shock waves a and b are given by [13]

$$tg\delta_a = \frac{2}{tg\beta_a}\left[\frac{M_1^2 sin^2\beta_a - 1}{M_1^2\left(\kappa + cos2\beta_a\right) + 2}\right] \tag{5.13}$$

and

$$tg\delta_b = \frac{2}{tg\beta_b}\left[\frac{M_2^2 sin^2\beta_b - 1}{M_2^2\left(\kappa + cos2\beta_b\right) + 2}\right] \tag{5.14}$$

Thanks to that, the only necessary input data required for the analysis are incoming Mach numbers and trailing edge angle, showed in the Table 5.1.

Table 5.1: Oblique shock analysis input data

	Case I	**Case II**
M_1	1.51	2.29
M_2	1.27	1.15
δ_{TE}	15.1°	28.8°

Azimuthal flow angles ϑ_3 and ϑ_4 can be expressed as follows

$$\vartheta_3 = \vartheta_1 + \delta_a \tag{5.15}$$

and

$$\vartheta_4 = \vartheta_2 - \delta_b \tag{5.16}$$

The trailing edge angle is, of course

$$\delta_{TE} = \vartheta_2 - \vartheta_1 = \delta_a + \delta_b \tag{5.17}$$

Equations (5.9), (5.11) and (5.13) give final dependence of static to total pressure ratio p_3/p_{01} on turning angles δ_a for $M_1 = const.$ when

$$\beta_a = var, arcsin\frac{1}{M_1} < \beta_a < 90 \tag{5.18}$$

The dependence is depicted in diagrams in the Figures 5.12 and 5.13 as a blue curve. Equations (5.10), (5.12) and (5.14) give final dependence of ratio of static pressure p_4/p_{01} on turning angles δ_b for $M_2 = const.$ when

$$\beta_b = var, arcsin\frac{1}{M_2} < \beta_b < 90 \tag{5.19}$$

The dependence is depicted for assumption in Eq. (5.6) in diagrams in the Figures 5.12 and 5.13 as a red curve.

Noting that thanks to ambiguous character of the supersonic flow, such relations give two values of pressure ratio for each possible wave angle which fulfill conditions in Equations (5.6) and (5.7) [24] up to the maximum value where the wave detaches and change to normal shock. The solution with higher value of p/p_{01} represents the unstable strong shock solution and the solution with lower value of p/p_{01} represents weak stable solution. Points of intersection define overall solution of the supersonic flow past sharp trailing edge. Results of this analysis are the shock polars. Every "half-heart" shaped line represents one side of the profile and vertical line is the value of trailing edge angle.

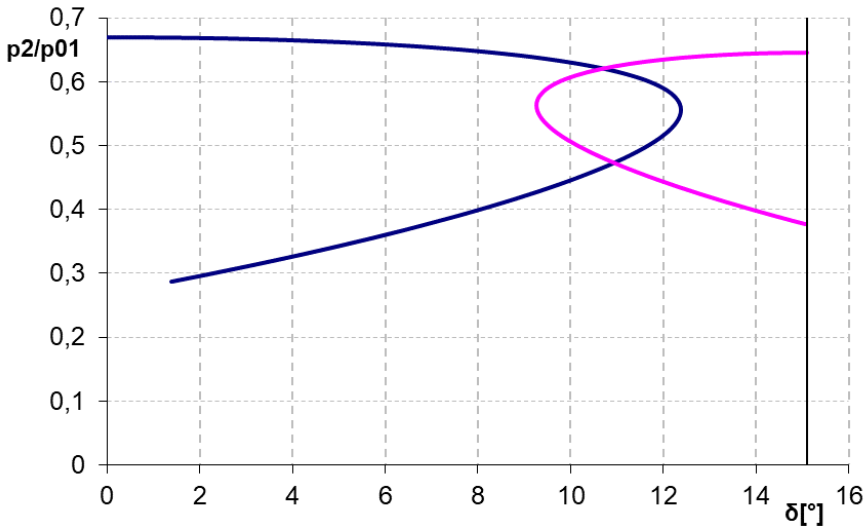

Figure 5.12: Shock polars for Case I

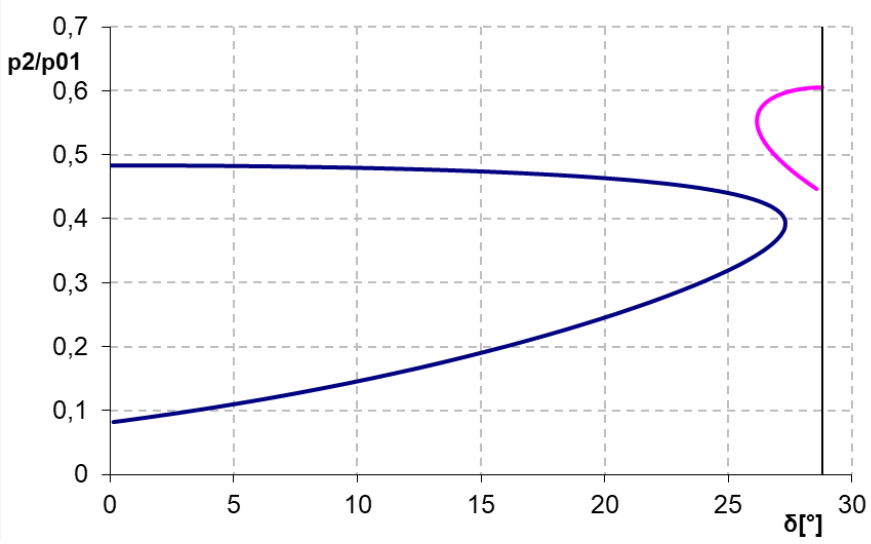

Figure 5.13: Shock polars for Case II

Shock polars for the airfoil configuration Case I with the solid vertical line representing the trailing edge angle of a value of $15.1°$ are depicted in the Figure 5.12. Both polars intersect twice and considering that the stable solution is the natural one, the result is the lower point of intersection. The flow turning angle in absolute value on the upper side of the profile is approximately $10.8°$ and on the lower side $4.3°$. To compare these numbers with the CFD results, the values from the nearest cell of the shock are approximately $10.9°$ for the upper side and $4.0°$ for the lower side. That is very satisfying result considering finite character of the computational mesh on one side and ideal gas dynamics theory on the other.

In the Figure 5.13, the shock polars for the airfoil of Case II, thicker and more cambered profile and limit variant with the trailing edge angle $28.8°$, are shown. The first noticeable difference is the fact that the polars do not intersect ending with questionable irregular solution for this configuration. But the contour in the Figure 5.6 above with no obvious oblique shock on the lower side of the profile already predicted nonstandard behavior.

For deeper investigation of this problem, the model of nonsymmetrical supersonic flow past a trailing edge [25] is proposed in the Figure 5.14. The nonsymmetrical supersonic flow past a trailing edge can be reduced to symmetric case by means of following relations to obtain some results also for analysis of irregular configuration. Reduced value of azimuthal angle of the flow upstream and downstream (namely azimuthal angle of discontinuity (d) of symmetric trailing edge is given by

$$\vartheta_{red} = \frac{\vartheta_1 + \nu_1 + \vartheta_2 - \nu_2}{2} \tag{5.20}$$

and reduced value of Prandtl-Meyer function

$$\nu_{red} = \vartheta_1 + \nu_1 - \vartheta_{red} = \vartheta_{red} - \vartheta_2 + \nu_2 \tag{5.21}$$

where Prandtl-Meyer function is [13]

$$\nu\left(M\right) = -\sqrt{\frac{\kappa+1}{\kappa-1}} arctg \sqrt{\frac{\kappa-1}{\kappa+1}\left(M^2-1\right)} + arctg\sqrt{M^2-1}. \tag{5.22}$$

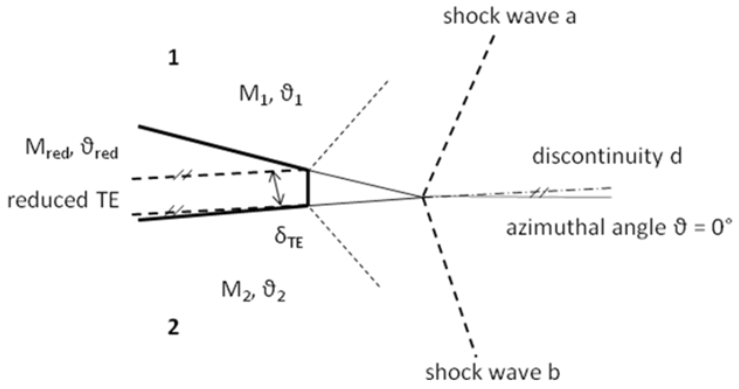

Figure 5.14: Reduced parameters trailing edge configuration

Reduced parameters analysis proved the possibility of application of the model in the Figure 5.14 also for sharp trailing edges. Application of Equations (5.20) and (5.21) for the Case I of the cusped airfoil proved regular interaction of supersonic flows on the sharp trailing edge. Reduced value of azimuthal angle is $\vartheta_{red} = 10.97°$ and reduced value of Prandtl-Meyer function is $\nu_{red} = 1.23°$. That confirmed previous numbers from basic analysis. For the Case II of the cusped airfoil, reduced value of azimuthal angle is $\vartheta_{red} = 30.23°$ and Prandtl-Meyer function is $\nu_{red} = 3.80$, while the flow angle obtained from the numerical simulation is approximately $30.8°$. That corresponds well with the reduced angle value as well, however, further analysis proved important fact that condition for upper branch of exit shock waves $\delta_a \leq \delta_{a,max}$ is not fulfilled. Angle of shock wave to incoming flow $\beta_{a,max}$ corresponding to maximum turning angle $\beta_{a,max}$ is given by the following expression [26]:

$$\beta_{a,max} = arcsin\sqrt{\frac{1}{\kappa M_1^2}\left[\frac{\kappa+1}{4}M_1^2 - 1 + \sqrt{(\kappa+1)}\left(1 + \frac{\kappa-1}{2}M_1^2 + \frac{\kappa+1}{16}M_1^4\right)\right]}. \tag{5.23}$$

The interaction of supersonic flows at the trailing edge for the Case II is not regular and the supersonic flow on the upper side of profile can be separated upstream of the trailing edge or can show some unstable unsteady character.

5.4 Off-Design Conditions

Using the sonic free stream condition, it has been already proved that it is possible to correctly simulate the analytical solutions, but the whole problem was limited by an ideal state of exact flow velocity. To get closer to the real world, even when this case is meant to be an academic example, it is always a benefit to think about some off-design conditions [JS4]. Especially here, when talking about very special and sensitive flow speed value, it can be very easily imagined that the velocity will oscillate around value of Mach number $M = 1$ and the problem can turn into a supersonic or on the other hand subsonic free stream case.

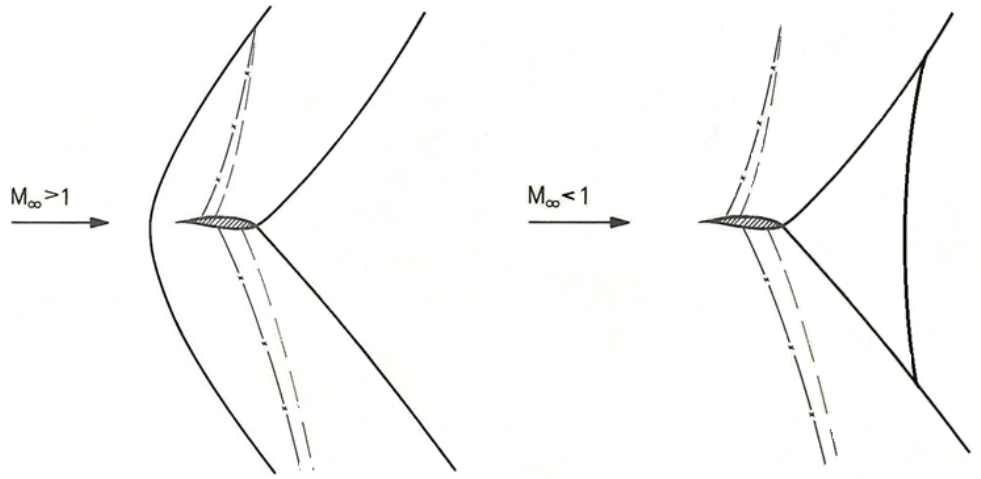

Figure 5.15: Supersonic (left) and subsonic (right) flow field [3]

These two off-design cases are symbolized in the Figure 5.15. On the left is the airfoil in mildly supersonic free stream what causes a creation of detached bow wave in front of the cusp. Detailed shape, strength and location of detached shock depending on the free stream Mach number is more explained in [3] and [17]. On the right side is the opposite case in slightly subsonic free stream. This problem has not been investigated much yet, but it is known that a fish tail wave should occur closing the local supersonic domain bounded by oblique shocks.

For such cases, the model had to be modified to prevent the interaction of the boundary with the flow field that could influence the results. For the off-design simulation, the symmetrical cusp with $\tau = 0.05$ was used, but the computational domain is now much larger comparing with the sonic flow conditions mainly because of the expected normal shock formed in front of the airfoil. Thanks to the dimensions disproportion between the cusp and the boundary, the triangular mesh had to be used due to grid size reduction. The Mach number gradient adaptation was then used to refine the

mesh in critical locations. The mesh size for this symmetrical case varied from 60000 – 80000 cells depending on the adaptation requirements. The numerical simulation setup remained same as for the sonic flow simulations with pressure far field boundary condition.

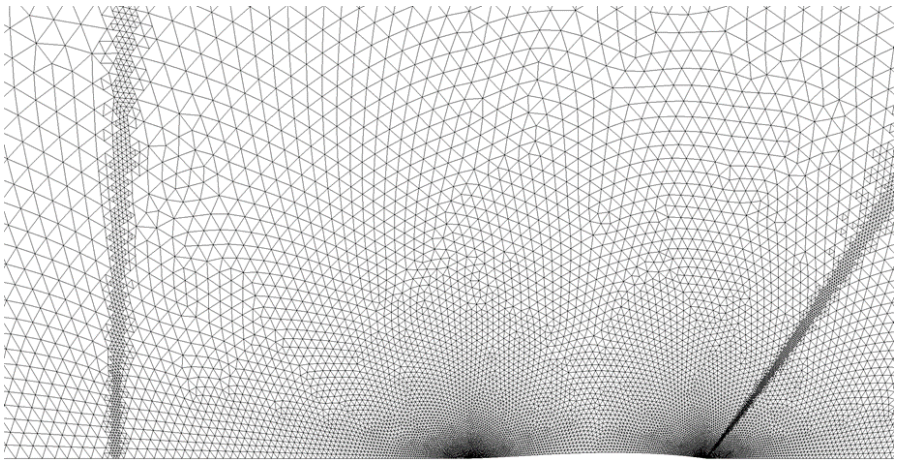

Figure 5.16: Adapted triangular mesh

The displayed mesh is already adapted one for $M_\infty = 1.05$ case and it is obvious where the shocks are corresponding to local mesh refinement. Graphical result of the numerical simulation for this setup is shown then in the Figure 5.17 with displayed Mach number isolines. The bow wave is clearly formed in front of the airfoil and from this view, it seems as it has almost a shape of normal shock. The scale of the figure does not allow to see here the whole bow wave, but it propagates further until it crosses the sonic line. The flow field is then very similar to the sonic free stream condition described in previous chapters. The flow is accelerated smoothly from subsonic to supersonic speeds past the airfoil until it forms oblique shocks starting from the trailing edge.

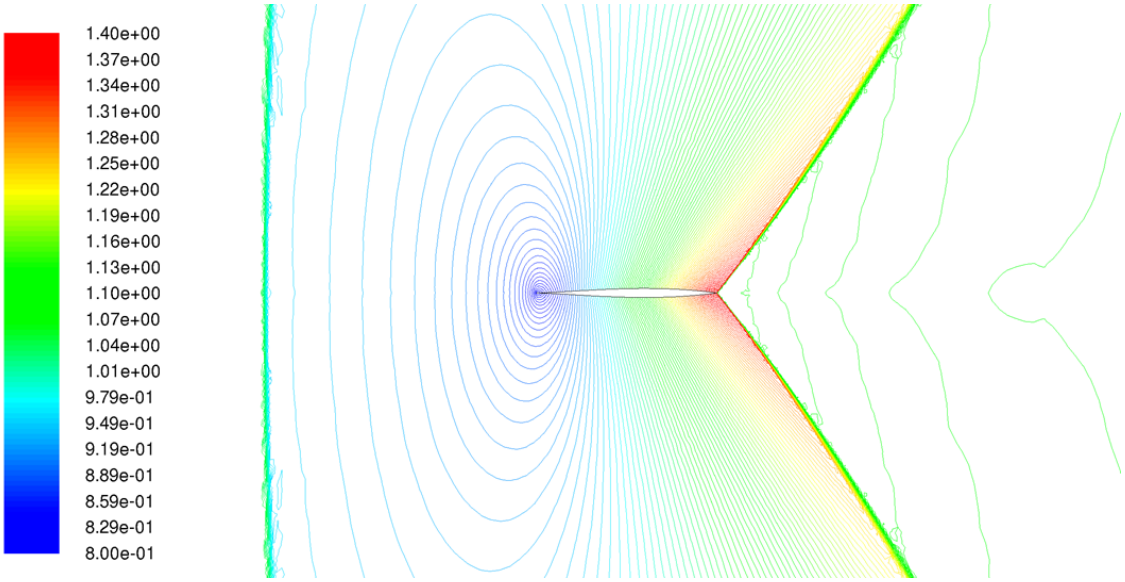

Figure 5.17: Mach number isolines $M_\infty = 1.05$

The location of the bow wave differs with rising free stream Mach number. Close to sonic conditions, the wave gets weaker and disappears, while with rising Mach number the wave gets stronger and approaches towards the leading edge until it attaches and form an oblique shock as well. Table 5.2. shows this phenomenon with the detached wave location corresponding to the Mach number with C being the chord length and d the wave distance from the leading edge

Table 5.2: Mach number and detached bow wave location

M_∞	d/C
1.1	0.19
1.075	0.53
1.05	1.51
1.025	6.37

From rheograph theory for this supersonic free stream case, it is possible to evaluate the ratio of the bow wave distance d and chord length C [3]. A new similarity parameter is defined:

$$\chi_\infty = \frac{M^2 - 1}{(\kappa+1)^{2/3}\,\tau^{2/3}\left[1 + 2^{12}\cdot 3\cdot 5^{-6}\left(\frac{\omega}{\tau}\right)^2\right]} \tag{5.24}$$

$$\frac{d}{C} = \lambda\left(\chi_\infty\right)\cdot\left[1 + 2^{12}\cdot 3\cdot 5^{-6}\left(\frac{\omega}{\tau}\right)^2\right] \tag{5.25}$$

And an asymptotic solution of $\lambda\left(\chi_\infty\right)$ for $\chi_\infty \to 0$ or also for $M_\infty \to 1$ can be obtained defined by:

$$\lambda\left(\chi_\infty \to 0\right) = 0.2916\cdot\chi_\infty^{-2}. \tag{5.26}$$

For this symmetrical profile, Equations (5.24) and (5.25) are significantly simplified and the dependency of wave position and free stream Mach number can be plotted in to a simple graph.

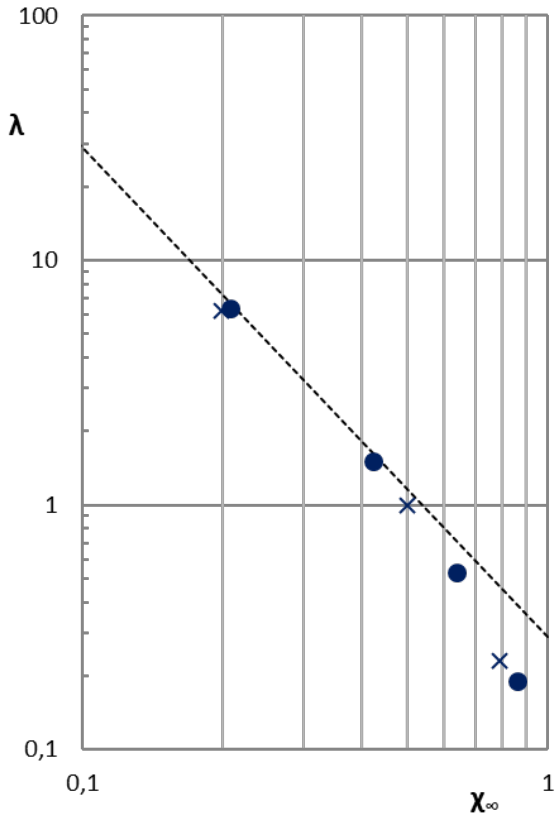

Figure 5.18: Bow wave location

Solid blue points in the Figure 5.18 are values form previous Table 5.2, x - points are results from DLR - Tau inviscid code [17] which were compared with analytical data obtained for same profile and free stream condition and showed a very good correspondence. And finally dashed line is the asymptote (Eq. (5.26)) valid for $M_\infty \to 1$. There is a good correspondence for low Mach numbers, where theoretical solution is exactly defined. The values for higher Mach numbers logically deviate from the asymptote because of upcoming wave attachment, but both numerical codes follow the same trend.

So it can be said, that acceptable results for supersonic free stream case were obtained, but the opposite problem of subsonic free stream remains. This solution is displayed again using Mach number isolines in the Figure 5.19. The setup for the simulation remained same as well, only the mesh was adapted for different gradient location.

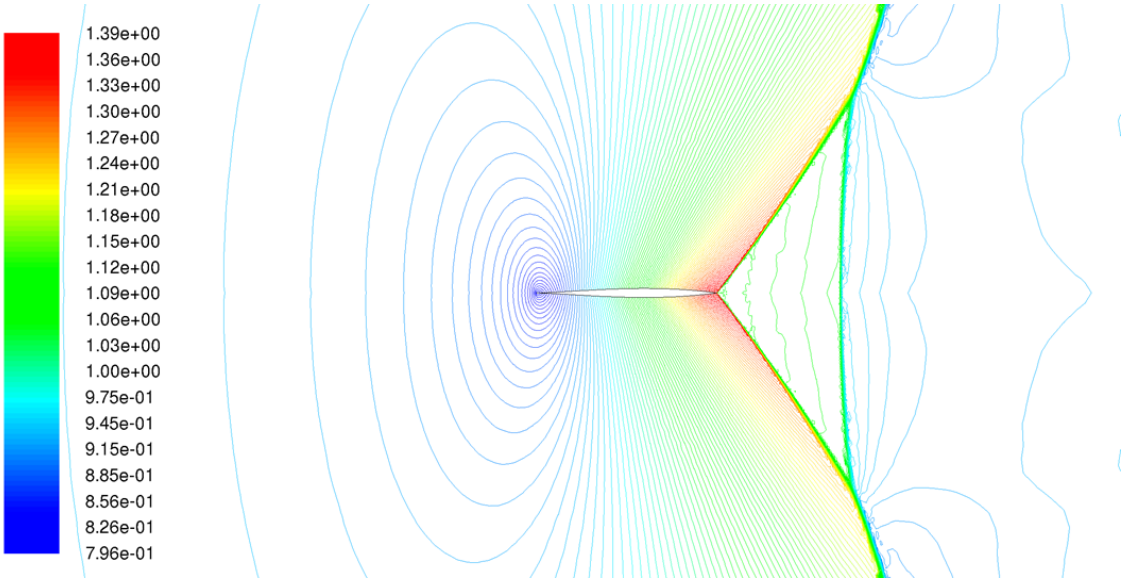

Figure 5.19: Mach number isolines $M_\infty = 0.95$

The Figure 5.19 shows nicely the expected solution resulting in the fish tail wave creation behind the cusp. The flow follows correct trend from leading to trailing edge past the profile accelerating smoothly from subsonic to supersonic velocities exiting with oblique shocks. The difference appears behind the trailing edge, where the flow is still locally supersonic while the rest of the flow field has to be subsonic given by the boundary condition value. That forms this local supersonic triangular domain bounded by shocks on all sides resembling the shape of a fish tail. For various setups, decreasing the value of the free stream Mach number is resulting in decreasing of this local supersonic triangle size and conversely. The zoom of this figure does not allow to see that here, but the oblique shocks then disappear relatively close to the airfoil in comparison with supersonic and sonic conditions, because the flow in the subsonic free stream is not accelerated that much around the profile to form strong lasting shocks far from the airfoil.

These two off-design setups extend the problematic of developed near sonic flow theory past sharp profile and describe the sensitivity of the transonic problems as a whole. It is clear how important is precise analysis when solving problems around sonic values and how a very small change in flow properties can change the whole behavior. And it has been confirmed here, that the numerical simulations followed the right trend as expected form theoretical analysis and proved as fast and reliable tool for design or verification. Vice-versa, analytical tools also prove their relevancy, as the predicted behavior is correct with high precision compared to all the simulations results.

At the end, it is important to remind that the problematics still covers only the potential or inviscid flow what keeps this topic still far from reality. But it would be very interesting to observe viscous effects and their influence on the flow in future and describe the differences between initial design and the real flow confrontation.

6 Supercritical Symmetric Nozzle

Classical transonic hodograph-based design methods described and validated in previous sections can be employed and revitalized as fast modern numerical tools and can be used to serve as tools to substitute analytical models for solution of differential Laplace/Poisson equations and the method of characteristics. And altogether, to illustrate the design of a symmetrical accelerating-decelerating nozzle throat. The concept of elliptic continuation is applied to solve transonic boundary value problems avoiding the inherently nonlinear nature of the basic equations and obtaining transonic flow examples using the method of characteristics in an inverse mode. Purpose of the case, besides describing a new special flow example, is to show how are the classical methods usable for design and as well education of a new generation of creative engineers.

This contribution makes use of particular solutions to the gasdynamic equations focusing on the transonic regime [JS2], hodograph representation of the well known Laval throat accelerated flow allows for some extensions resulting in a new type of nozzle flow [JS5]. This section begins, therefore, with reviewing the rheograph version of hodograph basic equations and the Laval throat flow is selected to be represented in this working space. With classical gas dynamics knowledge [5], analytical solutions at hand, numerical verification, but also numerical variations along modified boundary conditions are possible. For supersonic parts of selected examples, the method of characteristics is employed in an inverse mode to accommodate design procedures. Construction of exact flow fields with the methods applied here for an academic example, are the basis of practical transonic analysis and design in aeronautics and mainly turbomachinery, where the transonic regime and conditions play major role in the flow behavior.

The side benefit for engineering and scientific community is that the output geometry can then possibly serve as a validation test case for precise transonic codes.

6.1 Rheograph Formulation of Laval Nozzle Flow

A rheograph solution to the potential flow was already described in previous chapter.

$$\phi_{ss} + \phi_{tt} = \frac{K_s}{K}\phi_s + \frac{K_t}{K}\phi_t \tag{6.1}$$

$$\psi_{tt} + \psi_{tt} = \frac{K_s}{K}\psi_s + \frac{K_t}{K}\psi_t \tag{6.2}$$

$$\left(\frac{d\psi}{d\phi}\right)_{\xi,\mu=const.} = \pm K^{-1} \tag{6.3}$$

For flows with only small deviations from sonic velocity, only a simplified perturbation potential equation may be used instead of the full potential equation [6].

$$m\left(1-l\right)^{l}\left|\phi_{x}\right|^{l}\phi_{xx}-\phi_{yy}-\frac{k\phi_{y}}{y}=0 \tag{6.4}$$

with the three switch parameters k, l, m which can then convert the equation accordingly. Integer k distinguishes between plane $(k = 0)$ and axisymmetric $(k = 1)$ flow, l distinguishes between perturbed subsonic or supersonic flow $(l = 0)$ and perturbed sonic flow $(l = 1)$ and integer m distinguishes between locally subsonic $(m = -1)$ or supersonic $(m = 1)$ flow. Later rheograph transformation [6] converts Equation (6.4) into a set of coupled Beltrami equations for velocity variables U, V and physical coordinates X, Y, valid in a parametric "rheograph" plane (s, t)

$$V_{t}-Y^{k}\left(s,t\right)U_{s}=0 \tag{6.5}$$

$$V_{s}-mY^{k}\left(s,t\right)U_{t}=0 \tag{6.6}$$

$$X_{s}-U^{l/3}\left(s,t\right)Y_{t}=0 \tag{6.7}$$

$$X_{t}-mU^{l/3}\left(s,t\right)Y_{s}=0 \tag{6.8}$$

The use of this technique can be shown on the example of transonic area near the nozzle throat. Reduction of previous relations (Eqs. (6.5) - (6.8)) for two-dimensional planar flow in the Laval nozzle flow for subsonic domain $(k = 0, l = 1, m = -1)$ gives

$$V_{t}-U_{s}=0 \tag{6.9}$$

$$V_{s}+U_{t}=0 \tag{6.10}$$

$$X_{s}-U^{1/3}Y_{t}=0 \tag{6.11}$$

$$X_{t}+U^{1/3}Y_{s}=0 \tag{6.12}$$

Elimination of V or U and X or Y yields

$$U_{ss}+U_{tt}=0 \tag{6.13}$$

$$V_{ss}+V_{tt}=0 \tag{6.14}$$

$$X_{ss}+X_{tt}-\frac{1}{3}\left[\frac{U_{s}}{U}X_{s}+\frac{U_{t}}{U}X_{t}\right]=0 \tag{6.15}$$

$$Y_{ss} + Y_{tt} + \frac{1}{3}\left[\frac{U_s}{U}Y_s + \frac{U_t}{U}Y_t\right] = 0 \tag{6.16}$$

Now it arrived at the state that the linear second order differential Laplace (Poisson) equations (Eqs. (6.13) - (6.16)) are formulated for subsonic region and are ready to be solved numerically using finite difference methods for further purposes. It is good to mention that this particular set of equations can be very helpful for code and results validation because they also give a simple analytical solution in form of

$$U = 2st \tag{6.17}$$

$$V = t^2 - s^2 \tag{6.18}$$

$$X = \left(t^{4/3} + s^{4/3}\right) \tag{6.19}$$

$$Y = -2^{2/3}\left(t^{2/3} - s^{2/3}\right) \tag{6.20}$$

This solution is valid for subsonic domain, that means for $s < 0$, according to rheograph transformation, the $s = 0$ represents the sonic line.

6.2 Elliptic Continuation and Method of Characteristics

The solution of the whole problem now consists of two parts (see the Figure 6.1). At first, solving the elliptical domain in order to obtain the flow field up to the sonic line including the sonic line data, by an elliptic continuation of the boundary value problem beyond the sonic line location $(s = 0)$. Next is the extension into the hyperbolic supersonic domain, using the previously obtained sonic line data as initial conditions.

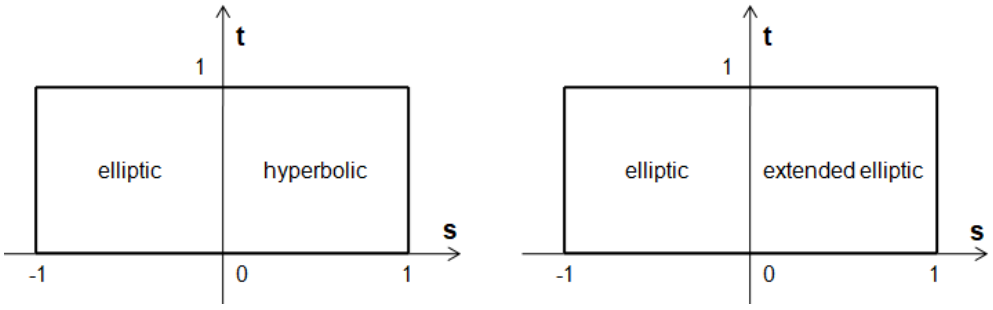

Figure 6.1: Rheograph s, t plane: Mapping of real transonic and partly fictitious flow

In direct CFD simulation of transonic flow in physical space, the location of the sonic line, dividing the subsonic from the supersonic part of the flow, is usually unknown, while a hodograph

formulation a priori prescribes the location of the sonic line. This allows a strong control of the geometry downstream the sonic line location, which will be the key to designing flows with desirable aerodynamic properties.

In an effort to understand the physical meaning of elliptic continuation as an auxiliary step to solve transonic flow problems, the solution within the continuation domain can be interpreted as a „Fictitious Gas“ subsonic flow, later to be corrected by a „Real“ supersonic flow calculation. Once the parameters along the sonic line are established, it can easily continue with the method of characteristics for the supersonic flow solution.

In pre-computational era, elliptic solutions had to be modeled using methods related to conformal mapping, but nowadays, with strong influence of the computing abilities, fast numerical methods can be used to find the solution of differential equation systems like (Eqs. (6.13) - (6.16)). This will give a correct subsonic portion of the flow, plus a temporary fictitious portion, separated by a resulting line where the flow velocity is equal to the speed of sound, from real subsonic flow.

The equations system for the planar nozzle geometry for fictitious part with application of Eq. (6.17) transforms the equations for X and Y means that they can now be solved separately:

$$U_{ss} + U_{tt} = 0 \tag{6.21}$$

$$V_{ss} + V_{tt} = 0 \tag{6.22}$$

$$X_{ss} + X_{tt} - \frac{1}{3}\left[\frac{1}{s}X_s + \frac{1}{t}X_t\right] = 0 \tag{6.23}$$

$$Y_{ss} + Y_{tt} + \frac{1}{3}\left[\frac{1}{s}Y_s + \frac{1}{t}Y_t\right] = 0 \tag{6.24}$$

This system of perturbed variables can be now solved on a simple rectangular grid describing the whole domain (elliptic + extended elliptic) in the rheograph s, t plane using finite difference methods with one of iteration schemes. Boundary conditions can be prescribed as Dirichlet conditions, for the special case of nozzle flow taken from the analytical solution. For this case, the Successive over-relaxation iteration method has been chosen in upcoming form [15]:

$$\Phi_{i,j}^{n+1} = \Phi_{i,j}^{n} + \sigma\left(\widehat{\Phi_{i,j}} - \Phi_{i,j}^{n}\right) \tag{6.25}$$

$$\widehat{\Phi_{i,j}} = \frac{1}{4}\left(\Phi_{i+1,j}^{n} + \widehat{\Phi_{i-1,j}} + \Phi_{i,j+1}^{n} + \widehat{\Phi_{i,j-1}}\right) + \Omega \tag{6.26}$$

The converged solution is shown in the form of contour images for individual variables in Figures 6.2 - 6.5.

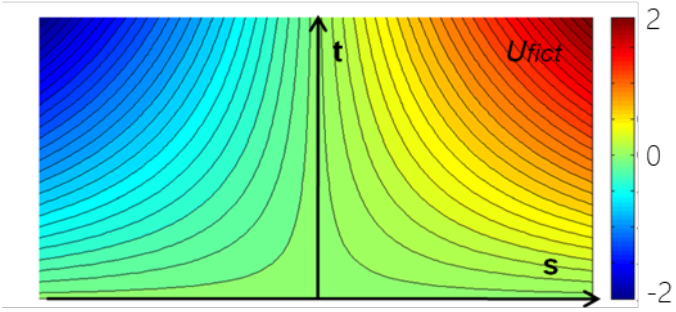

Figure 6.2: Fictitious gas results - U contour

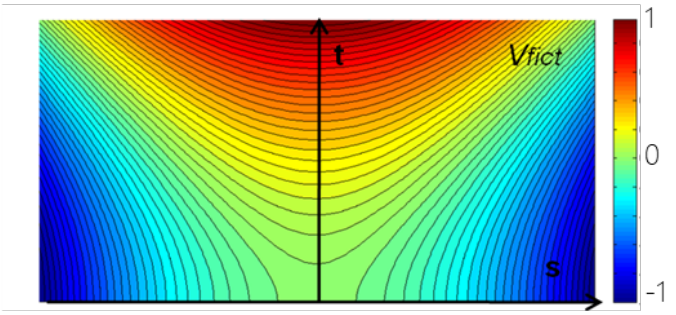

Figure 6.3: Fictitious gas results - V contour

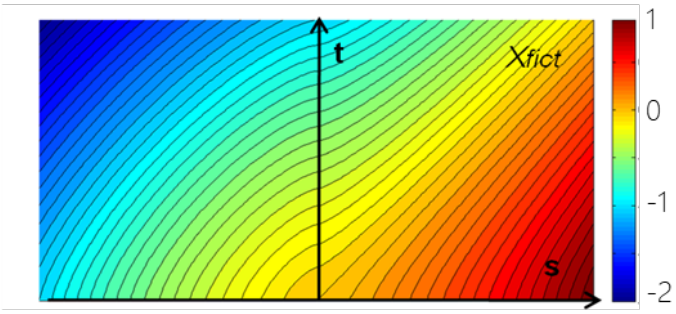

Figure 6.4: Fictitious gas results - X contour

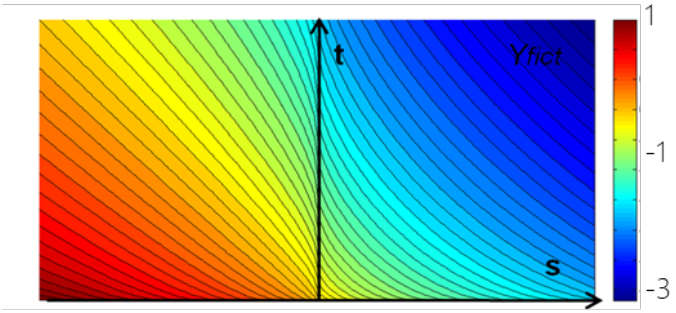

Figure 6.5: Fictitious gas results - Y contour

Now, noticing that the left half of the figures ($s < 0$) represents the valid subsonic solution, the data along t-axis are the data of the sonic line. To continue into supersonic domain ($s > 0$), the method of characteristic can be used but staying in described rheograph plane. The characteristic form of the basic equations, with ξ and η being the characteristics

$$\xi = \frac{(t+s)}{2} \tag{6.27}$$

$$\eta = \frac{(t-s)}{2} \tag{6.28}$$

is resulting into the systems:

$$V_\xi - U_\xi = 0 \tag{6.29}$$

$$V_\eta + U_\eta = 0 \tag{6.30}$$

$$X_\xi - U^{1/3} Y_\xi = 0 \tag{6.31}$$

$$Y_\eta + U^{1/3} Y_\eta = 0 \tag{6.32}$$

With already known solution of U and V from (Eqs. (6.17) - (6.20)), the X and Y can be solved as a initial value problem in the characteristic triangle

$$\frac{dY}{dX}_{\eta=const} = |U^{-1/3}| \tag{6.33}$$

$$\frac{dY}{dX}_{\xi=const} = -|U^{-1/3}| \tag{6.34}$$

Due to the $1/3$ power of U, some care needs to be taken in averaging the coefficient when taking the first step of this weak singularity at $s = 0$. In the result, the characteristic domain for the initial value problem in this case will be bounded by the sonic line and the limiting characteristics. The sketch of the investigated domain is shown in the Figure 6.6.

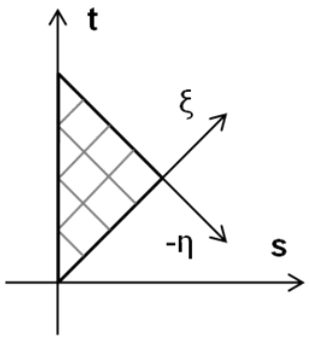

Figure 6.6: Characteristic domain in the s, t plane

The resulting domain visualized in the physical X, Y plane in the Figure 6.7 shows the local supersonic domain from the sonic line to the neutral characteristics. Special attention needs to be paid to the region near this neutral characteristic at the Laval throat point ($s = t = 0$), which in hodograph mapping is a singular point. The inaccuracies travel along characteristics and by amplification may corrupt the solution. Initial data distribution along the sonic line needs to be appropriately refined in order to obtain acceptable accuracy.

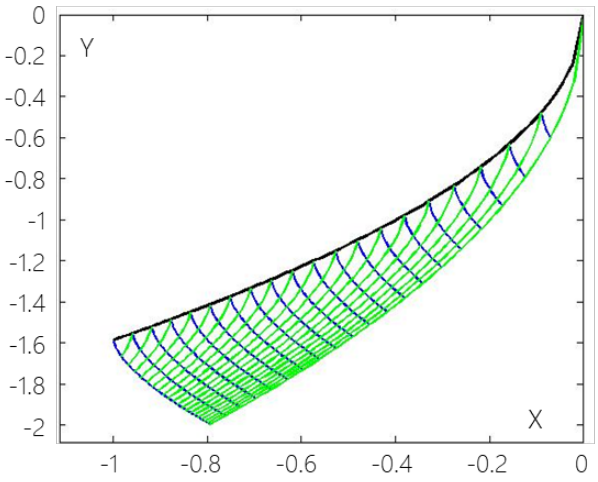

Figure 6.7: Characteristic domain in the X, Y coordinate system

For better understanding, the sketch of the transformation of both solved regions described above from the rheograph s, t plane to physical X, Y plane is shown in the Figure 6.8.

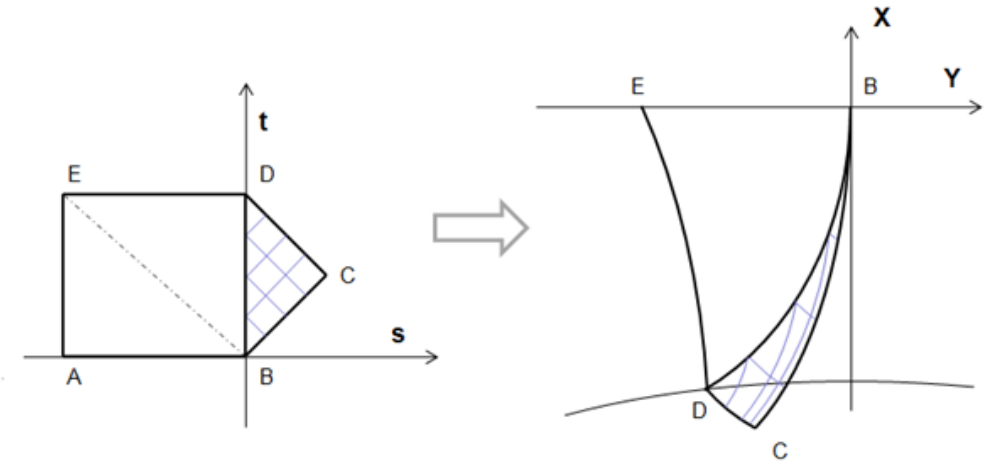

Figure 6.8: Rheograph (left) to physical (right) plane transformation

6.3 Symmetrical Accelerating-Deccelerating Transonic Nozzle Shape Integration

The space downstream the limiting characteristic is now free to continue without changing the upstream solution, but the ξ characteristic itself is not sufficient for continuing the characteristic pattern and some of the flow characteristics need to be prescribed. For a simple accelerating (basic Laval) nozzle, usually the parameters along the flow X axis are being used.

Here, it is proposed to use the solution for construction of a new flow model. For this case of symmetrical accelerating-decelerating nozzle, the symmetrical character of the hodograph solution can be used to calculate the mirrored quadratic region BCFC'. The sketch of the transformation of the middle region is shown in the figure (Fig. 6.9).

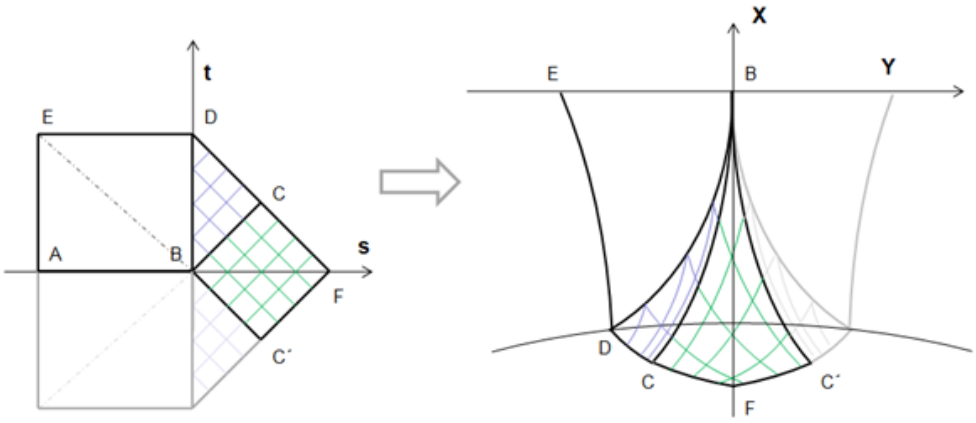

Figure 6.9: Rheograph to physical plane transformation of composing a flow using symmetry properties of the solution

The pattern in the Figure 6.10 shows both mirrored neutral characteristics used as initial condition to march into the gap, resulting in the full flow field description $U, V, X, Y(\xi, \eta)$.

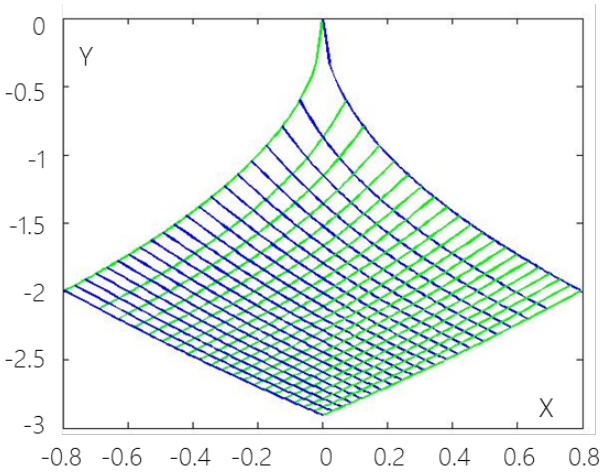

Figure 6.10: Characteristic symmetric domain in the X, Y coordinates

Now, the attention is paid to one flow-bounding streamline starting in the upstream accelerated Laval nozzle model and ending in its mirror image representing a decelerated outlet, both parts connected by fitting in the gap pattern. With the well-known Laval contours to be parabolas, the connection within the gap is still missing.

To obtain streamlines from the computed characteristic region, the values need to be evaluated along a constant stream function. For the chosen near sonic formulation, lines $Y = const$ represent such stream function. Interpolation of $V(X)$ along $Yc = const$ (see Fig. 6.11) defines the contour angle and allow for streamline shape integration (see Fig. 6.12). The scaling parameters A, B in Eqs. (6.35) - (6.38) represent transonic similarity parameters and allow for obtaining scaled flow fields $u, v(x, y)$ from the parametric solution $U, V, X, Y(\xi, \eta)$ in the rheograph.

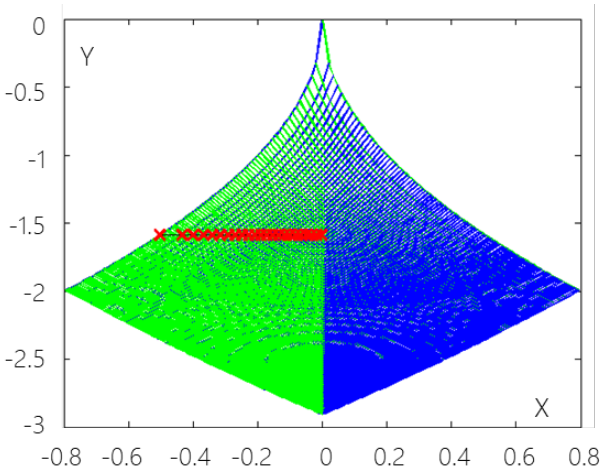

Figure 6.11: Shape integration

6.4 Shock-free Supercritical Nozzle

For the purpose of creating a new flow example, the upstream accelerated Laval flow and a mirror solution as downstream decelerated exit flow were used. The new symmetrical gap solution fits then exactly between the neutral characteristics, bridging the Laval portions of the flow and forming a complete accelerated and decelerated flow model, with chosen contour arc fitting together without curvature irregularities at the contact characteristics. Both Laval nozzle components show parabolic arc contours, these are bridged by a smoothly curved, symmetrical arc (Fig. 6.12) creating a flow boundary with reduced curvature in the plane of symmetry $X = 0$:

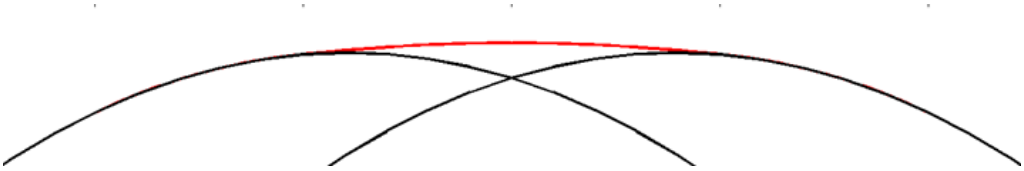

Figure 6.12: Resulting streamline shape for accelerated and decelerated part of the nozzle flow

Real geometric coordinates (x, y) and flow parameters (u, v) are obtained by the following equations, representing the transonic similarity laws:

$$x = AX \tag{6.35}$$

$$y = AB^{(-l/3(1+2k))}\left(\kappa+1\right)^{-l/2} Y \tag{6.36}$$

$$\frac{u}{u_{ref}} - 1 = B^{(1+k-(1-k)l/3)}\left(1^l U\right)^{1-l/3} \tag{6.37}$$

$$y^k \frac{v}{v_{ref}} - 1 = A^k B^{(1+k)}\left(\kappa+1\right)^{(l(1-k)/2)}\left(1-l/3\right) V \tag{6.38}$$

Free similarity parameters A, B in Eqs. (6.35) - (6.38) allow for obtaining scaled flow fields $u, v(x, y)$ from the parametric solution $U, V, X, Y(\xi, \eta)$ in the rheograph.

The final shape of a symmetric shock free accelerating-decelerating scaled nozzle is shown in the Figure 6.13. Sonic lines are depicted along with the limiting characteristics, illustrating the range of the accelerated inlet and the decelerated outlet Laval flow, connected by the new symmetrical pattern responsible for the flattened throat region. The flow is choked but not accelerated due to the unique throat geometry.

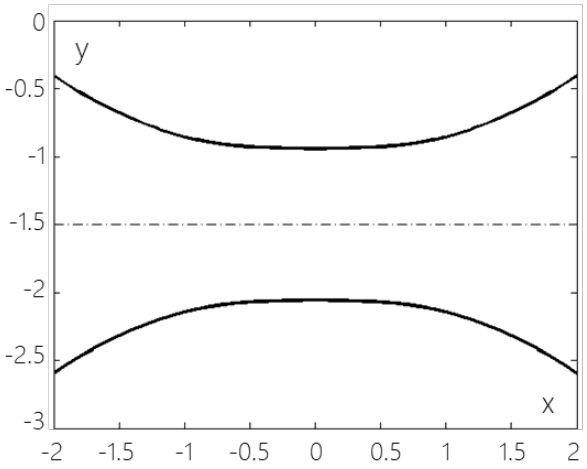

Figure 6.13: Symmetric accelerating-decelerating nozzle

Velocity distribution along a nozzle wall shows two characteristic slope discontinuities at the contact locations, which stem from the weakly singular behavior in the nozzle throat, Fig. 6.14.

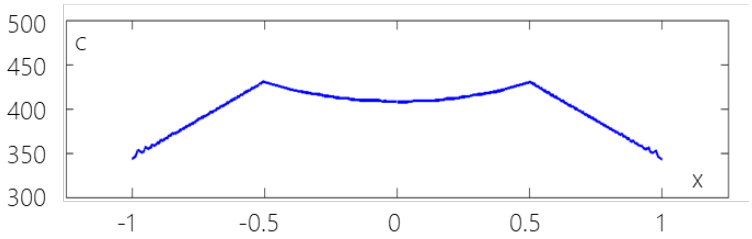

Figure 6.14: Velocity distribution along nozzle contour [m/s]

6.5 Validity and Resume

The main intention of this chapter was to show that the rheograph transformation method used together with modern computational and evaluation techniques may even nowadays still be a working tool for creative aerodynamic design. Manual based analytical methods for solution of equations describing underlying flow may led to unpopularity of this design methods between some of the general community in the past. The much simpler numerical solution of differential equations as showed above now makes the approach simpler, more user friendly and applicable even for engineers with lesser background in advanced mathematics.

The outcome is a special novel nozzle solution of up to sonic conditions accelerating nozzle that subsequently decelerates the flow to subsonic regime without formation of the shock. This example, however academic case study may be, shows that not only wing design for aeronautics can profit from this method, but also the high speed internal aerodynamics is a field where analytical flow

models can be useful and can provide deeper understandings of the underlying flow phenomena and potentially new and innovative solutions.

On the top of that, this particular case can now possibly serve as an academic validation or a test case for specialized compressible flow numerical codes, as such specific flow pattern needs very precise simulation to be captured usually unable to reach using general all-purpose codes. The specific geometry and unique very sensitive transonic flow field with weakly singular nozzle throat point is a sophisticated challenge for a CFD code.

For a short demonstration, in the figures below are quick simulations done by ANSYS Fluent code to describe a complexity of this issue. As expected, obvious from Figure 6.15, in fully subsonic regime, the flow field is smooth and really symmetric. But already here, the two max velocity regions are visible.

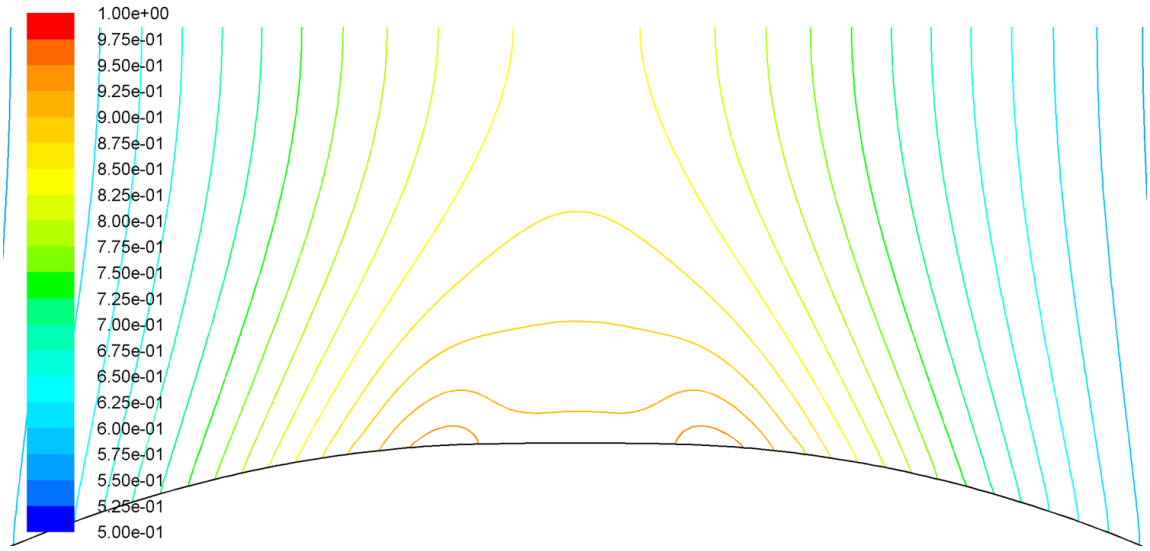

Figure 6.15: Nozzle flow Mach number - subsonic conditions

However, the sonic regime is unable to be precisely captured using common AUSM scheme and second order upwind spatial discretization even on an extra fine, quad computational mesh. The supersonic region just immediately starts to collapse and forms rather chaotic shape with closing shock instead of shock-free symmetrical pattern as can be seen in the Figure 6.16. In this case, it might be the singularity or the inability to calculate precisely the sonic line or just the overall sensitivity of the case. In order to simulate correctly the accelerating, sonic and decelerating section with the symmetric sonic lines, the used schemes must be more accurate and the solution more refined.

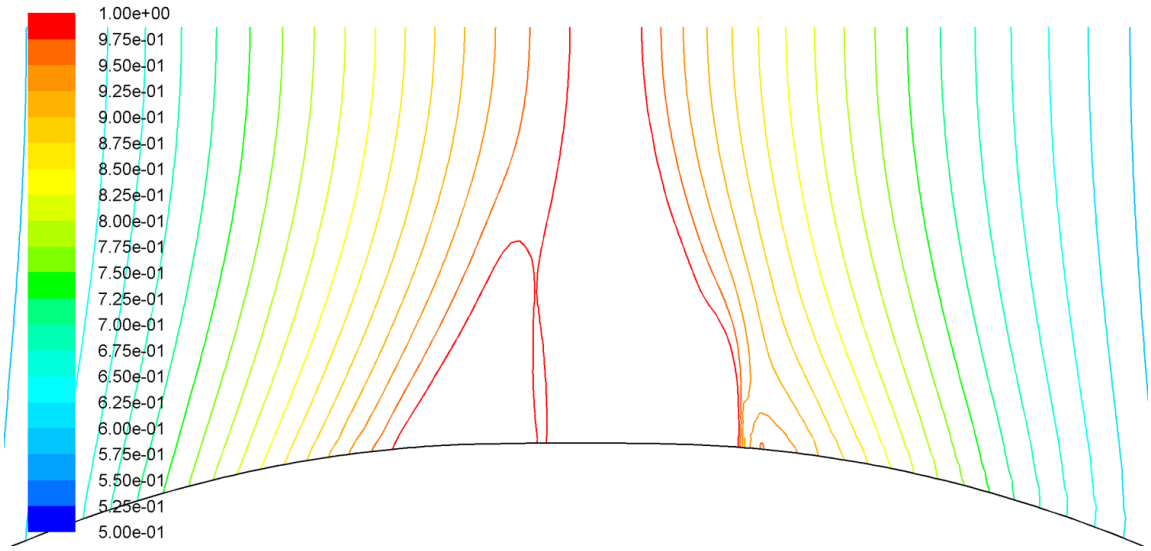

Figure 6.16: Nozzle flow Mach number - sonic conditions

These results prove the complexity of the case and due to the singularity hardly possible to reach the correct using finite mesh methods. But even a get near to the expected behavior would be a good result for any numerical method or scheme.

7 SE 1050 Blade Cascade Analysis

The academic examples might be interesting and beneficial for explaining, understanding and developing new methods, but for engineering purposes, it is appropriate to arrive with a practical case to demonstrate the abilities in the real world problems. As a great example to demonstrate the abilities of the above described methods, a well-known turbine blade cascade SE 1050 from ERCOFTAC database as an application challenge AC 6-12 [7] can be used.

The specific shaping of this blade cascade leads to the formation of re-compression area in the supersonic section caused by rapid change in curvature followed by the discontinuity and straightening of the surface in the expansion section. There might be reasons why the geometry is shaped like this and it might be designed on purpose, but for needs of this thesis, it will be considered as undesirable. The goal here, in general, is not to create new version of this cascade with better overall performance to, but more to show the possible way of situation analysis and possible solution to change the current flow field.

7.1 Case Description

Blade cascades belong to the most important elements in turbomachinery as they form the defining shape of the turbine or compressor. The chosen profile SE 1050 was designed for the last stage of a steam turbine and it is a section of 1085 mm long rotor blade at the distance 320 mm from the root. The geometrical description or scheme of the blade cascade is shown in the Figure 7.1.

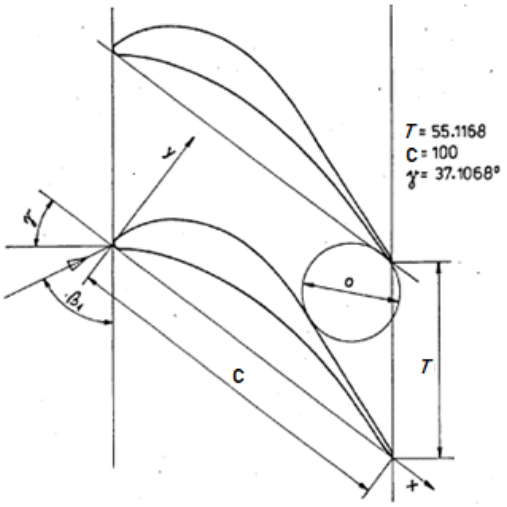

Figure 7.1: SE1050 blade cascade scheme [7]

Necessary geometrical properties and dimensions of the blade and the experimental setup are described in the Table 7.1. The profile coordinates are also available at [7].

Table 7.1: SE1050 basic dimensions

chord length	100 mm
blade span	160 mm
pitch	55.12 mm
stagger angle	37.11°
number of blades	8
inlet angle	70.7°
incidence angle	0°

Although the case was tested and measured for various operating conditions, the cascade for such large power output machine was designed primarily to operate in the transonic regime. The initial design is designed for inlet flow angle $70.7°$ and exit isoentropic Mach number 1.208. Results closest to design conditions achieved in the wind tunnel experiments respond to exit isoentropic Mach number 1.198 and are shown in the Table 7.2.

Table 7.2: Flow parameters

M_1	M_{2is}	β_1	p_{01}	T_{01}
0.375	1.198	70.7°	98 071.7 Pa	298.65 K

Very unique interferogram image of the flow field for this transonic regime is visualized in the Figure 7.2 [9]. Density isolines show subsonic flow accelerated into supersonic region resulting in oblique shock waves leaving the trailing edges. Next to all those expected phenomena, this case exceeds other transonic cascades with specific unusual behavior as can be clearly seen from the interferogram. A small area of compressed flow appears in the expansion section and forms very noticeable hump in isolines.

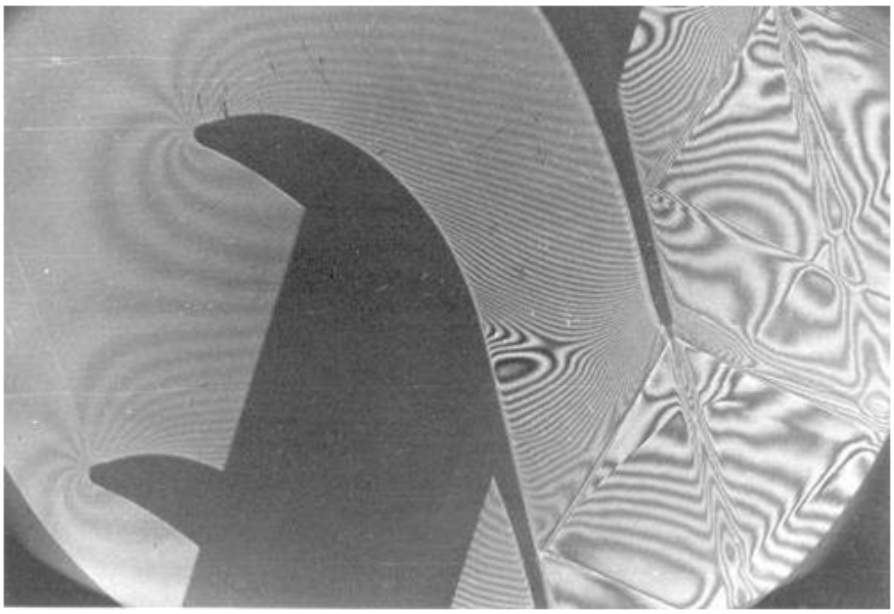

Figure 7.2: SE1050 blade cascade interferogram [7]

Various CFD simulations and analysis were also carried out using different models and approaches [10], [27], showing good correspondence to measured and visualized data. Inviscid flow was solved using custom in-house codes and turbulent simulations were solved in ANSYS Fluent using RANS turbulent models. Result of such simulation is shown in the Figure 7.3.

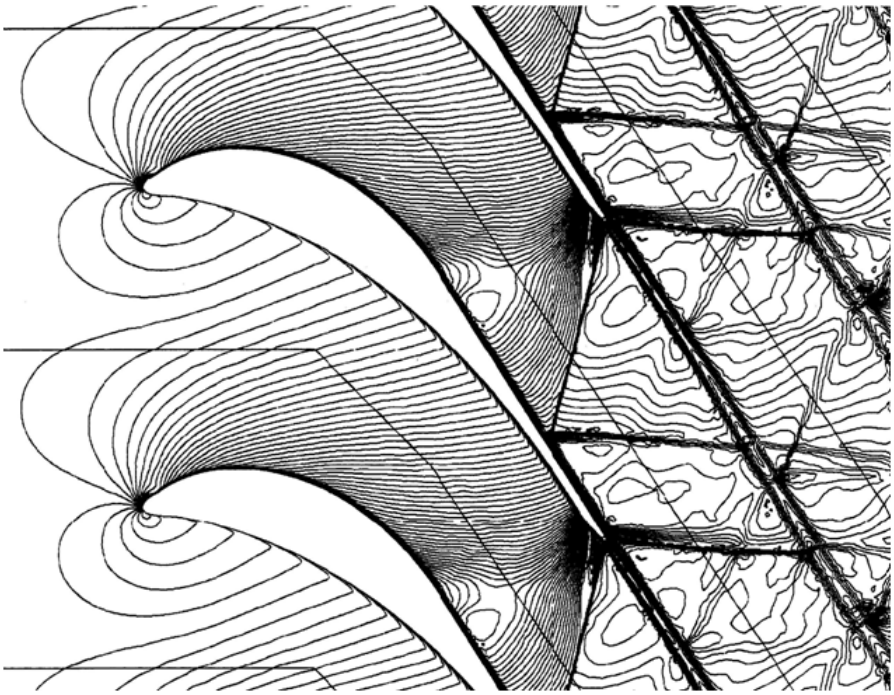

Figure 7.3: SE1050 blade cascade CFD results [7]

The original purpose of the ERCOFTAC case is to provide obtained unique data from experimental measurements to help to validate CFD codes used for numerical simulations and allow engineers to improve turbine design for even higher efficiency and reliability. But for purposes of this thesis, the main concentration aims on the small disturbed section in the expansion region caused by unsensitive blade shaping and intense changes in the blade surface curvature. This phenomenon is specifically called the supersonic compression accompanying transonic expansion and may have a negative effect on the flow in the cascade in terms of losses and probably boundary layer behavior too. In the next sections, the hodograph transformation method will be used to analyze the situation and to outline possible solutions in order to get rid of or minimize this issue. The actual flow field will be computed via CFD to get all the necessary data to see if there is any possibility of minor geometry modification that will improve the situation without drastically changing the geometrical and flow parameters.

7.2 Numerical Simulation

Although many simulations were done for this particular blade cascade, full flow data are required for further investigation and the first task is therefore to repeat the numerical simulation and obtain as similar results to the test as possible. The computational domain was modeled with respect to the nature of flow in transonic applications. The distance from the inlet to leading edge is approximately the length of 1-1.5 chords, similar to the distance from the trailing edge to the outlet boundary. Periodic boundaries are used for repeating blades. The high quality two-dimensional computational mesh was created using block-generation technique in ANSYS ICEM CFD meshing tool. The size of the mesh is around 30000 elements and the detail around the blade can be seen in the Figure 7.4. In order to meet the recommended requirements for the turbulence model, the mesh was accordingly refined in the boundary layer area to satisfy the y^+ criterion around 0.5 and secure around 15-20 cells in the physical boundary layer.

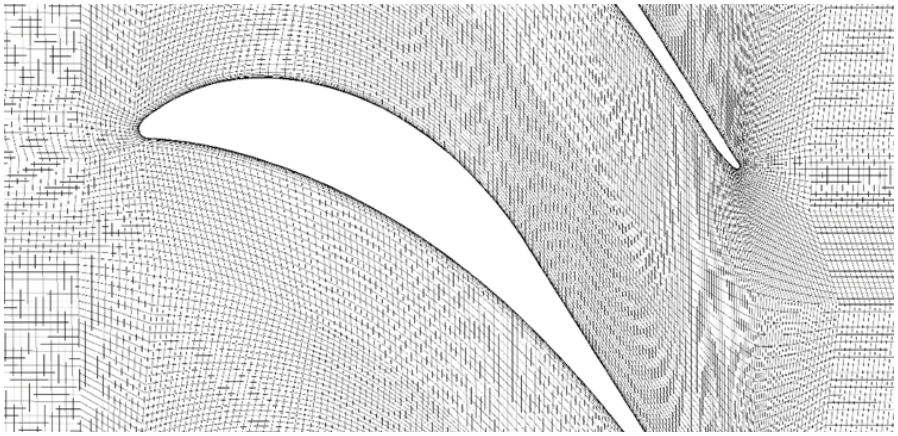

Figure 7.4: Computational mesh

For the simulation itself, the well tested ANSYS Fluent code was used. For case with expected shock waves and strong compressibility effect, density based solver was chosen with flow medium set to normal air treated as ideal gas. Turbulence model was set to two equational SST k-omega model. Boundary conditions for pressure inlet and pressure outlet were calculated to correspond with the operating conditions from the experimental test and are written down in the Table 7.3. The outlet pressure boundary with non-reflecting wave model and average pressure specification should be able to cancel out or at least minimize the effect of shock reflection. For this type of cases with the combination of accelerated flow and strong abrupt changes in solution, an implicit formulation and AUSM flux calculation method allow relatively smooth and fast convergence with Courant number up to the value of 5-10. For the spatial discretization the solution converged with the second order upwind.

Table 7.3: Boundary conditions

p_{01}	p_1	T_{01}	*turb. intensity*	*visc. ratio*	p_2
98 071 Pa	88 997 Pa	298.65 K	2	10	40 547 Pa

Graphical output of the simulation is shown in the Figure 7.5 in form of Mach number isolines, which should correspond with previous Figures 7.2 and 7.3 from ERCOFTAC database. At the first sight, the results already satisfy the expectations of how the flow filed should look like. Relatively slow flow at Mach number around 0.4 near the leading edge accelerated through the channel between blades reaches sonic velocity and continues up to the trailing edge, where the change in gas properties forms the oblique shock wave. The flow field downstream the cascade also behaves in expected

manner. Oblique and reflected shocks interact with the wake leaving the domain with no outlet boundary reflection visible. However, the situation on the suction side is much more complicated than on the pressure side. The flow accelerates smoothly up to the sonic line as well, but right after here, the geometry causes the flow to slow down to be later again accelerated until the interaction of the surface and shock leaving the trailing edge of the neighboring blade. The wobble in flow velocity forms the kink obvious from the contour lines and shows the rough flow behavior resulting in the compression that occurred during the flow expansion.

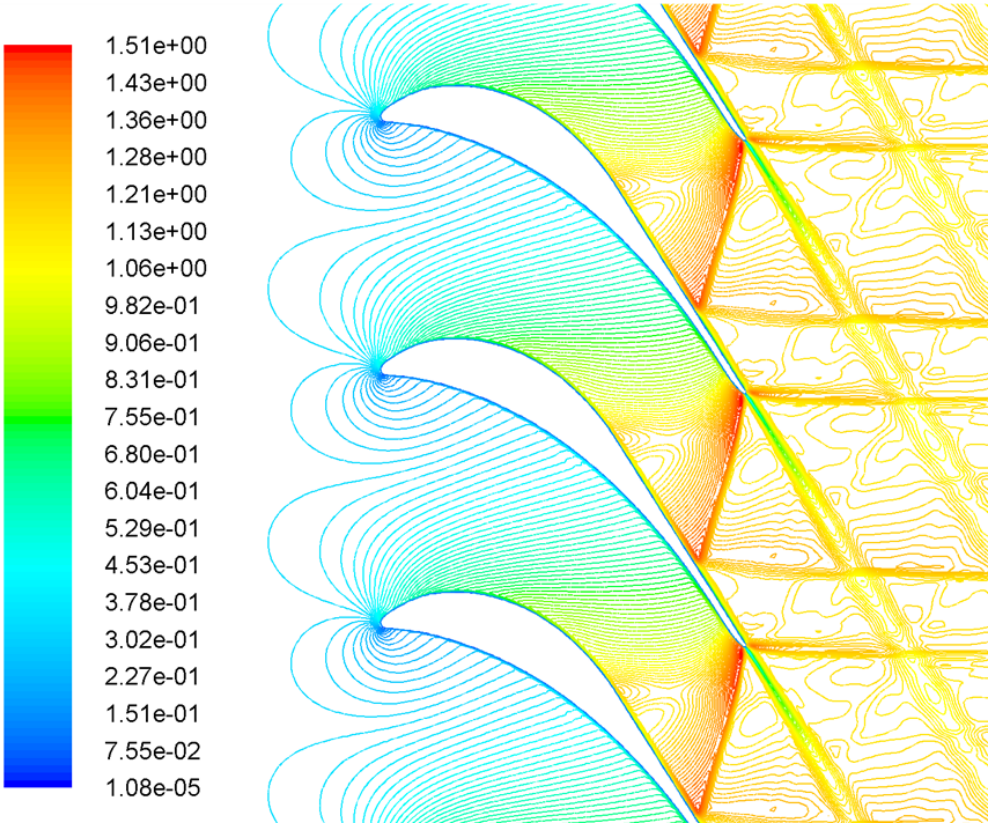

Figure 7.5: Mach number isolines

The same can be observed in the pressure field in the Figure 7.6. From the maximal pressure at the stagnation point, the pressure values decrease with the expansion up to the shock waves with exception in the problematic region where the compression area is obvious from this contour. The insensitive shape design causes very rapid flow expansion which is not followed by further concave surface shape and leads to the formation of the compression region. Intensive drop followed by pressure increase is even more obvious from blade surface pressure distribution in the Figure 7.7.

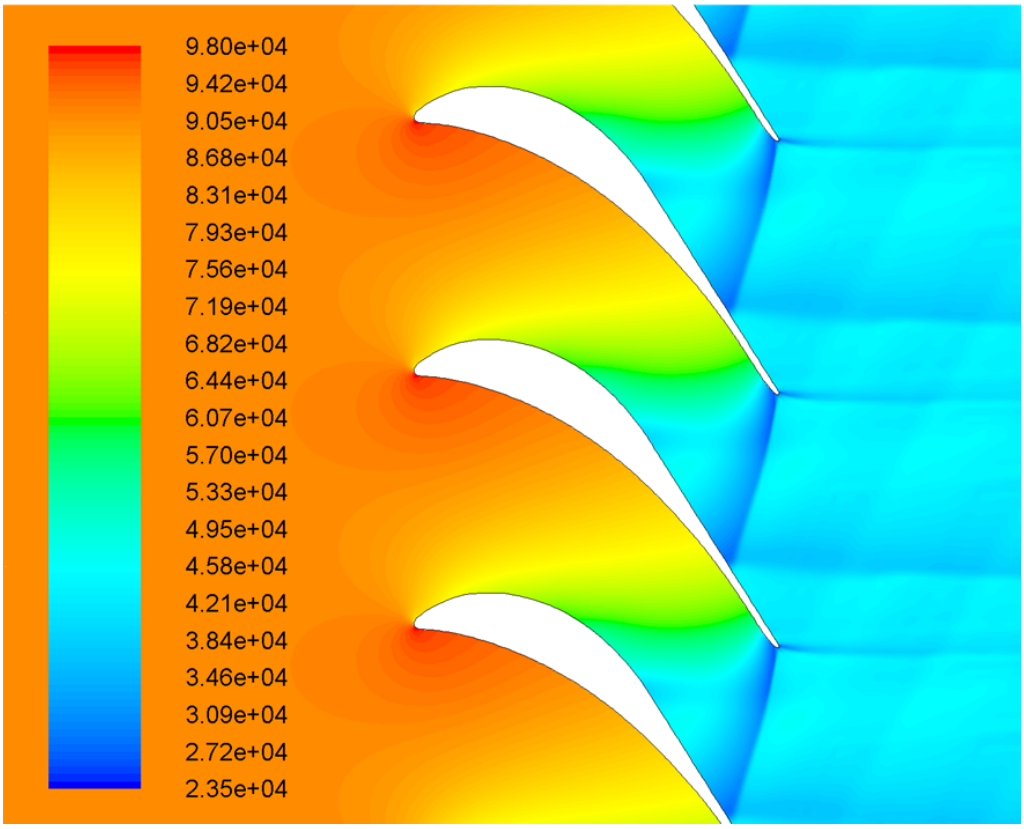

Figure 7.6: Contours of static pressure [Pa]

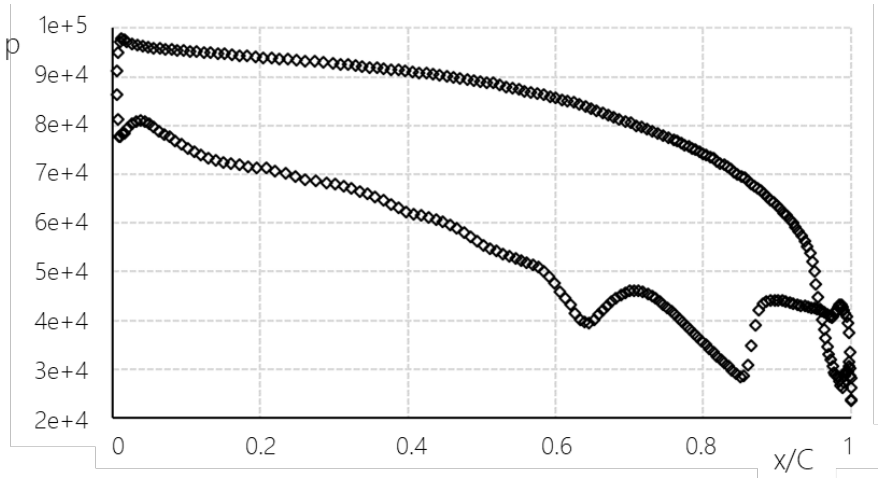

Figure 7.7: Surface static pressure distribution [Pa]

7.3 Flow Analysis and Design Modification

For detailed flow and shape analysis, a similar approach as in the previous chapter solving Laval nozzle flows can be applied, only this time the simulated flow field will be used as the initial condition for rheograph study. Flow data from extracted sonic line can be transformed like depicted in the

Figure 7.8. This boundary provides a perfect initial condition for building the characteristic region.

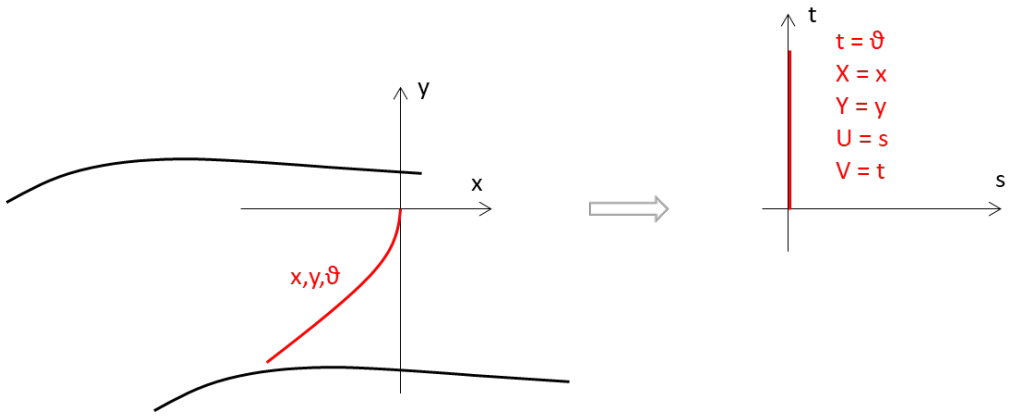

Figure 7.8: Physical plane to rheograph transformation

The possible continuation is described in [5] as a non-symmetrical nozzle exit design by prescribing velocity distribution along the nozzle axis. This approach once more demonstrates the difference between classical hodograph and characteristic or rheography plane, where the structure may be controlled to show a single-valued characteristic grid instead of multivalued “folded” hodograph. The sketch of the situation is depicted in the Figure 7.9.

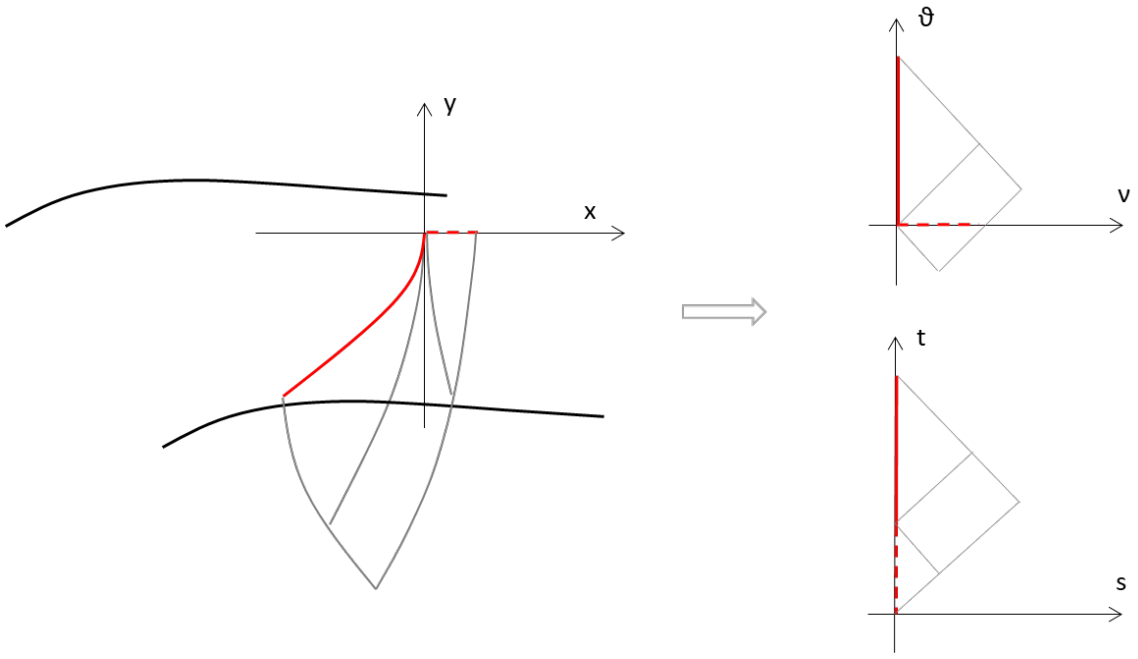

Figure 7.9: Physical plane to rheograph transformation

The shape of the characteristic region formed from the sonic line to the neutral characteristic is shown in the Figure 7.10 and already here, without the need of computing the further accelerated

flow, it is obvious that the position of curvature discontinuity (yellow point) lies very close to the neutral characteristic. Until this point, the surface is curved more progressively, but suddenly, the curvature goes down to zero to the trailing edge. This discontinuity leads to an infinite pressure coefficient gradient and later supersonic re-compression.

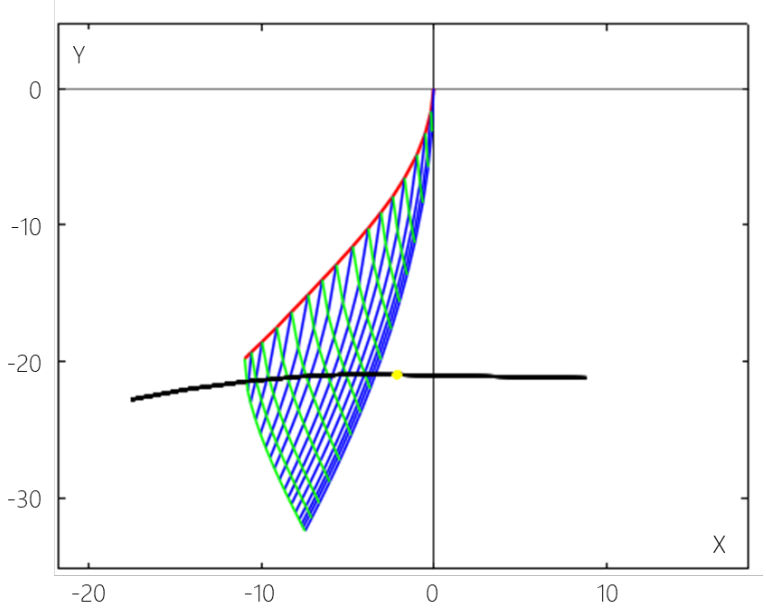

Figure 7.10: Characteristic region in X,Y plane

After transformation of this characteristic pattern back in to physical plane, the mapped region can be easily combined with obtained flow filed results. In the Figure 7.11, both, the results from CFD simulation and interferogram image, are put together in one visualization with added rheograph solution highlights. Red solid line is the extracted sonic line and dashed blue line is the calculated neutral characteristics. Note, that the sonic line does not continue up to the blade surface due to viscous behavior of boundary layer. The yellow point then shows the change in curvature of the blade surface shape. Both sub-images in the Figure 7.11 on one hand confirm very good correspondence in flow field between simulation and experiment in formation of compression region as well as position of shock waves and wake, but on the other hand very problematic location of curvature discontinuity.

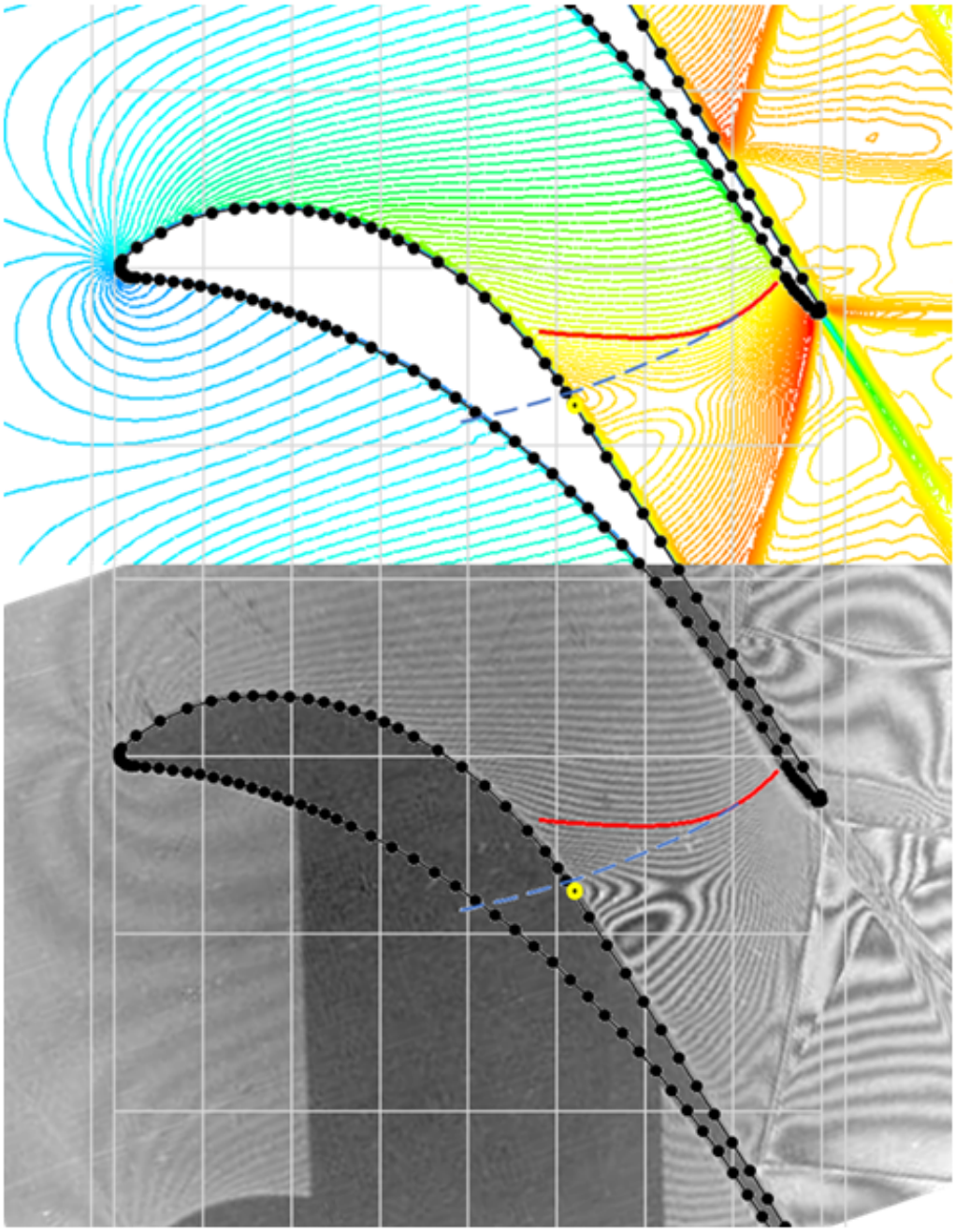

Figure 7.11: Results with sonic line and neutral characteristic position

Considering these facts, shape modification of this particular case is very challenging task. If the problematic area was further away, the method from Chapter 6 applied here as depicted in the Figure 7.8 could be used to easily find appropriate streamline shape downstream from the neutral characteristic, without disturbing the sonic line and thus the upstream conditions. There is a theoretical way how to reshape the supersonic section of the blade to obtain expanding nozzle-like solution, but the real thickness of the blade and a trailing edge fixed position makes only a little room for such

intensive intervention. A sketched solution from the principle described in the Figure 7.9 is shown in the Figure 7.12 with the red dotted red line as new surface shape downstream the neutral characteristics. The extension of the concave surface however requires manual connection with the trailing edge (blue dotted line) resulting in significant convex shape and thus inevitable compression. Note that the solution in this figure is slightly exaggerated for better visual description.

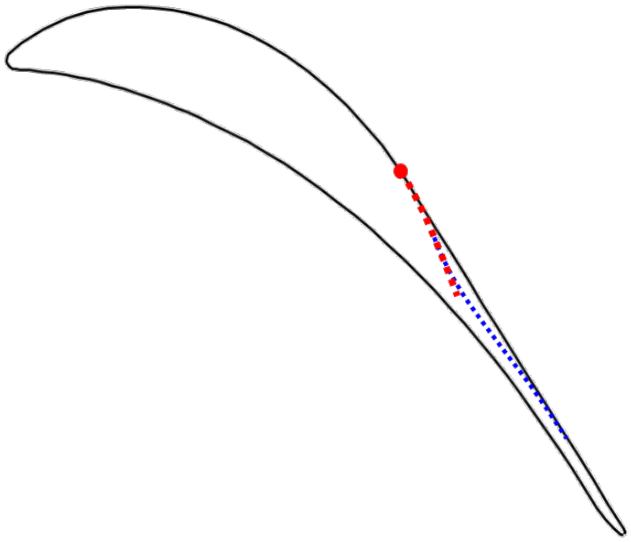

Figure 7.12: Rheograph solution resulting shape modification

The result of this effect is obvious in the Figure 7.13. The intensive convex curvature would just move the compression further downstream and make it worse. So that, in order to preserve basic characteristics of the cascade like exit flow angle and throat area, the modification of shape in subsonic region is necessary.

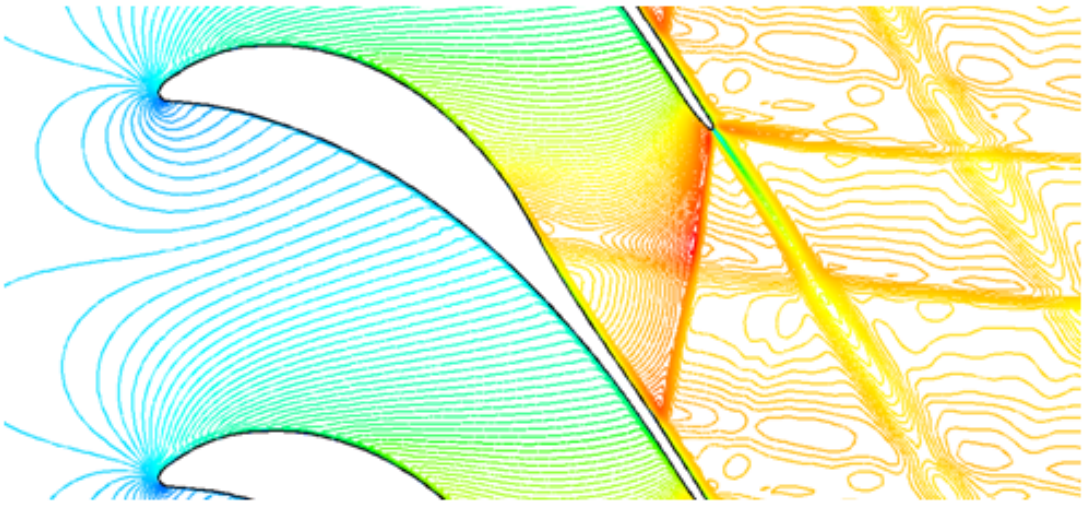

Figure 7.13: Convex shape flow field

Without the possibility of quick, purely supersonic hodograph based design modification as described in previous chapter, the shape must be changed in more sensitive manner manually and the update of the subsonic and near sonic regions is inevitable. One way to improve current state is just a minor change in area of the sonic line and surface curvature discontinuity, that in very sensitive phenomenon like transonic flow has major effect on the flow field. In general, the goal is to make the shape curvature slightly more moderate and extend it further downstream, like depicted in the Figure 7.14 (red), over the discontinuous original surface.

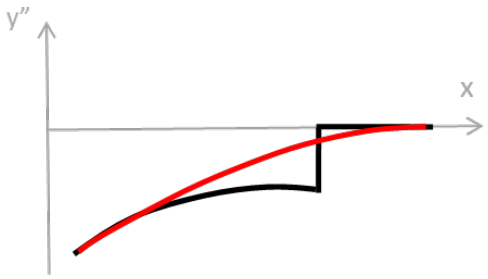

Figure 7.14: Blde surface curvature

With such solution, it is not easy to obtain impressive results without significantly changing the whole flow field, but visible changes are possible to reach. Such blade with slightly modified curvature is shown in the Figure 7.15.

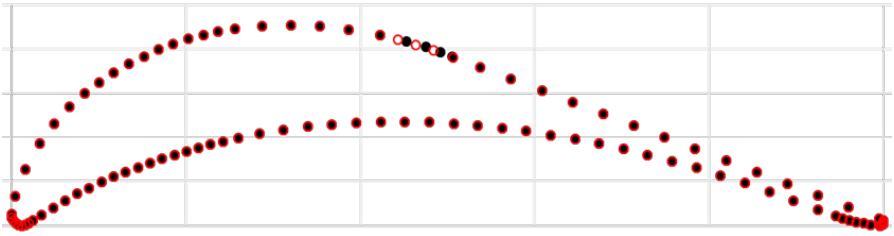

Figure 7.15: Modified blade shape

Mach number isolines in the Figure 7.16, in comparison with the original flow field, show some improvement, but the situation is not fully resolved. This is due to the still persistent presence of a straight surface in the expansion area.

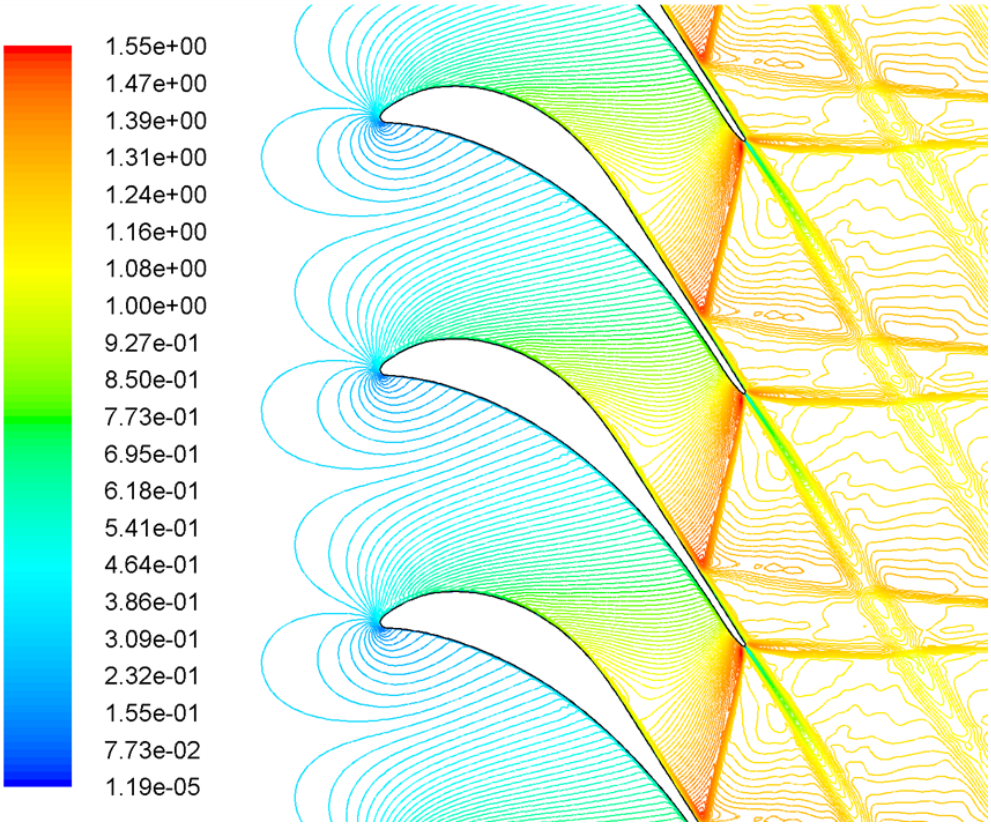

Figure 7.16: Isolines of Mach number

From the static pressure contour in the Figure 7.17, it can be said that the pressure field looks improved and better from this point of view as well and the re-compression hump is smoothed out.

The effect on the performance parameters of the blade is small, but the overall efficiency should be higher due to the more uniform flow expansion. The lift force on the other hand may not be increased because of the extensive expansion before the re-compression area in the original case. These thoughts are confirmed latter in the Figure 7.21, where pressure distributions on the blade surface are compared.

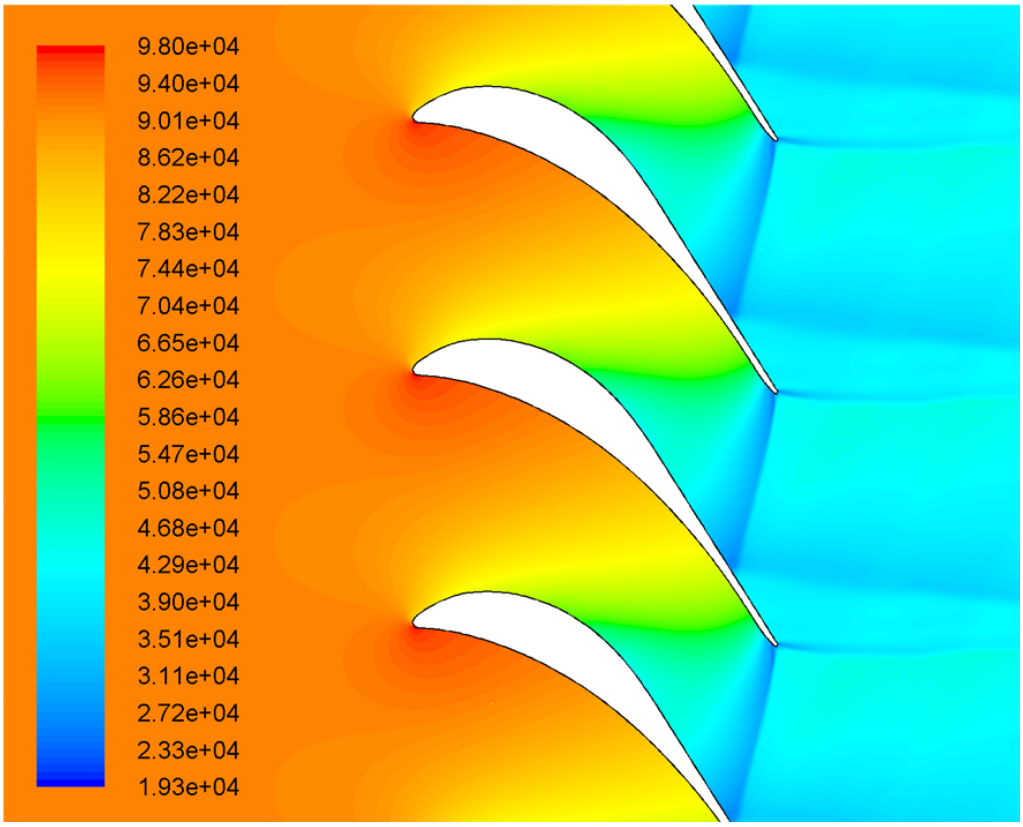

Figure 7.17: Contours of static pressure [Pa]

Another possibility is the whole blade shape modification or optimization. There is many to be said about airfoils or blades parametrization and optimization processes and different methods, but this in not the purpose of this work and the next geometry modification serves as just a hint or a suggestion of other possible solutions. Using a parametric tool [28], for e.g. a PARSEC application [29], a shape very similar to the SE1050 can be quickly generated with paying extra attention to the previous discontinuity location. The new blade design with different transition from curved to straight section is shown in the Figure 7.18.

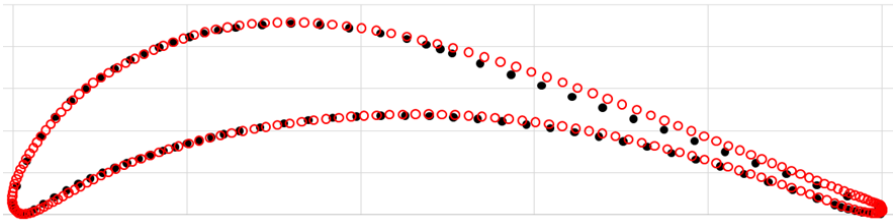

Figure 7.18: Modified blade shape

Flow field around the optimized blade is obviously even further in terms of re-compression elim-

ination. The overall shape change allows to smooth the transition between the curved and straight section, but the of use the complex parametric description changes the overall shape of the blade and thus the flow parameters in other sections as well. The Mach number isolines in the Figure 7.19 confirm continuous expansion and flow acceleration. This geometry change was however more intense and the difference in flow parameters causes also a small but visible change in the shock waves configuration.

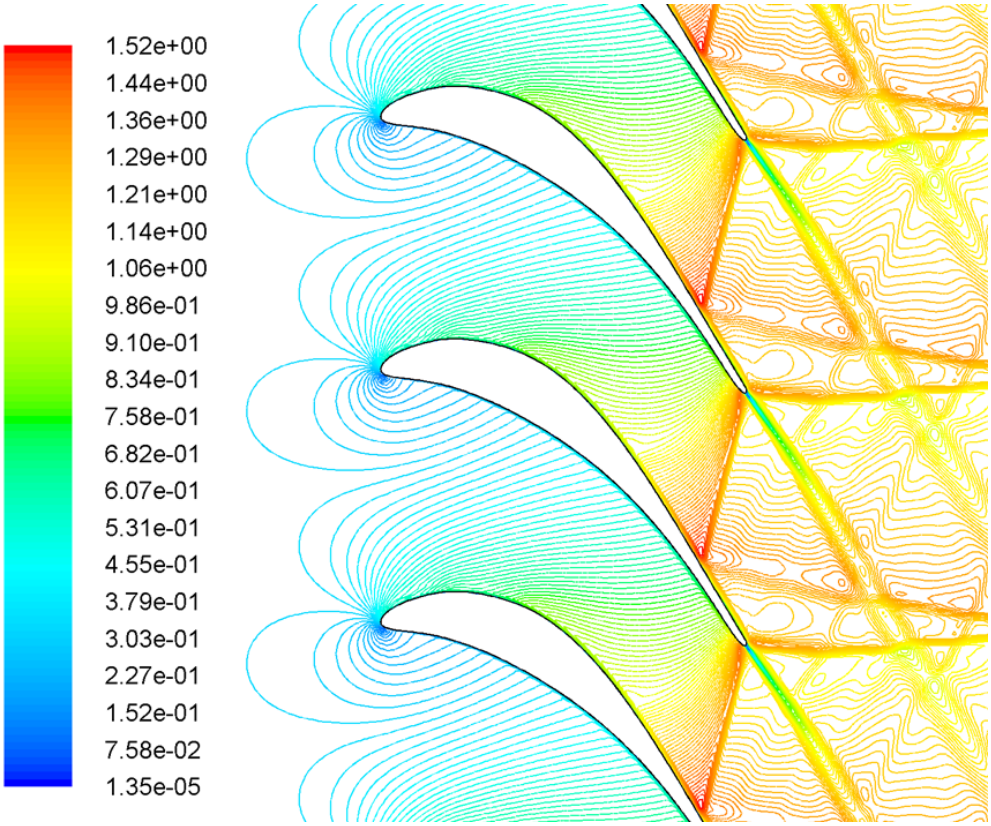

Figure 7.19: Isolines of Mach number

Pressure contours also confirms reduction of compression region, the smooth expansion continue through the whole channel up to the trailing edge shock without any noticeable kink in contours. But as the blade was reshaped as a whole, there are sections of the blade that have been modified significantly and the overall shape and parameters of the cascade are now different, that is why some changes in flow in other areas appear as well.

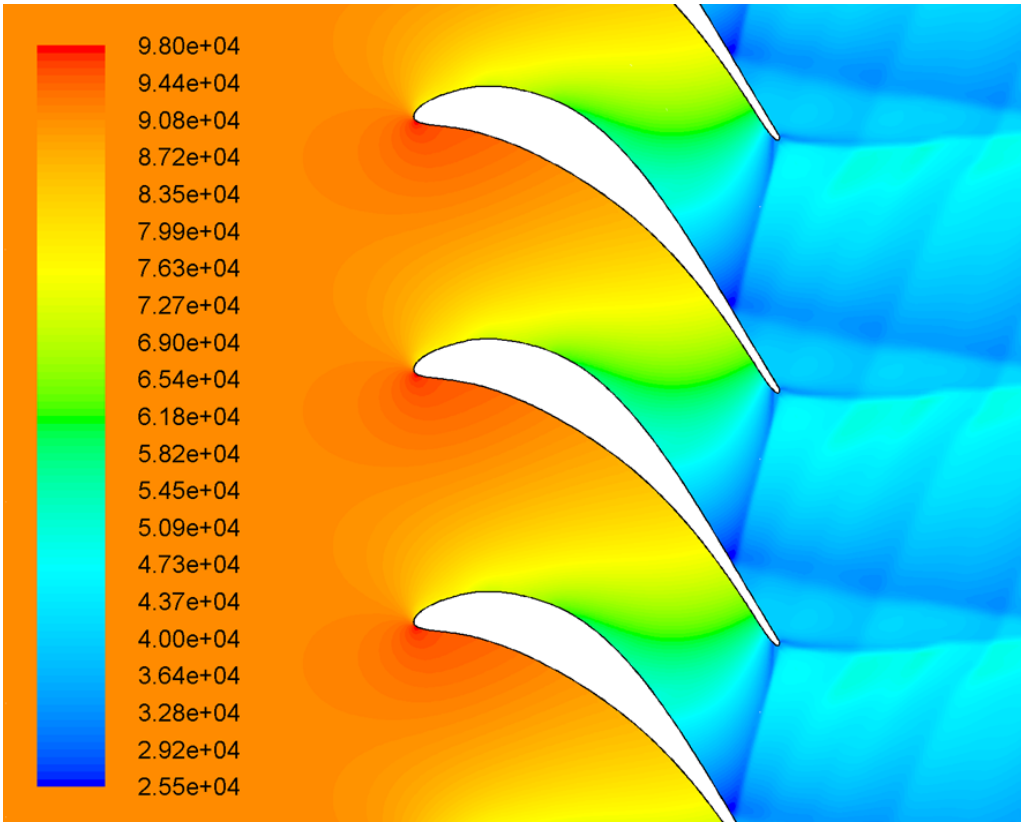

Figure 7.20: Contours of static pressure [Pa]

The effect of made changes is nicely comparable by plotting surface pressure values. Figure 7.21 shows static pressure distribution on the blade surface with dashed grey line representing the curvature discontinuation point. Local modification of the blade and more sensitive shaping in terms of curvature leads to dispersal of the expansion-compression region. The fully optimized blade eliminated the rapid expansion, what disposed the strong re-compression to occur, but the shape does not avoid minor oscillation in the problematic area. Due to complex shape change, the other parts of the blade surface obviously report changes in pressure distribution. From the point of view of aerodynamic forces, the change in geometry of the fully optimized blade to higher overall pressures at the suction side.

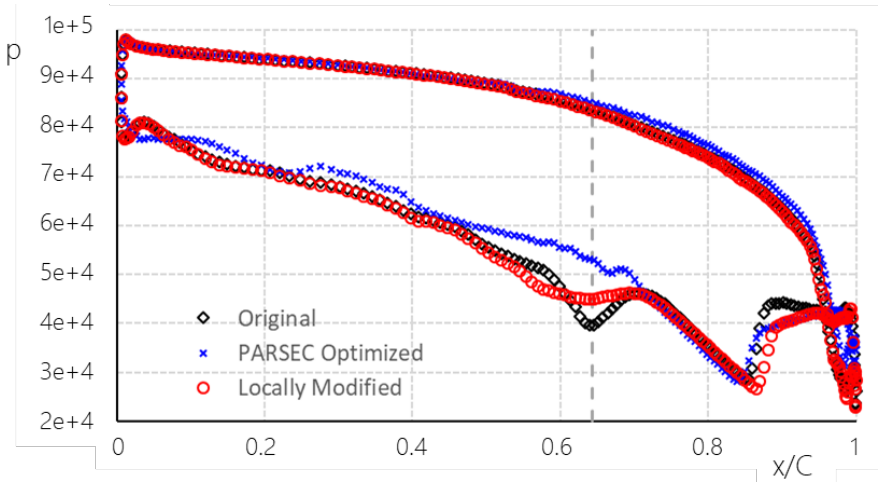

Figure 7.21: Surface static pressure distribution [Pa] - comparison

In terms of efficiency, or losses, both new shapes show some improvement over original geometry and the best values are presented by the locally modified blade shape. Individual values for static to static loss coefficient are shown in the Table 7.4.

$$\varsigma = 1 - \frac{h_1 - h_2}{h_1 - h_{02is}} \tag{7.1}$$

Table 7.4: Loss coefficient

original	**locally modified**	**optimized**
0.033	0.029	0.032

7.4 Results and Evaluation

After the theoretical introduction and academic examples, the SE1050 blade cascade case shows a practical potential of revitalized hodograph based transformation methods together with numerical solutions. The flow field calculated from numerical simulation can serve as a great input for rheograph analysis and as the initial condition for design modification. Using such approach on the case of SE1050 blade cascade confirms a specific behavior of the flow and computation of a characteristic field unveiled that the insensitive shape change and curvature discontinuity lies, specifically due to the transonic flow sensitivity, at the inappropriate location very close to the sonic line almost right at the position of the neutral characteristic. This fact means that there is no simple solution to resolve the noncontinuous expansion.

The upstream undisturbing design is based on after-sonic line characteristics build up, but due to the complicated location of the problematic area, the relevancy of such solution is very limited. From the practical point of view, this issue is impossible to eliminate by modification of just supersonic section of the blade. Therefore, in order to arrive with relevant solution without changing the basic cascade characteristics, the geometry modification has to encroach upstream to the subsonic region. The shape can be modified locally to secure continuous curvature change or reshape as a whole using parametrization or optimization tool. These solutions may more or less smooth the flow field and decrease the losses, but hardly improve aerodynamic forces.

Even though the solution of described problem needs much more attention than it may initially look like, there is an important outcome and that is once again the importance of complex knowledge of physical and mathematical principles. The rheograph transformation provides here a more advanced view onto the problematics and do not necessarily has to serve only for design purposes but effectively for flow analysis as well.

8 Discussion

All previous results and conclusions share a common attribute. In transonic flow field, the change in flow character between subsonic and supersonic regime results in extensive sensitivity and often in indirect cause of a flow character. Even a negligible change in shape, curvature or boundary conditions can result in entirely different flow field, especially near the sonic conditions. Many studied issues may then be caused by, for unexperienced analyst, at first sight unexpected and illogical origin. The solution to an issue also usually lies at different place then where the problem occurred. This perfectly stresses the need for special treatment and deeper understandings for flow design and analysis as incorrect assumptions and wrong solution approach can easily lead to faulty analysis and nonfunctional design even with convenient working tool.

8.1 Summary

High speed aerodynamics and the nature of the compressible fluid flows brings specific problems and phenomena that requires special solutions, but only some of them can be directly described by simplified relations and laws of the gas dynamics. The need for complete analytical solution of the transonic flow fields requires deeper understandings and methods standing on the basis of potential flow transformed in linearized hodograph based planes close to conformal and characteristic mapping were developed in past. Modern computational era then arrived with new solutions which can simulate the flows by numerical methods and direct discretization of basic differential equations. This also allowed very rapid rate of various cases simulations and data, but also led to the lack of some of the general knowledge of the compressible flow characteristics.

The all three approaches, the classical gas dynamics relations, rheograph transformation method and numerical modeling, were described and validated on the case of Guderley's cusp. The near sonic flow theory using conformal together with characteristic mapping for both velocity regions gives a precise modified hodograph solution of the whole flow field past the profile as well as the lift and drag information represented by the pressure coefficient distribution. Due to availability of modern computational fluid dynamics codes, the numerical experiment using verified schemes enables to receive data on parameters and flow structures past these airfoils very fast and effectively to be compared with the theory. Obtained results confirmed well the accordance between numerical and exact analytical data by means of described near sonic flow theory. And finally, detailed

analysis based on classical gas dynamics proved a good accordance of shock waves parameters at the trailing edge for regular interaction of supersonic flows. Reduced parameters analysis proved that the transonic flow past the limits of the sonic case results into irregular interaction. Off-design condition setups added a bit more practical view on the problematic and proved that even here, it is still possible to predict and simulate the flow behavior correctly. Especially for such cases, the numerical simulation is the only way how to compare and discuss obtained results and theories. It would be probably extremely difficult, if not impossible, to prepare an experimental setup for our problems containing large spreading shocks and waves. The setup precision and investigated domain limitations would make the experiment irrelevant or the material and time costs would be absolutely incomparable with the numerical requirements. Posted results also confirmed significant sensitivity of transonic flows, especially when talking about sonic and near sonic problems.

To show that the rheograph analysis and design methods used with modern computational techniques may even nowadays still be a working tool for creative aerodynamic design, the special case of symmetric supercritical nozzle was introduced and solved. The numerical modification of the elliptic continuation method combined with a method of characteristics have been shown to calculate the hitherto unknown mathematical inviscid flow example of a symmetric accelerating-decelerating nozzle throat. This computational extension removed one of the significant drawbacks of the analytical methods, the mathematically challenging manual solution of initial underlying transformed flow equations, what led to some unpopularity and incomprehension between general community. The nozzle geometry has been designed as an accelerated flow Laval nozzle reaching supersonic conditions, but continuing using a novel solution and subsequently decelerates to the subsonic regime without creation of a shock. This example, however academic case study may be, shows that not only wing design for aeronautics, but also internal high speed aerodynamics is a field where analytical flow models as available in rheograph formulation, can still be useful for design and provide a deeper understanding of the underlying flow phenomena. On the top of that, the special nozzle geometry and the specific singular behavior of the flow field can now be used as a test case for exact compressible flow simulation codes.

As a proof that rheograph solutions may be beneficial to practical problems, the simulated flow through the SE1050 blade cascade known as an ERCOFTAC test example with specific flow pattern with the re-compression area was analyzed. The flow field data, as a result of numerical simulation, can be used as an initial condition for the method of characteristics to obtain a neutral characteristics

position necessary for situation analysis and following solution proposal. The rheograph analysis shows that the curvature discontinuity and subsequent shape change lies right at the position of the extremely sensitive near sonic region and thus, there is no simple upstream flow independent design solution to this issue. In order to preserve general cascade flow parameters like the throat area and exit flow angle, resulting shape leads to formation of concave surface section and latter compression wave. Nevertheless, a hint of possible ways how to improve the situation were proposed. Local curvature based shape modification and full geometry parametric optimization were suggested with positive results in terms of re-compression area elimination, in slightly improved losses but neutral to more or less negative effect on the overall aerodynamic forces.

8.2 Conclusions

To conclude the work, the main goals defined for this thesis needs to be evaluated. Various solutions of transonic flows described in all previous chapters may follow different path to the result, but in the end nicely correspond with each other. The classical gas dynamic provide solid basics for compressible flows, the hodograph transformation methods extend the analytical abilities and allow to solve complex flow fields and create novel designs and finally, computational fluid dynamics can effectively use still growing software and hardware capabilities and simulate almost any problem with sufficient precision. This was proved on the Guderley's cusp example, where predicted flow field and parameters correspond with numerical simulation data. The supercritical symmetric nozzle case shows that the renovation of hodograph based methods, even now just on academic example, is possible. Combination of rheograph transformation and modern computational techniques can lead to interesting design tool which is also easier to understand and use than the original analytical approach. This method is also fully applicable not only on airfoil geometries, but for internal flows as well. The application on a practical case of SE 1050 blade cascade proves the functionality on relevant real life problems. The rheograph analysis shows that the only effective design modification must intervene the subsonic domain upstream the sonic conditions. Previous cases are a good example of usage range and a proof, that this approach can provide real benefits for different practical and academical problems. It may not be fully redeeming, sometimes the issue just does not have a possible simple solution, but it is also important to explain and understand the origin of a unwanted behavior. All the conclusions previously mentioned may not be easy to acquire in today's fast times, but if so, the results could extend the possibilities and deliver new sights for various topics.

Throughout the whole thesis, unique characteristics of transonic flow are solved and discussed, but all the non trivial individual examples or cases and their solutions repeatedly show the importance of deeper understandings of the problematics. Without the knowledge, many obtained results, no matter if from simulation or experiment, can be interpreted incorrectly because of at first sight hidden origin of the problem, especially at the regime of high speed aerodynamics. Any scientist or engineer working in this field of study should keep this in mind.

References

[1] Christianowitsch, S.A.: *Flow over Bodies at High Subsonic Velocities,* Tr. Joukowski Central Aero-Hydrodynamics Institute, No. 481, 1940

[2] Guderley, K.G.: *Theory of Trnsonic Flow,* Springer, Berlin - Goettingen - Heidelberg, 1957

[3] Sobieczky, H.: *Tragende Schnabelprofile in Stossfreier Schallanstromung,* ZAMP 26, Issue 6, pp. 819-830, 1975

[4] Sobieczky, H.: *Related Analytical, Analog and Numerical Methods in Transonic Airfoil Design,* AIAA 79-1566, 1979

[5] Sobieczky, H., Qian, Y.J.: *Extended Mapping and Characteristics Techniques for Inverse Aerodynamic Design,* ICIDES III Conv., 1991

[6] Sobieczky, H.: *Transonic Singularities,* Computationl Fluid Dynamics Journal, Vol 12, No 1, 2003

[7] *ERCOFTAC Application Challenge AC 6-12* [online], 1.12.2018 http://qnet-ercoftac.cfms.org.uk/w/index.php/Abstr:Steam-turbinerotor-cascade

[8] Sobieczky, H.: *Die Abgeloste Transsonische Kopfwelle,* Zeitschrift fur Flugwissenschaften 22, No 3, pp. 66-73, 1974

[9] Šťastný M., Šafařík P.: *Experimental Analysis Data on the Transonic Flow Past a Plane Turbine Cascade,* ASME Paper 90-GT-313, 1990

[10] Fořt J., Fürst J., Halama J., Kozel K.: *Numerical Solution of 2D and 3D Transonic Flows through a Cascade,* Proceedings of 4th International Symposium on Experimental and Computational Aerothermodynamics of Internal Flows, Dresden, Vol.1., pp. 231-240, 1999

[11] Šafařík, P.: *Theoretical Analysis of Transonic Expansion in Blade Cascade,* Report of IT CAS No. Z-856/83, 1983 (in Czech)

[12] Anderson J.D.: *Modern Compressible Flow, with Historical Perspective,* McGraw-Hill, New York, 1990

[13] Shapiro A.H.: *The Dynamics and Thermodynamics of Compressible Flow,* The Ronald Press Company, New York, 1957

[14] Chung, T.J.: *Computational Fluid Dynamics,* Cambridge University Press, Cambridge, 2002

[15] Moin, P.: *Fundamentals of Engineering Numerical Analysis,* Cambridge University Press, Cambridge, 2001

[16] Oswatitsch, K.: *Special Problems of Inviscid Steady Transonic Flow,* Internatinal Journal of Engineering Science, Vol 20, No. 4, pp. 497-540, 1982

[17] Trenkner, M., Sobieczky, H.: *Using the Gasdynamics Knowledge Base for Aerodynamic Design and Optimization in the Sonic Speed,* Proceedings of International Symposium on Inverse Problems in Engineering Mechanics, Nagano, 2001

[18] ANSYS Inc, *ANSYS®Fluent, Release 16.2, Theory Guide,* 2014

[19] Blažek, J.: *Computational Fluid Dynamics: Principles and Applications,* Elsevier, New York, 2001

[20] *Compressible Aerodynamics Calculator* [online], 1.12.2018, http://www.dept.aoe.vt.edu/ devenpor/aoe3114/calc.html

[21] Kozel, K., Fürst, J.: *Numerical Methods for Flow Problems Solutions I,* Vydavatelství ČVUT, Praha, 2001 (in czech)

[22] Punčochářová, P., Kozel, K., Fürst, J., Horáček, J.: *Numerical Solution of Unsteady Viscous Compressible Flows in a Channel,* Topical Problems of Fluid Mechanics, Institute of Thermomechanics AS CR, Prague, pp. 220-228, 2006

[23] Gottlieb, S., Shu, Ch-W.: *Total Variation Diminishing Runge-Kutta Schemes,* Mathematics for Computation, vol 67, 1998

[24] Šafařík, P.: *The Flow in the Supersonic Exit of Blade Cascades,* Archives of Mechanics, Vol.26, No.3, pp. 529-533, 1974 (in Czech)

[25] Šafařík, P.: *Application of Method of Characteristics at Calculation of Flow Past Blade Cascades,* Report of IT CAS No. T-178/75, 1975 (in Czech)

[26] Zucrow, M.J., Hoffman, J.D.: *Gas Dynamics,* John Wiley and Sons, INC, New York, 1976

[27] Fialová, M., Hyhlík, T., Kozel, K., Šafařík, P.: *Numerical Analysis Data on the Transonic Flow Past the Profile Cascade SE 1050,* Proceedings of the Seminar "Topical Problems of Fluid Mechanics", Institute of Thermomechanics, Prague, pp. 45-48, 2001

[28] Sobieczky, H.: *Parametric Airfoils and Wings,* K. Fuji and G. S. Dulikravich (Eds.): Notes on Numerical Fluid Mechanics, vol. 68, pp. 71-88, Wiesbaden: Vieweg, 1998

[29] *PARSEC - Airfoil Generator* [online], 1.12.2018, http://www.as.dlr.de/hs/d.PARSEC/Parsec.html

[JS1] Stodůlka, J.: *Numerical Solution of Oblique Shock with Wall Interaction Using Finite Difference Method,* SKMTaT 2013, Žilina, pp. 275-278, 2013

[JS2] Stodůlka J., Sobieczky, H.: *On Transonic Flow Models for Optimized Design and Experiment,* EPJ Web of Conferences 67, 02111, 2014

[JS3] Stodůlka, J., Šafařík, P.: *Analysis of Transonic Flow Past Cusped Airfoil Trailing Edge,* Acta Polytechnica, Prague, pp. 193-198, 2015

[JS4] Stodůlka, J., Sobieczky, H.: *Theoretical and Numerical Solution of a Near Sonic Flow Considering the Off-Design Conditions,* Engineering Mechanics 2014, Svratka, pp.588-591, 2014

[JS5] Stodůlka, J., Sobieczky, H., Šafařík, P.: *Analytical and Numerical Modifications of Transonic Nozzle Flows,* Journal of Thermal Science, Vol 27, Issue 4, pp. 382-388, 2018